Thin–Walled Structures 198 (2024) 111751

Contents lists available at ScienceDirect

Thin-Walled Structures

journal homepage: www.elsevier.com/locate/tws

Full length article

Equivalent layer-wise theory for the hygro-thermo-magneto-electro-elastic analysis of laminated curved shells

Francesco Tornabene *, Matteo Viscoti, Rossana Dimitri

Department of Engineering for Innovation, University of Salento, 73100, Lecce, Italy

ARTICLE INFO

Keywords:
Adaptive wood
Equivalent Layer-Wise
Generalized Differential Quadrature
Multifield formulation
Navier solution
Recovery procedure
Smart structures

ABSTRACT

The paper presents a multifield formulation involving five different physical problems under the equilibrium thermodynamic conditions for laminated doubly-curved shell structures. More specifically, the study focuses on the coupling between the mechanical elasticity and the thermo-hygrometric problem, while also considering the magneto-electricity of the solid. The configuration variables are described with a generalized formulation based on the Equivalent Layer Wise (ELW) approach, taking into account higher order polynomial interpolations along the thickness direction. The fundamental relations are derived from the Master Balance principle and solved using the Navier's method. Furthermore, the three-dimensional response of the doubly-curved shell solid in terms of primary and secondary variables is recovered from the two-dimensional solution with a methodology based on the three-dimensional multifield balance equations and the Generalized Differential Quadrature (GDQ) numerical technique. Some examples are then presented in which panels of different curvatures and lamination schemes are investigated. The results are compared with success to those coming from three-dimensional numerical models developed with a commercial software. It is shown that the present analytical solution is a valid tool for modelling multifield problems for the evaluation of the response of doubly-curved shells under generalized external actions and pre-determined values of the configuration variables.

1. Introduction

Recent applications in many engineering fields adopt structures of very complex shapes made of innovative materials [1–2]. More specifically, the so-called smart structures [3] are extensively employed, which can react not only to external surface tractions, but also to other general actions like hygrothermal loads, as well as electric and magnetic fields. As a consequence, the bending and vibrational response of a smart structure can be oriented according to the design needs by applying an external field [4–7]. Another interesting application of this kind of structures concerns the influence of thermal loads, since the deformations induced by high temperatures [8–9] or by moisture diffusion processes can be easily controlled with an application of an electric field to the structure [10–12]. The coupling between two physical problems considers both the direct and the converse effects, therefore several practical applications can be made. For instance, in case of piezoelectric devices [13–15], the direct piezoelectric effect consists of a deformation of the structure under the application of an electric field, whereas for the converse piezoelectric effect an electric voltage is generated from a strain distribution. In other words, the direct and converse piezoelectric properties of a structural component can be used in actuators and sensors, respectively [16–17]. Furthermore, multifield simulations can be adopted to investigate the effects of external electromagnetic fields, vibrations in a thermal environment, and the influence of mass diffusion processes on the structural response [18–20].

When a smart structure is studied, the derivation of a theoretical model can be carried out using both coupled and uncoupled formulations [21–23]. In case of uncoupled model, each physical problem is solved separately, and a distribution of additional strains is derived, which is embedded in the mechanical elasticity problem as an additional volume load [24–26]. On the other hand, when a fully-coupled formulation is adopted the constitutive equations of each physical problem consider the coupling between the different fields [27–29]. As a consequence, the energy of the system shows some additional terms and the fundamental equations of each field are solved within the same system. A multifield problem can be developed using either a three-dimensional (3D) or two-dimensional (2D) approach, and an approximate solution is usually obtained through a numerical procedure [30–33]. However, the

* Corresponding author.
E-mail address: francesco.tornabene@unisalento.it (F. Tornabene).

https://doi.org/10.1016/j.tws.2024.111751
Received 20 January 2024; Received in revised form 22 February 2024; Accepted 25 February 2024
Available online 1 March 2024

computational cost can be very high due to the significative number of Degrees of Freedom (DOFs) that are involved, especially in 3D formulations. To this end, closed-form and semi-analytical solutions [34–41] can be derived for some specific cases, such as plates, cylindrical and shallow spherical panels characterized by antisymmetric cross-ply and angle-ply lamination schemes. All these methods can be combined for a more convenient derivation of the solution of the system of partial differential equations governing each physical field [42–43].

When developing a multifield two-dimensional formulation, two different approaches can be followed, namely the Equivalent Single Layer (ESL) and the Layer-Wise (LW) models [44–47]. In addition, a hybrid approach named Equivalent Layer-Wise (ELW) formulation [48] can be also adopted. Several thickness functions can be selected, including both polynomial and non-polynomial functions [49–51]. Furthermore, zigzag functions [52–53] can be employed to depict the slope change of the deflection in the interface between two adjacent laminae. In this way, each unknown field variable is described using pre-determined thickness functions which only depend on the thickness coordinate. Some generalized variables are thus introduced, which represent the DOFs of the formulation. When an ESL model is used, these variables can be found on a reference surface located in the middle thickness of the panel under consideration [54–55], whereas LW and ELW variables are distributed along the thickness of the solid [56]. In addition, in LW models an axiomatic assumption is made in each lamina of the panel, whereas in ELW and ESL formulations the description of the field variables refers to the entire lamination scheme. Since each variable of a multifield problem may have a different behavior within the same layer with respect to the other ones, the structural model should be based on a generalized formulation in which a particular thickness function is adopted for each field. In order to achieve this, the unified formulation [57–58], presented for the first time in the works by Washizu and Reddy for the mechanical elastic problem [59–60], can be used. As far as the external loads are concerned, in mechanical problems an external surface traction is usually applied to the structure [61–62], or alternatively a pre-determined distribution of the displacement field can be prescribed in some regions. In the same way, in multifield analysis a prescribed value of the unknown field variable is typically enforced to the panel [63–68]. Furthermore, an external surface flux can be assigned for each field, depending on the modeling requirements. When coupled multifield formulations are presented, different expressions of the total energy of the structural system are provided in literature [69–71], depending on the physical problems that are coupled. In a more general case, the total free energy [72–73] can be seen as a generalization of several multifield energies in which only two or three physical problems are coupled, considering the elastic strain energy, the electric energy, the magnetic energy, the entropy energy and the chemical energy of the system. The total free energy can be interpreted as the internal work done by all the generalized actions associated with each physical problem. It should be noted that the governing equations of a multifield problem can be easily derived if the energy of the system is a thermodynamic potential. In this way, the Master balance principle can be applied. If a smaller number of fields is considered, some energetic contributions are neglected and the corresponding thermodynamic potential for the specific problem under consideration is derived. For example, when the coupling between the heat transfer problem and the mechanical elasticity is studied, a stationary configuration of the Helmholtz free energy function is derived, which depends on the deformation gradient and the absolute temperature. As it is well-known, the heat conduction problem is caused by a temperature gradient, whereas a mass concentration gradient leads to a mass diffusion. These two phenomena are traditionally modeled using the Fourier and Fick equations [74–77]. However, experimental results show that moisture diffusion and heat transfer are related to each other [78]. The coupling between these two systems of equations is conducted through the Onsager reciprocity relations [79–80]. In this way, the Dufour effect can be modeled, which consists of an additional heat flow coming from a concentration gradient. In the same way, the increment of mass flow caused by heat transfer is known as Soret effect [81–83].

Once the governing equations are derived, a closed-form solution can be found for only specific load cases, lamination schemes and geometries. Starting from the pioneering works by Pagano [84–85], several three-dimensional [86] and two-dimensional analytical solutions have been developed for laminated plates and shells based on the Classical Plate Theory (CPT), First Order Shear Deformation Theory (FSDT) and Third Order Shear Deformation Theory (TSDT) [87–89]. Analytical solutions are typically employed to validate numerical models. Nevertheless, a correct implementation of a semi-analytical method can provide a solution of practical interest by expanding some closed-form solutions, as happens in the well-known Navier and Levy methods [90–91]. On the other hand, the reconstruction of the actual distribution of primary and secondary variables from two-dimensional generalized variables may lead to inaccurate predictions of the real structural response because two-dimensional models do not a-priori satisfy the equilibrium conditions in the thickness direction. As a consequence, a post-processing correction of these profiles is essential, as shown in Refs. [92–94]. The correction of primary and secondary variable requires a numerical method to integrate the balance equations of each physical problem along the thickness direction. Among various numerical techniques, the Finite Element Method (FEM) is widely used in several commercial codes [95–96]. Based on local interpolation of the unknown variables through shape functions, it requires the definition of a discrete computational grid where the governing equations are solved. A grid refinement can yield more accurate results, even though the computational cost is increased. For this reason, spectral collocation methods, such as the Generalized Differential Quadrature (GDQ) method [97], are commonly employed to reduce the number of DOFs. To this class belongs the GDQ method [98–100], which allows one to approximate the derivative of an arbitrary order as a weighted sum of the values assumed by the unknown function on a discrete grid. Weighting coefficients are determined using various approaches. The Lagrange interpolating polynomials are very frequently adopted as basis functions [101]. When the unknown function is approximated with Taylor's series, the Taylor-based Differential Quadrature (TDQ) is obtained, whereas the Harmonic Differential Quadrature (HDQ) is based on the adoption of Fourier trigonometric series [102–103]. Several papers show that GDQ-based procedures are highly efficient and accurate, especially when the discrete problem is built on non-uniform grids [104–105]. The GDQ method has been applied to a series of structural problems, including laminated shell structures made of advanced materials [106–108]. Furthermore, in Refs.[109–112] it has been used to derive an approximate solution in various coupled multifield problems.

In the present work, a two-dimensional multifield problem is developed for laminated doubly-curved shell structures. The present model includes the mechanical elasticity problem, the electric and magnetic fields, as well as the hygro-thermal coupling all presented in a fully-coupled formulation. Once the geometry of the doubly-curved panel is described through principles of differential geometry, the multifield fundamental equations are derived from the Master Balance principle, taking into account all the coupling effects between the investigated physical problems. The unknown field variables are described using a generalized ELW formulation, involving higher order through-the-thickness kinematic assumptions. Furthermore, the interactions between two adjacent laminae are described with an improved version of the Murakami zigzag function. A semi-analytical two-dimensional solution is derived with the Navier method for cross-ply plates, cylinders and shallow spherical panels. Then, the GDQ

method is employed to correct the through-the-thickness profile of the primary and secondary variable of each physical problem through a recovery procedure based on multifield three-dimensional balance equations. Three examples of investigation are presented in which the model is used to derive the multifield response of various structures, considering different levels of coupling between the involved physical problems. For each case, the semi-analytical predictions of this formulation are successfully compared with the results obtained from refined Finite Element numerical models developed with a commercial software. To the best of author's knowledge, the present work provides, for the first time, a generalized model that considers the complete coupling between the hygrometric, thermal, magnetic, electric and mechanical fields. Furthermore, the equilibrium-based recovery procedure, initially developed for the mechanical elasticity problem, is extended here to a multifield formulation. This extension enables the derivation of highly accurate predictions of the outcomes computational expensive three-dimensional models starting from a two-dimensional semi-analytical solution. Finally, the proposed methodology can be a valid tool for studying a complete multifield problem with a high level of accuracy despite limited computational resources.

2. Geometric description of a doubly-curved shell

In this section, an abitrary doubly-curved shell structure is described according to the ESL approach. The position vector $\mathbf{R}$ of a doubly-curved shell solid depends on three parameters denoted by $\alpha_i = \alpha_1, \alpha_2, \alpha_3$, which are defined in a closed interval $\alpha_i \in [\alpha_i^0, \alpha_i^1]$ with extremes $\alpha_i^0 < \alpha_i^1$. If the unit vectors of a global cartesian coordinate system are denoted by $\mathbf{e}_1, \mathbf{e}_2, \mathbf{e}_3$, the following relation can be introduced:

$$\mathbf{R}(\alpha_1, \alpha_2, \alpha_3) = f_1(\alpha_1, \alpha_2, \alpha_3)\mathbf{e}_1 + f_2(\alpha_1, \alpha_2, \alpha_3)\mathbf{e}_2 + f_3(\alpha_1, \alpha_2, \alpha_3)\mathbf{e}_3 \tag{1}$$

where f_1, f_2, f_3 are smooth functions. Following the ESL approach, a reference surface is defined in the middle thickness of the solid. The position vector $\mathbf{r}(\alpha_1, \alpha_2)$ of any point on this surface is determined by the parameters α_1, α_2, which are the principal coordinates of the surface itself. In this way, the quantity $\mathbf{R}$ of Eqn. (1) can be expressed as follows [45]:

$$\mathbf{R}(\alpha_1, \alpha_2, \zeta) = \mathbf{r}(\alpha_1, \alpha_2) + \frac{h(\alpha_1, \alpha_2)}{2} z \mathbf{n}(\alpha_1, \alpha_2) \tag{2}$$

being h the total thickness of the doubly-curved shell solid. In addition, $z = 2\zeta / h$ is a dimensionless parameter that identifies the points located along the normal direction of the reference surface, with its unit vector denoted as $\mathbf{n}(\alpha_1, \alpha_2)$. If the symbol $\mathbf{r}_{,i} = \partial \mathbf{r} / \partial \alpha_i$ with the subscript $i = 1, 2$ is adopted for the first order partial derivatives of the reference surface position vector $\mathbf{r}$ with respect to the principal coordinates α_1, α_2, the outward normal unit vector can be evaluated according to the following relation:

$$\mathbf{n}(\alpha_1, \alpha_2) = \frac{\mathbf{r}_{,1} \wedge \mathbf{r}_{,2}}{\left| \mathbf{r}_{,1} \wedge \mathbf{r}_{,2} \right|} \tag{3}$$

At this point, the geometric properties of the reference surface $\mathbf{r}(\alpha_1, \alpha_2)$ can be evaluated using the well-known differential geometry principles. In particular, the principal radii of curvature R_1, R_2 along α_1 and α_2, respectively, are calculated as follows:

$$R_i(\alpha_1, \alpha_2) = -\frac{\mathbf{r}_{,i} \cdot \mathbf{r}_{,i}}{\mathbf{r}_{,ii} \cdot \mathbf{n}} \quad i = 1, 2 \tag{4}$$

where $\mathbf{r}_{,ij} = \partial^2 \mathbf{r} / (\partial \alpha_i \partial \alpha_j)$ with $i, j = 1, 2$ denotes the second order derivative of $\mathbf{r}(\alpha_1, \alpha_2)$ with respect to $\alpha_i, \alpha_j = \alpha_1, \alpha_2$. Furthermore, Eqn. (4) allows one to define the principal curvature $k_{ni} = 1 / R_i$ along the directions $\alpha_i = \alpha_1, \alpha_2$. In this way, the scaling parameters $H_i = H_1, H_2$, associated with each principal direction of the shell, can thus be introduced for each point of the doubly-curved shell solid. They are computed as $H_i(\alpha_1, \alpha_2, \zeta) = 1 + \zeta / R_i$ with $i = 1, 2$, where ζ is the thickness coordinate of the shell. Note that for the sampling points located on the reference surface, it leads to $H_i = 1$.

The length s_i of an arbitrary curve along $\alpha_i = \alpha_1, \alpha_2$ principal direction can be evaluated from the differential relation reported below which allows one to compute the infinitesimal arch length $ds_i = ds_1, ds_2$ [45]:

$$ds_i = A_i d\alpha_i \quad i = 1, 2 \tag{5}$$

Note that $s_i \in [0, L_i]$, where L_i is the total length of the parametric line along $\alpha_i = \alpha_1, \alpha_2$. Furthermore, $A_i = A_1, A_2$ denotes the Lamè parameter of the reference surface for the $\alpha_i = \alpha_1, \alpha_2$ principal direction. These parameters are evaluated in each point of the physical domain according to the following relation:

$$A_i(\alpha_1, \alpha_2) = \sqrt{\mathbf{r}_{,i} \cdot \mathbf{r}_{,i}} \quad i = 1, 2 \tag{6}$$

Finally, a general equation is provided for the evaluation of the total shell thickness in each point of the physical domain. Recalling that each k-th lamina of the stacking sequence with $k = 1, \ldots, l$ is located between its top and bottom surfaces, associated to the thickness coordinate value ζ_k and ζ_{k+1}, respectively, the total thickness $h(\alpha_1, \alpha_2)$ of an arbitrary doubly-curved shell solid can be calculated as [45]:

$$h(\alpha_1, \alpha_2) = \sum_{k=1}^{l} h_k(\alpha_1, \alpha_2) = \sum_{k=1}^{l} (\zeta_{k+1} - \zeta_k) \tag{7}$$

In the previous equation, h_k denotes the thickness of the k-th layer of the lamination scheme.

3. Configuration variables and definition equations

The present section deals with the assessment of a generalized higher order ESL model for a multifield problem in a laminated doubly-curved shell structure. More specifically, the vector $\mathbf{\Delta}^{(k)}(\alpha_1, \alpha_2, \zeta)$ is introduced in each point of an arbitrary k-th layer of a three-dimensional solid, collecting the configuration variables of the problem under consideration [45]:

$$\mathbf{\Delta}^{(k)}(\alpha_1, \alpha_2, \zeta) = \begin{bmatrix} U_1^{(k)} & U_2^{(k)} & U_3^{(k)} & \Delta\phi^{(k)} & \Delta\psi^{(k)} & \Delta\mathrm{T}^{(k)} & \Delta\mathrm{C}^{(k)} \end{bmatrix}^T \tag{8}$$

More specifically, $U_1^{(k)}, U_2^{(k)}$ and $U_3^{(k)}$ represent the three-dimensional displacement field components along $\alpha_1, \alpha_2, \zeta$, while $\Delta\phi^{(k)} = \phi^{(k)} - \phi_0$ and $\Delta\psi^{(k)} = \psi^{(k)} - \psi_0$ denote the variation of the electrostatic and magnetostatic potential, respectively, with respect to the reference values ϕ_0 and ψ_0 associated with the natural state of the system. Finally, $\Delta\mathrm{T}^{(k)} = \mathrm{T}^{(k)} - \mathrm{T}_0$ and $\Delta\mathrm{C}^{(k)} = \mathrm{C}^{(k)} - \mathrm{C}_0$ are the temperature and mass concentration gradients associated with the reference values T_0 and C_0. It should be noted that the quantities introduced in Eqn. (9) are expressed in accordance to the International Standards (SI). Therefore, the displacement field variables are in meters [m], whereas the units of magnetic and electric potential are Ampere [A] and Volt [V], respectively. On the other hand, the mass concentration problem involves the effects of the moisture concentration $\mathrm{C}^{(k)}$, expressed in $[\mathrm{kg}/\mathrm{m}^3]$, whereas $\mathrm{T}^{(k)}$ refers to the absolute temperature expressed in Kelvin [K]. Following the ESL approach, the vector $\mathbf{\Delta}^{(k)}$ of the three-dimensional configuration variables of Eqn. (9) is expanded up to the $(N+1)$-th order as follows:

$$\boldsymbol{\Delta}^{(k)} = \sum_{\tau=0}^{N+1} \mathbf{F}_{\tau}^{(k)} \boldsymbol{\delta}^{(\tau)} \quad \Leftrightarrow \quad \begin{bmatrix} U_1^{(k)} \\ U_2^{(k)} \\ U_3^{(k)} \\ \Delta\phi^{(k)} \\ \Delta\psi^{(k)} \\ \Delta \mathrm{T}^{(k)} \\ \Delta \mathrm{C}^{(k)} \end{bmatrix} = \sum_{\tau=0}^{N+1} \begin{bmatrix} F_{\tau}^{(k)\alpha_1} & 0 & 0 & 0 & 0 & 0 & 0 \\ 0 & F_{\tau}^{(k)\alpha_2} & 0 & 0 & 0 & 0 & 0 \\ 0 & 0 & F_{\tau}^{(k)\alpha_3} & 0 & 0 & 0 & 0 \\ 0 & 0 & 0 & F_{\tau}^{(k)\alpha_4} & 0 & 0 & 0 \\ 0 & 0 & 0 & 0 & F_{\tau}^{(k)\alpha_5} & 0 & 0 \\ 0 & 0 & 0 & 0 & 0 & F_{\tau}^{(k)\alpha_6} & 0 \\ 0 & 0 & 0 & 0 & 0 & 0 & F_{\tau}^{(k)\alpha_7} \end{bmatrix} \begin{bmatrix} u_1^{(\tau)} \\ u_2^{(\tau)} \\ u_3^{(\tau)} \\ \phi^{(\tau)} \\ \psi^{(\tau)} \\ \xi^{(\tau)} \\ \kappa^{(\tau)} \end{bmatrix} \tag{9}$$

Further details regarding the generalized ESL description of the unknown field variables can be found in Ref. [45]. In the previous equation, a generalized set of thickness functions denoted by $F_{\tau}^{(k)\alpha_i} = F_{\tau}^{(k)\alpha_i}(\alpha_1, \alpha_2)$ with $i = 1, ..., 7$ are introduced, which are collected in the matrix $\mathbf{F}_{\tau}^{(k)}$, defined for each $\tau = 0, ..., N+1$. In this way, the vector $\boldsymbol{\Delta}^{(k)}$, defined in each point within the three-dimensional shell solid, is expressed in terms of the vector $\boldsymbol{\delta}^{(\tau)}(\alpha_1, \alpha_2)$ containing the generalized configuration variables. It is worth noting that Eqn. (10) provides a generalized expression of the unknown field variables up to an arbitrary order. The selection of a particular expression of $F_{\tau}^{(k)\alpha_i}$ allows one to obtain several multifield formulations for shell structures that are available in literature, including well-established classical theories like CPT, FSDT and TSDT. Furthermore, by considering higher order polynomials for the kinematic expansion, refined models can be developed to predict the stretching effects within each lamina. On the other hand, Eqn. (10) can be employed to model the zigzag multifield effects that occur at the interface between two different adjacent by assigning different slopes to the profile of each configuration variable. In this study the following expressions of the thickness functions are adopted for $\tau = 0, ..., N+1$, setting $i = 1, ..., 7$:

$$F_{\tau}^{(k)\alpha_i} = \begin{cases} \dfrac{1-z}{2} & \text{for } \tau = 0 \\ z^{\tau+1} - z^{\tau-1} & \text{for } \tau = 1, .., N-1 \\ \dfrac{1+z}{2} & \text{for } \tau = N \end{cases} \tag{10}$$

The quantity $z = 2\zeta/h$, employed in Eqn. (11), allows one to express the thickness functions with $\tau = 0, ..., N$ in terms of the thickness coordinate ζ. On the other hand, the thickness function associated with $\tau = N+1$ accounts for the previously discussed zigzag effects. The following relation is adopted, setting $i = 1, ..., 7$:

$$F_{N+1}^{(k)\alpha_i} = \begin{cases} (-1)^k \widehat{z}_k = -\dfrac{\zeta - \zeta_1}{\zeta_2 - \zeta_1} & \text{for } k = 1 \\ (-1)^k z_k = (-1)^k \left(\dfrac{2}{\zeta_{k+1} - \zeta_k} \zeta - \dfrac{\zeta_{k+1} + \zeta_k}{\zeta_{k+1} - \zeta_k} \right) & \text{for } k = 2, ..., l-1 \\ (-1)^k \breve{z}_k = (-1)^l \dfrac{\zeta - \zeta_{l+1}}{\zeta_{l+1} - \zeta_l} & \text{for } k = l \end{cases} \tag{11}$$

where l is the total number of laminae in the stacking sequence. Note that if the thickness functions set (11) is adopted, the arbitrary element $\delta_i^{(\tau)}$ of the generalized vector $\boldsymbol{\delta}^{(\tau)}$ associated with $\tau = 0$ and $\tau = N+1$ is equal to the values assumed by the elements of the vector $\boldsymbol{\Delta}^{(k)}$ at the top and bottom surfaces of the doubly-curved laminated shell, respectively [45]:

$$\begin{aligned} \Delta_i^{(1)} \left(\alpha_1, \alpha_2, \zeta = -\frac{h}{2} \right) &= \delta_i^{(0)}(\alpha_1, \alpha_2) \\ \Delta_i^{(l)} \left(\alpha_1, \alpha_2, \zeta = \frac{h}{2} \right) &= \delta_i^{(N)}(\alpha_1, \alpha_2) \end{aligned} \tag{12}$$

At this point, the following nomenclature adopted to identify the axiomatic assumptions in Eqn. (10):

$$\begin{aligned} &\mathrm{ELD} - N \\ &\mathrm{ELDZL} - N \end{aligned} \tag{13}$$

More specifically, "EL" indicates that the ELW approach is adopted for describing the unknown variables, whereas "D" means that the fundamental equations are derived in terms of the configuration variables, and N denotes the maximum kinematic expansion order. Finally, the letter "ZL" is used when the model includes zigzag effects, following Eqn. (12).

At this point, the multifield definition equations are written, taking into account the higher order kinematic assumptions of Eqn. (10). To this end, the vectors $\boldsymbol{\varepsilon}^{(k)}, \mathbf{E}^{(k)}, \mathbf{H}^{(k)}, \widehat{\Delta \mathrm{T}}^{(k)}, \widehat{\Delta \mathrm{C}}^{(k)}, \boldsymbol{\theta}^{(k)}, \boldsymbol{\lambda}^{(k)}$ of the three-dimensional primary variables of the mechanical, electrostatic, magnetostatic, thermal and hygrometric problem are introduced at each point within an arbitrary k-th layer:

$$\begin{aligned} \boldsymbol{\varepsilon}^{(k)} &= \left[\varepsilon_1^{(k)} \;\; \varepsilon_2^{(k)} \;\; \gamma_{12}^{(k)} \;\; \gamma_{13}^{(k)} \;\; \gamma_{23}^{(k)} \;\; \varepsilon_3^{(k)} \right]^T \\ \mathbf{E}^{(k)} &= \left[E_1^{(k)} \;\; E_2^{(k)} \;\; E_3^{(k)} \right]^T, \quad \mathbf{H}^{(k)} = \left[H_1^{(k)} \;\; H_2^{(k)} \;\; H_3^{(k)} \right]^T \\ \widehat{\Delta \mathrm{T}}^{(k)} &= \widehat{\Delta \mathrm{T}}^{(k)}, \quad \widehat{\Delta \mathrm{C}}^{(k)} = \widehat{\Delta \mathrm{C}}^{(k)} \\ \boldsymbol{\theta}^{(k)} &= \left[\theta_1^{(k)} \;\; \theta_2^{(k)} \;\; \theta_3^{(k)} \right]^T, \quad \boldsymbol{\lambda}^{(k)} = \left[\lambda_1^{(k)} \;\; \lambda_2^{(k)} \;\; \lambda_3^{(k)} \right]^T \end{aligned} \tag{14}$$

The three-dimensional definition equations of the multifield problem can be expressed in a compact matrix notation as follows, where $\boldsymbol{\pi}^{(k)}$ represents the vector of the primary variables and $\mathbf{D}$ is a differential operator [45]:

$$\boldsymbol{\pi}^{(k)} = \mathbf{D}\boldsymbol{\Delta}^{(k)} = \mathbf{D}_{\zeta}\mathbf{D}_{\Omega}\boldsymbol{\Delta}^{(k)} \tag{15}$$

More specifically, the matrix $\mathbf{D}_{\zeta}$, which accounts for all the terms depending on the thickness coordinate ζ and its derivatives, has the following form:

$$\mathbf{D}_\zeta = \begin{bmatrix} \mathbf{D}_{\zeta(1)} & \mathbf{0} & \mathbf{0} & \mathbf{0} & \mathbf{0} & \mathbf{0} & \mathbf{0} \\ \mathbf{0} & \mathbf{D}_{\zeta(2)} & \mathbf{0} & \mathbf{0} & \mathbf{0} & \mathbf{0} & \mathbf{0} \\ \mathbf{0} & \mathbf{0} & \mathbf{D}_{\zeta(2)} & \mathbf{0} & \mathbf{0} & \mathbf{0} & \mathbf{0} \\ \mathbf{0} & \mathbf{0} & \mathbf{0} & \mathbf{D}_{\zeta(3)} & \mathbf{0} & \mathbf{0} & \mathbf{0} \\ \mathbf{0} & \mathbf{0} & \mathbf{0} & \mathbf{0} & \mathbf{D}_{\zeta(3)} & \mathbf{0} & \mathbf{0} \\ \mathbf{0} & \mathbf{0} & \mathbf{0} & \mathbf{0} & \mathbf{0} & \mathbf{D}_{\zeta(2)} & \mathbf{0} \\ \mathbf{0} & \mathbf{0} & \mathbf{0} & \mathbf{0} & \mathbf{0} & \mathbf{0} & \mathbf{D}_{\zeta(2)} \end{bmatrix} \tag{16}$$

The sub-operators $\mathbf{D}_{\zeta(1)}, \mathbf{D}_{\zeta(2)}$ and $\mathbf{D}_{\zeta(3)}$ introduced in the previous equation are defined as follows:

$$\mathbf{D}_{\zeta(1)} = \begin{bmatrix} \frac{1}{H_1} & 0 & 0 & 0 & 0 & 0 & 0 & 0 & 0 \\ 0 & \frac{1}{H_2} & 0 & 0 & 0 & 0 & 0 & 0 & 0 \\ 0 & 0 & \frac{1}{H_1} & \frac{1}{H_2} & 0 & 0 & 0 & 0 & 0 \\ 0 & 0 & 0 & 0 & \frac{1}{H_1} & 0 & \frac{\partial}{\partial \zeta} & 0 & 0 \\ 0 & 0 & 0 & 0 & 0 & \frac{1}{H_2} & 0 & \frac{\partial}{\partial \zeta} & 0 \\ 0 & 0 & 0 & 0 & 0 & 0 & 0 & 0 & \frac{\partial}{\partial \zeta} \end{bmatrix}, \quad \mathbf{D}_{\zeta(2)} = \begin{bmatrix} \frac{1}{H_1} & 0 & 0 \\ 0 & \frac{1}{H_2} & 0 \\ 0 & 0 & \frac{\partial}{\partial \zeta} \end{bmatrix}, \quad \mathbf{D}_{\zeta(3)} = 1 \tag{17}$$

On the other hand, the differential operator $\mathbf{D}_\Omega$, which contains the partial derivatives with respect to the principal coordinates α_1, α_2, is defined as:

$$\mathbf{D}_\Omega = \begin{bmatrix} \mathbf{D}_{\Omega(1)} & \mathbf{0} & \mathbf{0} & \mathbf{0} & \mathbf{0} \\ \mathbf{0} & \mathbf{D}_{\Omega(2)} & \mathbf{0} & \mathbf{0} & \mathbf{0} \\ \mathbf{0} & \mathbf{0} & \mathbf{D}_{\Omega(2)} & \mathbf{0} & \mathbf{0} \\ \mathbf{0} & \mathbf{0} & \mathbf{0} & \mathbf{D}_{\Omega(3)} & \mathbf{0} \\ \mathbf{0} & \mathbf{0} & \mathbf{0} & \mathbf{0} & \mathbf{D}_{\Omega(3)} \\ \mathbf{0} & \mathbf{0} & \mathbf{0} & \mathbf{D}_{\Omega(2)} & \mathbf{0} \\ \mathbf{0} & \mathbf{0} & \mathbf{0} & \mathbf{0} & \mathbf{D}_{\Omega(2)} \end{bmatrix} \tag{18}$$

The matrices $\mathbf{D}_{\Omega(1)}, \mathbf{D}_{\Omega(2)}$ and $\mathbf{D}_{\Omega(3)}$ introduced in the previous equation take the following aspect:

$$\begin{gathered} \mathbf{D}_{\Omega(1)} = \begin{bmatrix} \overline{\mathbf{D}}_\Omega^{\alpha_1} & \overline{\mathbf{D}}_\Omega^{\alpha_2} & \overline{\mathbf{D}}_\Omega^{\alpha_3} \end{bmatrix} \\ \mathbf{D}_{\Omega(2)} = \begin{bmatrix} -\frac{1}{A_1}\frac{\partial}{\partial \alpha_1} & -\frac{1}{A_2}\frac{\partial}{\partial \alpha_2} & -1 \end{bmatrix}^T \\ \mathbf{D}_{\Omega(3)} = 1 \end{gathered} \tag{19}$$

The quantities $\overline{\mathbf{D}}_\Omega^{\alpha_1}, \overline{\mathbf{D}}_\Omega^{\alpha_2}, \overline{\mathbf{D}}_\Omega^{\alpha_3}$ are defined as:

$$\begin{aligned} \overline{\mathbf{D}}_\Omega^{\alpha_1} &= \begin{bmatrix} \frac{1}{A_1}\frac{\partial}{\partial \alpha_1} & \frac{1}{A_1 A_2}\frac{\partial A_2}{\partial \alpha_1} & -\frac{1}{A_1 A_2}\frac{\partial A_1}{\partial \alpha_2} & \frac{1}{A_2}\frac{\partial}{\partial \alpha_2} & -\frac{1}{R_1} & 0 & 1 & 0 & 0 \end{bmatrix}^T \\ \overline{\mathbf{D}}_\Omega^{\alpha_2} &= \begin{bmatrix} \frac{1}{A_1 A_2}\frac{\partial A_1}{\partial \alpha_2} & \frac{1}{A_2}\frac{\partial}{\partial \alpha_2} & \frac{1}{A_1}\frac{\partial}{\partial \alpha_1} & -\frac{1}{A_1 A_2}\frac{\partial A_2}{\partial \alpha_1} & 0 & -\frac{1}{R_2} & 0 & 1 & 0 \end{bmatrix}^T \\ \overline{\mathbf{D}}_\Omega^{\alpha_3} &= \begin{bmatrix} \frac{1}{R_1} & \frac{1}{R_2} & 0 & 0 & \frac{1}{A_1}\frac{\partial}{\partial \alpha_1} & \frac{1}{A_2}\frac{\partial}{\partial \alpha_2} & 0 & 0 & 1 \end{bmatrix}^T \end{aligned} \tag{20}$$

It is useful to express the differential operator $\mathbf{D}_\Omega$ as the sum of the matrices $\mathbf{D}_\Omega^{\alpha_i}$ with $i = 1,...,7$, as shown below [45]:

$$\mathbf{D}_\Omega = \sum_{i=1}^{7} \mathbf{D}_\Omega^{\alpha_i} \tag{21}$$

The quantities $\mathbf{D}_\Omega^{\alpha_i}$ in Eqn. (22) are defined as follows:

$$\mathbf{D}_\Omega^{\alpha_1} = \begin{bmatrix} \overline{\mathbf{D}}_\Omega^{\alpha_1} & \mathbf{0} & \mathbf{0} & \mathbf{0} & \mathbf{0} & \mathbf{0} & \mathbf{0} \\ \mathbf{0} & \mathbf{0} & \mathbf{0} & \mathbf{0} & \mathbf{0} & \mathbf{0} & \mathbf{0} \\ \mathbf{0} & \mathbf{0} & \mathbf{0} & \mathbf{0} & \mathbf{0} & \mathbf{0} & \mathbf{0} \\ \mathbf{0} & \mathbf{0} & \mathbf{0} & \mathbf{0} & \mathbf{0} & \mathbf{0} & \mathbf{0} \\ \mathbf{0} & \mathbf{0} & \mathbf{0} & \mathbf{0} & \mathbf{0} & \mathbf{0} & \mathbf{0} \\ \mathbf{0} & \mathbf{0} & \mathbf{0} & \mathbf{0} & \mathbf{0} & \mathbf{0} & \mathbf{0} \\ \mathbf{0} & \mathbf{0} & \mathbf{0} & \mathbf{0} & \mathbf{0} & \mathbf{0} & \mathbf{0} \end{bmatrix}, \quad \mathbf{D}_\Omega^{\alpha_2} = \begin{bmatrix} \mathbf{0} & \overline{\mathbf{D}}_\Omega^{\alpha_2} & \mathbf{0} & \mathbf{0} & \mathbf{0} & \mathbf{0} & \mathbf{0} \\ \mathbf{0} & \mathbf{0} & \mathbf{0} & \mathbf{0} & \mathbf{0} & \mathbf{0} & \mathbf{0} \\ \mathbf{0} & \mathbf{0} & \mathbf{0} & \mathbf{0} & \mathbf{0} & \mathbf{0} & \mathbf{0} \\ \mathbf{0} & \mathbf{0} & \mathbf{0} & \mathbf{0} & \mathbf{0} & \mathbf{0} & \mathbf{0} \\ \mathbf{0} & \mathbf{0} & \mathbf{0} & \mathbf{0} & \mathbf{0} & \mathbf{0} & \mathbf{0} \\ \mathbf{0} & \mathbf{0} & \mathbf{0} & \mathbf{0} & \mathbf{0} & \mathbf{0} & \mathbf{0} \\ \mathbf{0} & \mathbf{0} & \mathbf{0} & \mathbf{0} & \mathbf{0} & \mathbf{0} & \mathbf{0} \end{bmatrix}, \quad \mathbf{D}_\Omega^{\alpha_3} = \begin{bmatrix} \mathbf{0} & \mathbf{0} & \overline{\mathbf{D}}_\Omega^{\alpha_3} & \mathbf{0} & \mathbf{0} & \mathbf{0} & \mathbf{0} \\ \mathbf{0} & \mathbf{0} & \mathbf{0} & \mathbf{0} & \mathbf{0} & \mathbf{0} & \mathbf{0} \\ \mathbf{0} & \mathbf{0} & \mathbf{0} & \mathbf{0} & \mathbf{0} & \mathbf{0} & \mathbf{0} \\ \mathbf{0} & \mathbf{0} & \mathbf{0} & \mathbf{0} & \mathbf{0} & \mathbf{0} & \mathbf{0} \\ \mathbf{0} & \mathbf{0} & \mathbf{0} & \mathbf{0} & \mathbf{0} & \mathbf{0} & \mathbf{0} \\ \mathbf{0} & \mathbf{0} & \mathbf{0} & \mathbf{0} & \mathbf{0} & \mathbf{0} & \mathbf{0} \\ \mathbf{0} & \mathbf{0} & \mathbf{0} & \mathbf{0} & \mathbf{0} & \mathbf{0} & \mathbf{0} \end{bmatrix},$$

$$\mathbf{D}_\Omega^{\alpha_4} = \begin{bmatrix} \mathbf{0} & \mathbf{0} & \mathbf{0} & \mathbf{0} & \mathbf{0} & \mathbf{0} & \mathbf{0} \\ \mathbf{0} & \mathbf{0} & \mathbf{0} & \overline{\mathbf{D}}_\Omega^{\alpha_4} & \mathbf{0} & \mathbf{0} & \mathbf{0} \\ \mathbf{0} & \mathbf{0} & \mathbf{0} & \mathbf{0} & \mathbf{0} & \mathbf{0} & \mathbf{0} \\ \mathbf{0} & \mathbf{0} & \mathbf{0} & \mathbf{0} & \mathbf{0} & \mathbf{0} & \mathbf{0} \\ \mathbf{0} & \mathbf{0} & \mathbf{0} & \mathbf{0} & \mathbf{0} & \mathbf{0} & \mathbf{0} \\ \mathbf{0} & \mathbf{0} & \mathbf{0} & \mathbf{0} & \mathbf{0} & \mathbf{0} & \mathbf{0} \\ \mathbf{0} & \mathbf{0} & \mathbf{0} & \mathbf{0} & \mathbf{0} & \mathbf{0} & \mathbf{0} \end{bmatrix}, \quad \mathbf{D}_\Omega^{\alpha_5} = \begin{bmatrix} \mathbf{0} & \mathbf{0} & \mathbf{0} & \mathbf{0} & \mathbf{0} & \mathbf{0} & \mathbf{0} \\ \mathbf{0} & \mathbf{0} & \mathbf{0} & \mathbf{0} & \mathbf{0} & \mathbf{0} & \mathbf{0} \\ \mathbf{0} & \mathbf{0} & \mathbf{0} & \mathbf{0} & \overline{\mathbf{D}}_\Omega^{\alpha_5} & \mathbf{0} & \mathbf{0} \\ \mathbf{0} & \mathbf{0} & \mathbf{0} & \mathbf{0} & \mathbf{0} & \mathbf{0} & \mathbf{0} \\ \mathbf{0} & \mathbf{0} & \mathbf{0} & \mathbf{0} & \mathbf{0} & \mathbf{0} & \mathbf{0} \\ \mathbf{0} & \mathbf{0} & \mathbf{0} & \mathbf{0} & \mathbf{0} & \mathbf{0} & \mathbf{0} \\ \mathbf{0} & \mathbf{0} & \mathbf{0} & \mathbf{0} & \mathbf{0} & \mathbf{0} & \mathbf{0} \end{bmatrix},$$

$$\mathbf{D}_\Omega^{\alpha_6} = \begin{bmatrix} \mathbf{0} & \mathbf{0} & \mathbf{0} & \mathbf{0} & \mathbf{0} & \mathbf{0} & \mathbf{0} \\ \mathbf{0} & \mathbf{0} & \mathbf{0} & \mathbf{0} & \mathbf{0} & \mathbf{0} & \mathbf{0} \\ \mathbf{0} & \mathbf{0} & \mathbf{0} & \mathbf{0} & \mathbf{0} & \mathbf{0} & \mathbf{0} \\ \mathbf{0} & \mathbf{0} & \mathbf{0} & \mathbf{0} & \mathbf{0} & \overline{\mathbf{D}}_\Omega^{\alpha_6} & \mathbf{0} \\ \mathbf{0} & \mathbf{0} & \mathbf{0} & \mathbf{0} & \mathbf{0} & \mathbf{0} & \mathbf{0} \\ \mathbf{0} & \mathbf{0} & \mathbf{0} & \mathbf{0} & \mathbf{0} & \widetilde{\mathbf{D}}_\Omega^{\alpha_6} & \mathbf{0} \\ \mathbf{0} & \mathbf{0} & \mathbf{0} & \mathbf{0} & \mathbf{0} & \mathbf{0} & \mathbf{0} \end{bmatrix}, \quad \mathbf{D}_\Omega^{\alpha_7} = \begin{bmatrix} \mathbf{0} & \mathbf{0} & \mathbf{0} & \mathbf{0} & \mathbf{0} & \mathbf{0} & \mathbf{0} \\ \mathbf{0} & \mathbf{0} & \mathbf{0} & \mathbf{0} & \mathbf{0} & \mathbf{0} & \mathbf{0} \\ \mathbf{0} & \mathbf{0} & \mathbf{0} & \mathbf{0} & \mathbf{0} & \mathbf{0} & \mathbf{0} \\ \mathbf{0} & \mathbf{0} & \mathbf{0} & \mathbf{0} & \mathbf{0} & \mathbf{0} & \mathbf{0} \\ \mathbf{0} & \mathbf{0} & \mathbf{0} & \mathbf{0} & \mathbf{0} & \mathbf{0} & \overline{\mathbf{D}}_\Omega^{\alpha_7} \\ \mathbf{0} & \mathbf{0} & \mathbf{0} & \mathbf{0} & \mathbf{0} & \mathbf{0} & \mathbf{0} \\ \mathbf{0} & \mathbf{0} & \mathbf{0} & \mathbf{0} & \mathbf{0} & \mathbf{0} & \widetilde{\mathbf{D}}_\Omega^{\alpha_7} \end{bmatrix} \tag{22}$$

where $\overline{\mathbf{D}}_{\Omega(2)}^{\alpha_4} = \overline{\mathbf{D}}_{\Omega(2)}^{\alpha_5} = \overline{\mathbf{D}}_{\Omega(2)}^{\alpha_6} = \overline{\mathbf{D}}_{\Omega(2)}^{\alpha_7} = \mathbf{D}_{\Omega(2)}$ and $\widetilde{\mathbf{D}}_{\Omega(3)}^{\alpha_6} = \widetilde{\mathbf{D}}_{\Omega(3)}^{\alpha_7} = \mathbf{D}_{\Omega(3)}$. Introducing the generalized kinematic model of Eqn. (10) in the three-dimensional definition (16), one gets [45]:

$$\boldsymbol{\pi}^{(k)} = \mathbf{D}\boldsymbol{\Delta}^{(k)} = \mathbf{D}_\zeta \mathbf{D}_\Omega \boldsymbol{\Delta}^{(k)} = \mathbf{D}_\zeta \sum_{i=1}^{7} \mathbf{D}_\Omega^{\alpha_i} \boldsymbol{\Delta}^{(k)} =$$
$$= \sum_{\tau=0}^{N+1} \sum_{i=1}^{7} \mathbf{D}_\zeta \mathbf{D}_\Omega^{\alpha_i} \mathbf{F}_\tau^{(k)} \boldsymbol{\delta}^{(\tau)} = \sum_{\tau=0}^{N+1} \sum_{i=1}^{7} \mathbf{D}_\zeta F_\tau^{(k)\alpha_i} \mathbf{D}_\Omega^{\alpha_i} \boldsymbol{\delta}^{(\tau)} = \sum_{\tau=0}^{N+1} \sum_{i=1}^{7} \mathbf{Z}^{(k\tau)\alpha_i} \mathbf{D}_\Omega^{\alpha_i} \boldsymbol{\delta}^{(\tau)} = \sum_{\tau=0}^{N+1} \sum_{i=1}^{7} \mathbf{Z}^{(k\tau)\alpha_i} \boldsymbol{\pi}^{(\tau)\alpha_i} \tag{23}$$

As can be seen, the vector $\boldsymbol{\pi}^{(k)}$ of the three-dimensional primary variables is expanded using a generalized kinematic model in terms of the generalized vector $\boldsymbol{\pi}^{(\tau)\alpha_i}$, defined for each $\tau = 0, ..., N+1$ and $i = 1, ..., 7$. In particular, $\boldsymbol{\pi}^{(\tau)\alpha_i}$ includes the algebraic vectors $\boldsymbol{\varepsilon}^{(\tau)\alpha_i}$, $\mathbf{E}^{(\tau)\alpha_i}$, $\mathbf{H}^{(\tau)\alpha_i}$, $\widehat{\Delta \mathrm{T}}^{(\tau)\alpha_i}$, $\widehat{\Delta \mathrm{C}}^{(\tau)\alpha_i}$, $\boldsymbol{\theta}^{(\tau)\alpha_i}$ and $\boldsymbol{\lambda}^{(\tau)\alpha_i}$, which contain the generalized strain characteristics of the mechanical, electrostatic, magnetostatic, thermal and hygrometric problem [45]:

$$\boldsymbol{\varepsilon}^{(\tau)\alpha_i}(\alpha_1,\alpha_2,t) = \left[\varepsilon_1^{(\tau)\alpha_i}\ \varepsilon_2^{(\tau)\alpha_i}\ \gamma_1^{(\tau)\alpha_i}\ \gamma_2^{(\tau)\alpha_i}\ \gamma_{13}^{(\tau)\alpha_i}\ \gamma_{23}^{(\tau)\alpha_i}\ \omega_{13}^{(\tau)\alpha_i}\ \omega_{23}^{(\tau)\alpha_i}\ \varepsilon_3^{(\tau)\alpha_i}\right]^T$$
$$\mathbf{E}^{(\tau)\alpha_i}(\alpha_1,\alpha_2,t) = \left[E_1^{(\tau)\alpha_i}\ E_2^{(\tau)\alpha_i}\ E_3^{(\tau)\alpha_i}\right]^T,\ \mathbf{H}^{(\tau)\alpha_i}(\alpha_1,\alpha_2,t) = \left[H_1^{(\tau)\alpha_i}\ H_2^{(\tau)\alpha_i}\ H_3^{(\tau)\alpha_i}\right]^T$$
$$\widehat{\Delta \mathrm{T}}^{(\tau)\alpha_i}(\alpha_1,\alpha_2,t) = \widehat{\Delta \mathrm{T}}^{(\tau)\alpha_i},\ \widehat{\Delta \mathrm{C}}^{(\tau)\alpha_i}(\alpha_1,\alpha_2,t) = \widehat{\Delta \mathrm{C}}^{(\tau)\alpha_i}$$
$$\boldsymbol{\theta}^{(\tau)\alpha_i}(\alpha_1,\alpha_2,t) = \left[\theta_1^{(\tau)\alpha_i}\ \theta_2^{(\tau)\alpha_i}\ \theta_3^{(\tau)\alpha_i}\right]^T,\ \boldsymbol{\lambda}^{(\tau)\alpha_i}(\alpha_1,\alpha_2,t) = \left[\lambda_1^{(\tau)\alpha_i}\ \lambda_2^{(\tau)\alpha_i}\ \lambda_3^{(\tau)\alpha_i}\right]^T \tag{24}$$

Eqn. (24) can be expressed more conveniently in the following compact form:

where the matrices $\mathbf{Z}_1^{(k\tau)\alpha_i}, \mathbf{Z}_2^{(k\tau)\alpha_i}$ and $\mathbf{Z}_3^{(k\tau)\alpha_i}$ assume the following aspect for each $k = 1, ..., l$, setting $m = 1, 2, 3$:

$$\mathbf{Z}_m^{(k\tau)\alpha_i} = \mathbf{D}_{\zeta(m)} F_\tau^{(k)\alpha_i} \tag{26}$$

4. Constitutive equations

An arbitrary k-th layer of the solid is modelled using a three-dimensional linear elastic constitutive relationship valid for generally anisotropic materials. With reference to the geometric reference system of the shell $O'\alpha_1\alpha_2\zeta$, the following constitutive equation is considered, with $\overline{\boldsymbol{\Gamma}}^{(k)}$ representing the multifield stiffness matrix of the k-th layer [45]:

$$\boldsymbol{\pi}^{(k)} = \sum_{\tau=0}^{N+1} \sum_{i=1}^{7} \mathbf{Z}^{(k\tau)\alpha_i} \boldsymbol{\pi}^{(\tau)\alpha_i} \quad \Leftrightarrow \quad \begin{bmatrix} \boldsymbol{\varepsilon}^{(k)} \\ \mathbf{E}^{(k)} \\ \mathbf{H}^{(k)} \\ \widehat{\Delta \mathrm{T}}^{(k)} \\ \widehat{\Delta \mathrm{C}}^{(k)} \\ \boldsymbol{\theta}^{(k)} \\ \boldsymbol{\lambda}^{(k)} \end{bmatrix} = \sum_{\tau=0}^{N+1} \sum_{i=1}^{7} \begin{bmatrix} \mathbf{Z}_1^{(k\tau)\alpha_i} & \mathbf{0} & \mathbf{0} & \mathbf{0} & \mathbf{0} & \mathbf{0} & \mathbf{0} \\ \mathbf{0} & \mathbf{Z}_2^{(k\tau)\alpha_i} & \mathbf{0} & \mathbf{0} & \mathbf{0} & \mathbf{0} & \mathbf{0} \\ \mathbf{0} & \mathbf{0} & \mathbf{Z}_2^{(k\tau)\alpha_i} & \mathbf{0} & \mathbf{0} & \mathbf{0} & \mathbf{0} \\ \mathbf{0} & \mathbf{0} & \mathbf{0} & \mathbf{Z}_3^{(k\tau)\alpha_i} & \mathbf{0} & \mathbf{0} & \mathbf{0} \\ \mathbf{0} & \mathbf{0} & \mathbf{0} & \mathbf{0} & \mathbf{Z}_3^{(k\tau)\alpha_i} & \mathbf{0} & \mathbf{0} \\ \mathbf{0} & \mathbf{0} & \mathbf{0} & \mathbf{0} & \mathbf{0} & \mathbf{Z}_2^{(k\tau)\alpha_i} & \mathbf{0} \\ \mathbf{0} & \mathbf{0} & \mathbf{0} & \mathbf{0} & \mathbf{0} & \mathbf{0} & \mathbf{Z}_2^{(k\tau)\alpha_i} \end{bmatrix} \begin{bmatrix} \boldsymbol{\varepsilon}^{(\tau)\alpha_i} \\ \mathbf{E}^{(\tau)\alpha_i} \\ \mathbf{H}^{(\tau)\alpha_i} \\ \widehat{\Delta \mathrm{T}}^{(\tau)\alpha_i} \\ \widehat{\Delta \mathrm{C}}^{(\tau)\alpha_i} \\ \boldsymbol{\theta}^{(\tau)\alpha_i} \\ \boldsymbol{\lambda}^{(\tau)\alpha_i} \end{bmatrix} \tag{25}$$

$$\boldsymbol{\chi}^{(k)} = \overline{\boldsymbol{\Gamma}}^{(k)} \boldsymbol{\pi}^{(k)} \quad \Leftrightarrow \quad \begin{bmatrix} \boldsymbol{\sigma}^{(k)} \\ \mathbf{D}^{(k)} \\ \mathbf{B}^{(k)} \\ \eta^{(k)} \\ \mu^{(k)} \\ \mathbf{h}^{(k)} \\ \mathbf{c}^{(k)} \end{bmatrix} = \begin{bmatrix} \overline{\boldsymbol{\Gamma}}_{\mathrm{C}}^{(k)} & -\overline{\boldsymbol{\Gamma}}_{\mathrm{P}}^{(k)T} & -\overline{\boldsymbol{\Gamma}}_{\mathrm{Q}}^{(k)T} & -\overline{\boldsymbol{\Gamma}}_{\mathrm{z}}^{(k)T} & -\overline{\boldsymbol{\Gamma}}_{\mathrm{e}}^{(k)T} & \mathbf{0} & \mathbf{0} \\ \overline{\boldsymbol{\Gamma}}_{\mathrm{P}}^{(k)} & \overline{\boldsymbol{\Gamma}}_{\mathrm{L}}^{(k)} & \overline{\boldsymbol{\Gamma}}_{\mathrm{D}}^{(k)} & \overline{\boldsymbol{\Gamma}}_{\mathrm{o}}^{(k)T} & \overline{\boldsymbol{\Gamma}}_{\mathrm{g}}^{(k)T} & \mathbf{0} & \mathbf{0} \\ \overline{\boldsymbol{\Gamma}}_{\mathrm{Q}}^{(k)} & \overline{\boldsymbol{\Gamma}}_{\mathrm{D}}^{(k)} & \overline{\boldsymbol{\Gamma}}_{\mathrm{M}}^{(k)} & \overline{\boldsymbol{\Gamma}}_{\mathrm{w}}^{(k)T} & \overline{\boldsymbol{\Gamma}}_{\mathrm{f}}^{(k)T} & \mathbf{0} & \mathbf{0} \\ \overline{\boldsymbol{\Gamma}}_{\mathrm{z}}^{(k)} & \overline{\boldsymbol{\Gamma}}_{\mathrm{o}}^{(k)} & \overline{\boldsymbol{\Gamma}}_{\mathrm{w}}^{(k)} & \overline{\boldsymbol{\Gamma}}_{\mathrm{TT}}^{(k)} & \overline{\boldsymbol{\Gamma}}_{\mathrm{TC}}^{(k)} & \mathbf{0} & \mathbf{0} \\ \overline{\boldsymbol{\Gamma}}_{\mathrm{e}}^{(k)} & \overline{\boldsymbol{\Gamma}}_{\mathrm{g}}^{(k)} & \overline{\boldsymbol{\Gamma}}_{\mathrm{f}}^{(k)} & \overline{\boldsymbol{\Gamma}}_{\mathrm{TC}}^{(k)} & \overline{\boldsymbol{\Gamma}}_{\mathrm{CC}}^{(k)} & \mathbf{0} & \mathbf{0} \\ \mathbf{0} & \mathbf{0} & \mathbf{0} & \mathbf{0} & \mathbf{0} & \overline{\boldsymbol{\Gamma}}_{\mathrm{K}}^{(k)} & \overline{\boldsymbol{\Gamma}}_{\mathrm{Y}}^{(k)} \\ \mathbf{0} & \mathbf{0} & \mathbf{0} & \mathbf{0} & \mathbf{0} & \overline{\boldsymbol{\Gamma}}_{\mathrm{X}}^{(k)} & \overline{\boldsymbol{\Gamma}}_{\mathrm{S}}^{(k)} \end{bmatrix} \begin{bmatrix} \boldsymbol{\varepsilon}^{(k)} \\ \mathbf{E}^{(k)} \\ \mathbf{H}^{(k)} \\ \widehat{\Delta \mathrm{T}}^{(k)} \\ \widehat{\Delta \mathrm{C}}^{(k)} \\ \boldsymbol{\theta}^{(k)} \\ \boldsymbol{\lambda}^{(k)} \end{bmatrix} \tag{27}$$

As can be seen, $\overline{\mathbf{\Gamma}}_{\alpha}^{(k)}$ with $\alpha = \mathrm{C, L, M, TT, CC, K, S}$ is the constitutive matrix of each field, whereas $\overline{\mathbf{\Gamma}}_{\beta}^{(k)}$ with $\beta = \mathrm{P, Q, D, z, o, w, e, g, f, TC, X, Y}$ accounts for the coupling between the primary and secondary variables of the current multifield problem. On the other hand, the vector $\boldsymbol{\chi}^{(k)}$ contains the secondary variables of the present formulation. In a more expanded form, the three-dimensional constitutive Eqn. (28) can be expressed as follows [45]:

$$
\begin{bmatrix}
\sigma_1^{(k)} \\ \sigma_2^{(k)} \\ \tau_{12}^{(k)} \\ \tau_{13}^{(k)} \\ \tau_{23}^{(k)} \\ \sigma_3^{(k)} \\ \hline
D_1^{(k)} \\ D_2^{(k)} \\ D_3^{(k)} \\ \hline
B_1^{(k)} \\ B_2^{(k)} \\ B_3^{(k)} \\ \hline
\eta^{(k)} \\ \hline
\mu^{(k)} \\ \hline
h_1^{(k)} \\ h_2^{(k)} \\ h_3^{(k)} \\ \hline
c_1^{(k)} \\ c_2^{(k)} \\ c_3^{(k)}
\end{bmatrix}
=
\left[\begin{array}{cccccc|ccc|ccc|cc|cccccc}
\overline{C}_{11}^{(k)} & \overline{C}_{12}^{(k)} & \overline{C}_{16}^{(k)} & \overline{C}_{14}^{(k)} & \overline{C}_{15}^{(k)} & \overline{C}_{13}^{(k)} & -\overline{p}_{11}^{(k)} & -\overline{p}_{21}^{(k)} & -\overline{p}_{31}^{(k)} & -\overline{q}_{11}^{(k)} & -\overline{q}_{21}^{(k)} & -\overline{q}_{31}^{(k)} & -\overline{\tau}_{11}^{(k)} & -\overline{e}_{11}^{(k)} & 0 & 0 & 0 & 0 & 0 & 0 \\
\overline{C}_{12}^{(k)} & \overline{C}_{22}^{(k)} & \overline{C}_{26}^{(k)} & \overline{C}_{24}^{(k)} & \overline{C}_{25}^{(k)} & \overline{C}_{23}^{(k)} & -\overline{p}_{12}^{(k)} & -\overline{p}_{22}^{(k)} & -\overline{p}_{32}^{(k)} & -\overline{q}_{12}^{(k)} & -\overline{q}_{22}^{(k)} & -\overline{q}_{32}^{(k)} & -\overline{\tau}_{22}^{(k)} & -\overline{e}_{22}^{(k)} & 0 & 0 & 0 & 0 & 0 & 0 \\
\overline{C}_{16}^{(k)} & \overline{C}_{26}^{(k)} & \overline{C}_{66}^{(k)} & \overline{C}_{46}^{(k)} & \overline{C}_{56}^{(k)} & \overline{C}_{36}^{(k)} & -\overline{p}_{16}^{(k)} & -\overline{p}_{26}^{(k)} & -\overline{p}_{36}^{(k)} & -\overline{q}_{16}^{(k)} & -\overline{q}_{26}^{(k)} & -\overline{q}_{36}^{(k)} & -\overline{\tau}_{12}^{(k)} & -\overline{e}_{12}^{(k)} & 0 & 0 & 0 & 0 & 0 & 0 \\
\overline{C}_{14}^{(k)} & \overline{C}_{24}^{(k)} & \overline{C}_{46}^{(k)} & \overline{C}_{44}^{(k)} & \overline{C}_{45}^{(k)} & \overline{C}_{34}^{(k)} & -\overline{p}_{14}^{(k)} & -\overline{p}_{24}^{(k)} & -\overline{p}_{34}^{(k)} & -\overline{q}_{14}^{(k)} & -\overline{q}_{24}^{(k)} & -\overline{q}_{34}^{(k)} & -\overline{\tau}_{13}^{(k)} & -\overline{e}_{13}^{(k)} & 0 & 0 & 0 & 0 & 0 & 0 \\
\overline{C}_{15}^{(k)} & \overline{C}_{25}^{(k)} & \overline{C}_{56}^{(k)} & \overline{C}_{45}^{(k)} & \overline{C}_{55}^{(k)} & \overline{C}_{35}^{(k)} & -\overline{p}_{15}^{(k)} & -\overline{p}_{25}^{(k)} & -\overline{p}_{35}^{(k)} & -\overline{q}_{15}^{(k)} & -\overline{q}_{25}^{(k)} & -\overline{q}_{35}^{(k)} & -\overline{\tau}_{23}^{(k)} & -\overline{e}_{23}^{(k)} & 0 & 0 & 0 & 0 & 0 & 0 \\
\overline{C}_{13}^{(k)} & \overline{C}_{23}^{(k)} & \overline{C}_{36}^{(k)} & \overline{C}_{34}^{(k)} & \overline{C}_{35}^{(k)} & \overline{C}_{33}^{(k)} & -\overline{p}_{13}^{(k)} & -\overline{p}_{23}^{(k)} & -\overline{p}_{33}^{(k)} & -\overline{q}_{13}^{(k)} & -\overline{q}_{23}^{(k)} & -\overline{q}_{33}^{(k)} & -\overline{\tau}_{33}^{(k)} & -\overline{e}_{33}^{(k)} & 0 & 0 & 0 & 0 & 0 & 0 \\ \hline
\overline{p}_{11}^{(k)} & \overline{p}_{12}^{(k)} & \overline{p}_{16}^{(k)} & \overline{p}_{14}^{(k)} & \overline{p}_{15}^{(k)} & \overline{p}_{13}^{(k)} & \overline{l}_{11}^{(k)} & \overline{l}_{12}^{(k)} & \overline{l}_{13}^{(k)} & \overline{d}_{11}^{(k)} & \overline{d}_{12}^{(k)} & \overline{d}_{13}^{(k)} & \overline{\sigma}_{11}^{(k)} & \overline{g}_{11}^{(k)} & 0 & 0 & 0 & 0 & 0 & 0 \\
\overline{p}_{21}^{(k)} & \overline{p}_{22}^{(k)} & \overline{p}_{26}^{(k)} & \overline{p}_{24}^{(k)} & \overline{p}_{25}^{(k)} & \overline{p}_{23}^{(k)} & \overline{l}_{12}^{(k)} & \overline{l}_{22}^{(k)} & \overline{l}_{23}^{(k)} & \overline{d}_{12}^{(k)} & \overline{d}_{22}^{(k)} & \overline{d}_{23}^{(k)} & \overline{\sigma}_{22}^{(k)} & \overline{g}_{22}^{(k)} & 0 & 0 & 0 & 0 & 0 & 0 \\
\overline{p}_{31}^{(k)} & \overline{p}_{32}^{(k)} & \overline{p}_{36}^{(k)} & \overline{p}_{34}^{(k)} & \overline{p}_{35}^{(k)} & \overline{p}_{33}^{(k)} & \overline{l}_{13}^{(k)} & \overline{l}_{23}^{(k)} & \overline{l}_{33}^{(k)} & \overline{d}_{13}^{(k)} & \overline{d}_{23}^{(k)} & \overline{d}_{33}^{(k)} & \overline{\sigma}_{33}^{(k)} & \overline{g}_{33}^{(k)} & 0 & 0 & 0 & 0 & 0 & 0 \\ \hline
\overline{q}_{11}^{(k)} & \overline{q}_{12}^{(k)} & \overline{q}_{16}^{(k)} & \overline{q}_{14}^{(k)} & \overline{q}_{15}^{(k)} & \overline{q}_{13}^{(k)} & \overline{d}_{11}^{(k)} & \overline{d}_{12}^{(k)} & \overline{d}_{13}^{(k)} & \overline{m}_{11}^{(k)} & \overline{m}_{12}^{(k)} & \overline{m}_{13}^{(k)} & \overline{w}_{11}^{(k)} & \overline{f}_{11}^{(k)} & 0 & 0 & 0 & 0 & 0 & 0 \\
\overline{q}_{21}^{(k)} & \overline{q}_{22}^{(k)} & \overline{q}_{26}^{(k)} & \overline{q}_{24}^{(k)} & \overline{q}_{25}^{(k)} & \overline{q}_{23}^{(k)} & \overline{d}_{12}^{(k)} & \overline{d}_{22}^{(k)} & \overline{d}_{23}^{(k)} & \overline{m}_{12}^{(k)} & \overline{m}_{22}^{(k)} & \overline{m}_{23}^{(k)} & \overline{w}_{22}^{(k)} & \overline{f}_{22}^{(k)} & 0 & 0 & 0 & 0 & 0 & 0 \\
\overline{q}_{31}^{(k)} & \overline{q}_{32}^{(k)} & \overline{q}_{36}^{(k)} & \overline{q}_{34}^{(k)} & \overline{q}_{35}^{(k)} & \overline{q}_{33}^{(k)} & \overline{d}_{13}^{(k)} & \overline{d}_{23}^{(k)} & \overline{d}_{33}^{(k)} & \overline{m}_{13}^{(k)} & \overline{m}_{23}^{(k)} & \overline{m}_{33}^{(k)} & \overline{w}_{33}^{(k)} & \overline{f}_{33}^{(k)} & 0 & 0 & 0 & 0 & 0 & 0 \\ \hline
\overline{\tau}_{11}^{(k)} & \overline{\tau}_{22}^{(k)} & \overline{\tau}_{12}^{(k)} & \overline{\tau}_{13}^{(k)} & \overline{\tau}_{23}^{(k)} & \overline{\tau}_{33}^{(k)} & \overline{\sigma}_{11}^{(k)} & \overline{\sigma}_{22}^{(k)} & \overline{\sigma}_{33}^{(k)} & \overline{w}_{11}^{(k)} & \overline{w}_{22}^{(k)} & \overline{w}_{33}^{(k)} & \overline{\varsigma}_{11}^{(k)} & \overline{\varsigma}_{12}^{(k)} & 0 & 0 & 0 & 0 & 0 & 0 \\ \hline
\overline{e}_{11}^{(k)} & \overline{e}_{22}^{(k)} & \overline{e}_{12}^{(k)} & \overline{e}_{13}^{(k)} & \overline{e}_{23}^{(k)} & \overline{e}_{33}^{(k)} & \overline{g}_{11}^{(k)} & \overline{g}_{22}^{(k)} & \overline{g}_{33}^{(k)} & \overline{f}_{11}^{(k)} & \overline{f}_{22}^{(k)} & \overline{f}_{33}^{(k)} & \overline{\varsigma}_{12}^{(k)} & \overline{\varsigma}_{22}^{(k)} & 0 & 0 & 0 & 0 & 0 & 0 \\ \hline
0 & 0 & 0 & 0 & 0 & 0 & 0 & 0 & 0 & 0 & 0 & 0 & 0 & 0 & \overline{k}_{11}^{(k)} & \overline{k}_{12}^{(k)} & \overline{k}_{13}^{(k)} & \overline{y}_{11}^{(k)} & \overline{y}_{12}^{(k)} & \overline{y}_{13}^{(k)} \\
0 & 0 & 0 & 0 & 0 & 0 & 0 & 0 & 0 & 0 & 0 & 0 & 0 & 0 & \overline{k}_{12}^{(k)} & \overline{k}_{22}^{(k)} & \overline{k}_{23}^{(k)} & \overline{y}_{12}^{(k)} & \overline{y}_{22}^{(k)} & \overline{y}_{23}^{(k)} \\
0 & 0 & 0 & 0 & 0 & 0 & 0 & 0 & 0 & 0 & 0 & 0 & 0 & 0 & \overline{k}_{13}^{(k)} & \overline{k}_{23}^{(k)} & \overline{k}_{33}^{(k)} & \overline{y}_{13}^{(k)} & \overline{y}_{23}^{(k)} & \overline{y}_{33}^{(k)} \\ \hline
0 & 0 & 0 & 0 & 0 & 0 & 0 & 0 & 0 & 0 & 0 & 0 & 0 & 0 & \overline{x}_{11}^{(k)} & \overline{x}_{12}^{(k)} & \overline{x}_{13}^{(k)} & \overline{z}_{11}^{(k)} & \overline{z}_{12}^{(k)} & \overline{z}_{13}^{(k)} \\
0 & 0 & 0 & 0 & 0 & 0 & 0 & 0 & 0 & 0 & 0 & 0 & 0 & 0 & \overline{x}_{12}^{(k)} & \overline{x}_{22}^{(k)} & \overline{x}_{23}^{(k)} & \overline{z}_{12}^{(k)} & \overline{z}_{22}^{(k)} & \overline{z}_{23}^{(k)} \\
0 & 0 & 0 & 0 & 0 & 0 & 0 & 0 & 0 & 0 & 0 & 0 & 0 & 0 & \overline{x}_{13}^{(k)} & \overline{x}_{23}^{(k)} & \overline{x}_{33}^{(k)} & \overline{z}_{13}^{(k)} & \overline{z}_{23}^{(k)} & \overline{z}_{33}^{(k)}
\end{array}\right]
\begin{bmatrix}
\varepsilon_1^{(k)} \\ \varepsilon_2^{(k)} \\ \gamma_{12}^{(k)} \\ \gamma_{13}^{(k)} \\ \gamma_{23}^{(k)} \\ \varepsilon_3^{(k)} \\ \hline
E_1^{(k)} \\ E_2^{(k)} \\ E_3^{(k)} \\ \hline
H_1^{(k)} \\ H_2^{(k)} \\ H_3^{(k)} \\ \hline
\widehat{\Delta \mathrm{T}}^{(k)} \\ \hline
\widehat{\Delta \mathrm{C}}^{(k)} \\ \hline
\theta_1^{(k)} \\ \theta_2^{(k)} \\ \theta_3^{(k)} \\ \hline
\lambda_1^{(k)} \\ \lambda_2^{(k)} \\ \lambda_3^{(k)}
\end{bmatrix}
\tag{28}
$$

The matrices $\overline{\mathbf{\Gamma}}_{\mathrm{z}}^{(k)}$ and $\overline{\mathbf{\Gamma}}_{\mathrm{e}}^{(k)}$ occurring in Eqn. (28) can be determined from the following relationship [45]:

$$
\overline{\mathbf{\Gamma}}_{\mathrm{z}}^{(k)T} = \overline{\mathbf{\Gamma}}_{\mathrm{C}}^{(k)} \overline{\mathbf{\Gamma}}_{\mathrm{a}}^{(k)}, \quad \overline{\mathbf{\Gamma}}_{\mathrm{e}}^{(k)T} = \overline{\mathbf{\Gamma}}_{\mathrm{C}}^{(k)} \overline{\mathbf{\Gamma}}_{\mathrm{b}}^{(k)}
\tag{29}
$$

where $\overline{\mathbf{\Gamma}}_{\mathrm{a}}^{(k)}$ and $\overline{\mathbf{\Gamma}}_{\mathrm{b}}^{(k)}$ contain the thermal and hygroscopic expansion coefficients $\overline{a}_{ij}^{(k)}$ and $\overline{b}_{ij}^{(k)}$ with $i,j = 1, \ldots, 3$, respectively.

Eqn. (28) and Eqn. (29) are expressed in the geometric reference system $O^{'}\alpha_1\alpha_2\zeta$ already introduced in the previous section. However, the multifield constitutive behavior of each k-th layer of the shell is usually provided in the material reference system denoted by $O^{'}\widehat{\alpha}_1^{(k)}\widehat{\alpha}_2^{(k)}\widehat{\zeta}^{(k)}$, whose axes coincides to the material symmetry directions of the lamina. Therefore, the following constitutive relation is considered:

$$
\widehat{\boldsymbol{\chi}}^{(k)} = \mathbf{\Gamma}^{(k)} \widehat{\boldsymbol{\pi}}^{(k)} \quad \Leftrightarrow \quad
\begin{bmatrix}
\widehat{\boldsymbol{\sigma}}^{(k)} \\ \widehat{\mathbf{D}}^{(k)} \\ \widehat{\mathbf{B}}^{(k)} \\ \eta^{(k)} \\ \mu^{(k)} \\ \widehat{\mathbf{h}}^{(k)} \\ \widehat{\mathbf{c}}^{(k)}
\end{bmatrix}
=
\begin{bmatrix}
\mathbf{\Gamma}_{\mathrm{C}}^{(k)} & -\mathbf{\Gamma}_{\mathrm{P}}^{(k)T} & -\mathbf{\Gamma}_{\mathrm{Q}}^{(k)T} & -\mathbf{\Gamma}_{\mathrm{z}}^{(k)T} & -\mathbf{\Gamma}_{\mathrm{e}}^{(k)T} & \mathbf{0} & \mathbf{0} \\
\mathbf{\Gamma}_{\mathrm{P}}^{(k)} & \mathbf{\Gamma}_{\mathrm{L}}^{(k)} & \mathbf{\Gamma}_{\mathrm{D}}^{(k)} & \mathbf{\Gamma}_{\mathrm{o}}^{(k)T} & \mathbf{\Gamma}_{\mathrm{g}}^{(k)T} & \mathbf{0} & \mathbf{0} \\
\mathbf{\Gamma}_{\mathrm{Q}}^{(k)} & \mathbf{\Gamma}_{\mathrm{D}}^{(k)} & \mathbf{\Gamma}_{\mathrm{M}}^{(k)} & \mathbf{\Gamma}_{\mathrm{w}}^{(k)T} & \mathbf{\Gamma}_{\mathrm{f}}^{(k)T} & \mathbf{0} & \mathbf{0} \\
\mathbf{\Gamma}_{\mathrm{z}}^{(k)} & \mathbf{\Gamma}_{\mathrm{o}}^{(k)} & \mathbf{\Gamma}_{\mathrm{w}}^{(k)} & \mathbf{\Gamma}_{\mathrm{TT}}^{(k)} & \mathbf{\Gamma}_{\mathrm{TC}}^{(k)} & \mathbf{0} & \mathbf{0} \\
\mathbf{\Gamma}_{\mathrm{e}}^{(k)} & \mathbf{\Gamma}_{\mathrm{g}}^{(k)} & \mathbf{\Gamma}_{\mathrm{f}}^{(k)} & \mathbf{\Gamma}_{\mathrm{TC}}^{(k)} & \mathbf{\Gamma}_{\mathrm{CC}}^{(k)} & \mathbf{0} & \mathbf{0} \\
\mathbf{0} & \mathbf{0} & \mathbf{0} & \mathbf{0} & \mathbf{0} & \mathbf{\Gamma}_{\mathrm{K}}^{(k)} & \mathbf{\Gamma}_{\mathrm{Y}}^{(k)} \\
\mathbf{0} & \mathbf{0} & \mathbf{0} & \mathbf{0} & \mathbf{0} & \mathbf{\Gamma}_{\mathrm{X}}^{(k)} & \mathbf{\Gamma}_{\mathrm{S}}^{(k)}
\end{bmatrix}
\begin{bmatrix}
\widehat{\boldsymbol{\varepsilon}}^{(k)} \\ \widehat{\mathbf{E}}^{(k)} \\ \widehat{\mathbf{H}}^{(k)} \\ \widehat{\Delta \mathrm{T}}^{(k)} \\ \widehat{\Delta \mathrm{C}}^{(k)} \\ \widehat{\boldsymbol{\theta}}^{(k)} \\ \widehat{\boldsymbol{\lambda}}^{(k)}
\end{bmatrix}
\tag{30}
$$

where $\widehat{\boldsymbol{\varepsilon}}^{(k)}, \widehat{\mathbf{E}}^{(k)}, \widehat{\mathbf{H}}^{(k)}, \widehat{\Delta \mathrm{T}}^{(k)}, \widehat{\Delta \mathrm{C}}^{(k)}, \widehat{\boldsymbol{\theta}}^{(k)}, \widehat{\boldsymbol{\lambda}}^{(k)}$ and $\widehat{\boldsymbol{\sigma}}^{(k)}, \widehat{\mathbf{D}}^{(k)}, \widehat{\mathbf{B}}^{(k)}, \eta^{(k)}, \mu^{(k)}, \widehat{\mathbf{h}}^{(k)}, \widehat{\mathbf{c}}^{(k)}$ are the vectors of the primary and secondary variables,

respectively, written in the material reference system, while $\mathbf{\Gamma}^{(k)}$ represents the three-dimensional constitutive matrix. It is assumed that both the origin of the material and geometric reference system coincides. Furthermore, for each $k = 1, \ldots, l$ it is assumed that the planes $\widehat{\alpha}_1^{(k)} - \widehat{\alpha}_2^{(k)}$ and $\alpha_1 - \alpha_2$ are parallel, therefore the relation $\widehat{\zeta}^{(k)} = \zeta$ is considered. As a consequence, the material reference system is rotated by an angular quantity, denoted by $\vartheta^{(k)}$, which is the angle between $\widehat{\alpha}_1^{(k)}$ and α_1 axes. The matrices $\overline{\mathbf{\Gamma}}_{\alpha}^{(k)}$ and $\overline{\mathbf{\Gamma}}_{\beta}^{(k)}$ of Eqn. (28) can be calculated from their corresponding ones $\mathbf{\Gamma}_{\alpha}^{(k)}$ and $\mathbf{\Gamma}_{\beta}^{(k)}$ of Eqn. (31), written in the material reference system, as follows [45]:

$$\mathbf{A}^{(k)} = \begin{bmatrix} a_{11}^{(k)} & a_{12}^{(k)} & a_{13}^{(k)} \\ a_{12}^{(k)} & a_{22}^{(k)} & a_{23}^{(k)} \\ a_{13}^{(k)} & a_{23}^{(k)} & a_{33}^{(k)} \end{bmatrix} = \begin{bmatrix} 1 & 2 & 2 \\ 2 & 1 & 2 \\ 2 & 2 & 1 \end{bmatrix} \odot \begin{bmatrix} \widehat{a}_{11}^{(k)} & \widehat{a}_{12}^{(k)} & \widehat{a}_{13}^{(k)} \\ \widehat{a}_{12}^{(k)} & \widehat{a}_{22}^{(k)} & \widehat{a}_{23}^{(k)} \\ \widehat{a}_{13}^{(k)} & \widehat{a}_{23}^{(k)} & \widehat{a}_{33}^{(k)} \end{bmatrix} = \mathbf{Y}_{\varepsilon} \odot \widehat{\mathbf{A}}^{(k)}$$
$$\mathbf{B}^{(k)} = \begin{bmatrix} b_{11}^{(k)} & b_{12}^{(k)} & b_{13}^{(k)} \\ b_{12}^{(k)} & b_{22}^{(k)} & b_{23}^{(k)} \\ b_{13}^{(k)} & b_{23}^{(k)} & b_{33}^{(k)} \end{bmatrix} = \begin{bmatrix} 1 & 2 & 2 \\ 2 & 1 & 2 \\ 2 & 2 & 1 \end{bmatrix} \odot \begin{bmatrix} \widehat{b}_{11}^{(k)} & \widehat{b}_{12}^{(k)} & \widehat{b}_{13}^{(k)} \\ \widehat{b}_{12}^{(k)} & \widehat{b}_{22}^{(k)} & \widehat{b}_{23}^{(k)} \\ \widehat{b}_{13}^{(k)} & \widehat{b}_{23}^{(k)} & \widehat{b}_{33}^{(k)} \end{bmatrix} = \mathbf{Y}_{\varepsilon} \odot \widehat{\mathbf{B}}^{(k)} \tag{35}$$

$$\overline{\mathbf{\Gamma}}^{(k)} = \begin{bmatrix} \mathbf{T}^{(k)}\mathbf{\Gamma}_{\mathrm{C}}^{(k)}\mathbf{T}^{(k)T} & -\mathbf{T}^{(k)}\mathbf{\Gamma}_{\mathrm{P}}^{(k)T}\mathbf{H}^{(k)} & -\mathbf{T}^{(k)}\mathbf{\Gamma}_{\mathrm{Q}}^{(k)T}\mathbf{H}^{(k)} & -\mathbf{T}^{(k)}\mathbf{\Gamma}_{\mathrm{C}}^{(k)}\mathbf{T}_{\mathrm{a}}^{(k)T-(k)} & -\mathbf{T}^{(k)}\mathbf{\Gamma}_{\mathrm{C}}^{(k)}\mathbf{T}_{\mathrm{b}}^{(k)T-(k)} & \mathbf{0} & \mathbf{0} \\ \mathbf{H}^{(k)T}\mathbf{\Gamma}_{\mathrm{P}}^{(k)}\mathbf{T}^{(k)T} & \mathbf{H}^{(k)T}\mathbf{\Gamma}_{\mathrm{L}}^{(k)}\mathbf{H}^{(k)} & \mathbf{H}^{(k)T}\mathbf{\Gamma}_{\mathrm{D}}^{(k)}\mathbf{H}^{(k)} & \mathbf{H}^{(k)T}\mathbf{\Gamma}_{\mathrm{o}}^{(k)T} & \mathbf{H}^{(k)T}\mathbf{\Gamma}_{\mathrm{g}}^{(k)T} & \mathbf{0} & \mathbf{0} \\ \mathbf{H}^{(k)T}\mathbf{\Gamma}_{\mathrm{Q}}^{(k)}\mathbf{T}^{(k)T} & \mathbf{H}^{(k)T}\mathbf{\Gamma}_{\mathrm{D}}^{(k)}\mathbf{H}^{(k)} & \mathbf{H}^{(k)T}\mathbf{\Gamma}_{\mathrm{M}}^{(k)}\mathbf{H}^{(k)} & \mathbf{H}^{(k)T}\mathbf{\Gamma}_{\mathrm{w}}^{(k)T} & \mathbf{H}^{(k)T}\mathbf{\Gamma}_{\mathrm{f}}^{(k)T} & \mathbf{0} & \mathbf{0} \\ \overline{\mathbf{\Gamma}}_{\mathrm{a}}^{(k)T}\mathbf{T}^{(k)T}\mathbf{\Gamma}_{\mathrm{C}}^{(k)}\mathbf{T}^{(k)} & \mathbf{\Gamma}_{\mathrm{o}}^{(k)}\mathbf{H}^{(k)} & \mathbf{\Gamma}_{\mathrm{w}}^{(k)}\mathbf{H}^{(k)} & \mathbf{\Gamma}_{\mathrm{TT}}^{(k)} & \mathbf{\Gamma}_{\mathrm{TC}}^{(k)} & \mathbf{0} & \mathbf{0} \\ \overline{\mathbf{\Gamma}}_{\mathrm{b}}^{(k)T}\mathbf{T}^{(k)T}\mathbf{\Gamma}_{\mathrm{C}}^{(k)}\mathbf{T}^{(k)} & \mathbf{\Gamma}_{\mathrm{g}}^{(k)}\mathbf{H}^{(k)} & \mathbf{\Gamma}_{\mathrm{f}}^{(k)}\mathbf{H}^{(k)} & \mathbf{\Gamma}_{\mathrm{TC}}^{(k)} & \mathbf{\Gamma}_{\mathrm{CC}}^{(k)} & \mathbf{0} & \mathbf{0} \\ \mathbf{0} & \mathbf{0} & \mathbf{0} & \mathbf{0} & \mathbf{0} & \mathbf{H}^{(k)T}\mathbf{\Gamma}_{\mathrm{K}}^{(k)}\mathbf{H}^{(k)} & \mathbf{H}^{(k)T}\mathbf{\Gamma}_{\mathrm{Y}}^{(k)}\mathbf{H}^{(k)} \\ \mathbf{0} & \mathbf{0} & \mathbf{0} & \mathbf{0} & \mathbf{0} & \mathbf{H}^{(k)T}\mathbf{\Gamma}_{\mathrm{X}}^{(k)}\mathbf{H}^{(k)} & \mathbf{H}^{(k)T}\mathbf{\Gamma}_{\mathrm{S}}^{(k)}\mathbf{H}^{(k)} \end{bmatrix} \tag{31}$$

Here, $\mathbf{H}^{(k)}$ and $\mathbf{T}^{(k)}$ are rotation matrices defined on each k-th layer, dependent on the previously introduced material orientation angle $\vartheta^{(k)}$. In a more extended form, they can be written as:

$$\mathbf{T}^{(k)} = \begin{bmatrix} \cos^2\vartheta^{(k)} & \sin^2\vartheta^{(k)} & -2\sin\vartheta^{(k)}\cos\vartheta^{(k)} & 0 & 0 & 0 \\ \sin^2\vartheta^{(k)} & \cos^2\vartheta^{(k)} & 2\sin\vartheta^{(k)}\cos\vartheta^{(k)} & 0 & 0 & 0 \\ \sin\vartheta^{(k)}\cos\vartheta^{(k)} & -\sin\vartheta^{(k)}\cos\vartheta^{(k)} & \cos^2\vartheta^{(k)} - \sin^2\vartheta^{(k)} & 0 & 0 & 0 \\ 0 & 0 & 0 & \cos\vartheta^{(k)} & -\sin\vartheta^{(k)} & 0 \\ 0 & 0 & 0 & \sin\vartheta^{(k)} & \cos\vartheta^{(k)} & 0 \\ 0 & 0 & 0 & 0 & 0 & 1 \end{bmatrix} \tag{32}$$

$$\mathbf{H}^{(k)} = \begin{bmatrix} \cos\vartheta^{(k)} & \sin\vartheta^{(k)} & 0 \\ -\sin\vartheta^{(k)} & \cos\vartheta^{(k)} & 0 \\ 0 & 0 & 1 \end{bmatrix} \tag{33}$$

The elements of the vectors $\overline{\mathbf{\Gamma}}_{\mathrm{a}}^{(k)}$ and $\overline{\mathbf{\Gamma}}_{\mathrm{b}}^{(k)}$ represent the transformed thermal and hygroscopic expansion coefficients $\overline{a}_{ij}^{(k)}$ and $\overline{b}_{ij}^{(k)}$ with $i, j = 1, \ldots, 3$ belonging to the matrices $\overline{\mathbf{A}}^{(k)}$ and $\overline{\mathbf{B}}^{(k)}$ defined as follows [45]:

$$\overline{\mathbf{A}}^{(k)} = \mathbf{Y}_{\varepsilon} \odot \left(\mathbf{H}^{(k)T}\widehat{\mathbf{A}}^{(k)}\mathbf{H}^{(k)}\right), \quad \overline{\mathbf{B}}^{(k)} = \mathbf{Y}_{\varepsilon} \odot \left(\mathbf{H}^{(k)T}\widehat{\mathbf{B}}^{(k)}\mathbf{H}^{(k)}\right) \tag{34}$$

where the matrix $\mathbf{Y}_{\varepsilon}$ yields the conversion of the three-dimensional strain components into the three-dimensional engineering strain components, while $\mathbf{A}^{(k)}$ and $\mathbf{B}^{(k)}$ are defined in terms of the matrices $\widehat{\mathbf{A}}^{(k)}$, $\widehat{\mathbf{B}}^{(k)}$ whose elements are the thermal and the hygroscopic expansion coefficients, respectively:

The variation $\Delta\mu^{(k)}$ of the chemical potential with respect to its reference value $\mu_0^{(k)}$ can be expressed in terms of the absolute temperature $\mathrm{T}^{(k)}$ and the concentration variation $\Delta\mathrm{C}^{(k)}$ variables as follows:

$$\Delta\mu^{(k)} = \mu^{(k)} - \mu_0^{(k)} = R_g \mathrm{T}^{(k)} \log\Delta\mathrm{C}^{(k)} \tag{36}$$

where $R_g = 461.9\,\mathrm{J/(kg\,K)}$ denotes the gas constant. In this way, the following definitions of can be considered for the constitutive coefficients $\xi_{11}^{(k)}, \xi_{22}^{(k)}$ and $\xi_{12}^{(k)}$ which belong to the matrices $\mathbf{\Gamma}_{\mathrm{TT}}^{(k)}, \mathbf{\Gamma}_{\mathrm{CC}}^{(k)}$ and $\mathbf{\Gamma}_{\mathrm{TC}}^{(k)}$, respectively [45]:

$$\xi_{11}^{(k)} = \left(\frac{\partial\eta^{(k)}}{\partial\mathrm{T}}\right)_{\boldsymbol{\varepsilon},\mathbf{E},\mathbf{H},\Delta\mathrm{C}} = \left(\frac{\partial\eta^{(k)}}{\partial\mathrm{T}}\right)_{\boldsymbol{\varepsilon},\mathbf{E},\mathbf{H},\mathrm{C}_\infty} = \frac{\rho^{(k)}c^{(k)}}{\mathrm{T}_0}$$
$$\xi_{22}^{(k)} = \left(\frac{\partial\mu^{(k)}}{\partial\mathrm{C}}\right)_{\boldsymbol{\varepsilon},\mathbf{E},\mathbf{H},\Delta\mathrm{T}} = \left(\frac{\partial\mu^{(k)}}{\partial\mathrm{C}}\right)_{\boldsymbol{\varepsilon},\mathbf{E},\mathbf{H},\mathrm{T}_0} = \frac{R_g\mathrm{T}_0}{\mathrm{C}_\infty^{(k)} - \mathrm{C}_0^{(k)}} \cong \frac{R_g\mathrm{T}_0}{\mathrm{C}_\infty^{(k)}} = \frac{R_g\mathrm{T}_0}{\rho^{(k)}M_\infty^{(k)}}$$
$$\xi_{12}^{(k)} = \left(\frac{\partial\mu^{(k)}}{\partial\mathrm{T}}\right)_{\boldsymbol{\varepsilon},\mathbf{E},\mathbf{H},\Delta\mathrm{C}} = \left(\frac{\partial\mu^{(k)}}{\partial\mathrm{T}}\right)_{\boldsymbol{\varepsilon},\mathbf{E},\mathbf{H},\mathrm{C}_\infty} = \left(\frac{\partial\eta^{(k)}}{\partial\mathrm{C}}\right)_{\boldsymbol{\varepsilon},\mathbf{E},\mathbf{H},\Delta\mathrm{T}} = \left(\frac{\partial\eta^{(k)}}{\partial\mathrm{C}}\right)_{\boldsymbol{\varepsilon},\mathbf{E},\mathbf{H},\mathrm{T}_0} =$$
$$= -\frac{\Delta\mu^{(k)}}{\mathrm{T}_0} = -R_g\log\left(\mathrm{C}_\infty^{(k)} - \mathrm{C}_0^{(k)}\right) \cong -R_g\log\mathrm{C}_\infty^{(k)} = -R_g\log\left(\rho^{(k)}M_\infty^{(k)}\right) \tag{37}$$

The coupled hygrothermal constitutive relations, which relate the temperature and concentration gradient vectors $\boldsymbol{\theta}^{(k)}$ and $\boldsymbol{\lambda}^{(k)}$ to the thermal and concentration vectors $\mathbf{h}^{(k)}$ and $\mathbf{c}^{(k)}$, respectively, are derived from the Onsager's reciprocity principle as follows:

$$\mathbf{h}^{(k)} = \overline{\mathbf{\Gamma}}_{\mathrm{K}}^{(k)}\boldsymbol{\theta}^{(k)} + \nu^{(k)}u_d^{(k)}\overline{\mathbf{\Gamma}}_{\mathrm{K}}^{(k)}\boldsymbol{\lambda}^{(k)} = \overline{\mathbf{\Gamma}}_{\mathrm{K}}^{(k)}\boldsymbol{\theta}^{(k)} + \overline{\mathbf{\Gamma}}_{\mathrm{Y}}^{(k)}\boldsymbol{\lambda}^{(k)}$$
$$\mathbf{c}^{(k)} = \frac{\lambda^{(k)}}{\rho^{(k)}c^{(k)}}\overline{\mathbf{\Gamma}}_{\mathrm{K}}^{(k)}\boldsymbol{\theta}^{(k)} + \frac{u_d^{(k)}}{\rho^{(k)}c^{(k)}}\overline{\mathbf{\Gamma}}_{\mathrm{K}}^{(k)}\boldsymbol{\lambda}^{(k)} = \overline{\mathbf{\Gamma}}_{\mathrm{X}}^{(k)}\boldsymbol{\theta}^{(k)} + \overline{\mathbf{\Gamma}}_{\mathrm{S}}^{(k)}\boldsymbol{\lambda}^{(k)} \tag{38}$$

In the previous relation, the matrices $\overline{\mathbf{\Gamma}}_{\mathrm{X}}^{(k)}$ and $\overline{\mathbf{\Gamma}}_{\mathrm{Y}}^{(k)}$ account for the Soret and Dufour effects, which couple the classical Fick diffusion equations and the Fourier relations of stationary heat conduction. In addition, the assumptions $u_d^{(k)} = 0.1$ and $\lambda^{(k)}\nu^{(k)} = 0.25$ are made in each

point of the panel, in line to the approach presented in the book by Sih [70]. In this way, the parameter $\nu^{(k)}$ is obtained from the following relation:

$$\nu^{(k)} = \frac{Q_h^{(k)}}{\rho^{(k)} c^{(k)}} \tag{39}$$

where $Q_h^{(k)}$ is the heat of transport ratio, which is the heat exchanged because of mass diffusion:

$$Q_h^{(k)} = \mathrm{T}_0 \sqrt{\frac{\rho^{(k)} c^{(k)} \lambda^{(k)} \nu^{(k)} R_g}{u_d^{(k)} \mathrm{C}_\infty^{(k)}}} = \mathrm{T}_0 \sqrt{\frac{c^{(k)} \lambda^{(k)} \nu^{(k)} R_g}{u_d^{(k)} M_\infty^{(k)}}} \tag{40}$$

Further details regarding the procedure presented above can be found in Ref. [45]. At this point, a generalized constitutive equation is derived for the doubly-curved shell solid, taking into account the kinematic assumption of Eqn. (10). To this end, the virtual variation of the total free energy Y of the system is evaluated:

$$\delta Y = \sum_{k=1}^{l} \int_{\alpha_1} \int_{\alpha_2} \int_{\zeta_k}^{\zeta_{k+1}} \left(\delta \overline{\boldsymbol{\pi}}^{(k)T} \overline{\boldsymbol{\chi}}^{(k)}\right) A_1 A_2 H_1 H_2 d\alpha_1 d\alpha_2 d\zeta = \sum_{k=1}^{l} \int_{\alpha_1} \int_{\alpha_2} \int_{\zeta_k}^{\zeta_{k+1}} \Big(\delta \boldsymbol{\varepsilon}^{(k)T} \boldsymbol{\sigma}^{(k)} - \delta \mathbf{E}^{(k)T} \mathbf{D}^{(k)} - \delta \mathbf{H}^{(k)T} \mathbf{B}^{(k)} - \eta^{(k)} \delta \widehat{\Delta \mathrm{T}}^{(k)} - \mu^{(k)} \delta \widehat{\Delta \mathrm{C}}^{(k)} + $$
$$- \delta \boldsymbol{\theta}^{(k)T} \left(\frac{\mathbf{h}^{(k)}}{\mathrm{T}_0} + \frac{\mu_\infty}{\mathrm{T}_0} \mathbf{c}^{(k)} \right) - \delta \boldsymbol{\lambda}^{(k)T} \left(\frac{\mu_\infty}{\mathrm{C}_\infty} \mathbf{c}^{(k)} \right) \Big) A_1 A_2 H_1 H_2 d\alpha_1 d\alpha_2 d\zeta \tag{41}$$

Note that in the previous equation the dissipation effects and the irreversible processes are neglected, because constant values have been selected for the quantities T_0, μ_∞ and C_∞. The vector $\overline{\boldsymbol{\pi}}^{(k)}$ and $\overline{\boldsymbol{\chi}}^{(k)}$ of primary and secondary variables, respectively, occurring in Eqn. (42) read as [45]:

$$\overline{\boldsymbol{\pi}}^{(k)} = \begin{bmatrix} \boldsymbol{\varepsilon}^{(k)T} & -\mathbf{E}^{(k)T} & -\mathbf{H}^{(k)T} & -\widehat{\Delta \mathrm{T}}^{(k)} & -\widehat{\Delta \mathrm{C}}^{(k)} & -\boldsymbol{\theta}^{(k)T} & -\boldsymbol{\lambda}^{(k)T} \end{bmatrix}^T$$

$$\overline{\boldsymbol{\chi}}^{(k)} = \mathbf{B} \boldsymbol{\chi}^{(k)} \quad \Leftrightarrow \quad \begin{bmatrix} \boldsymbol{\sigma}^{(k)} \\ \mathbf{D}^{(k)} \\ \mathbf{B}^{(k)} \\ \eta^{(k)} \\ \mu^{(k)} \\ \overline{\mathbf{h}}^{(k)} \\ \overline{\mathbf{c}}^{(k)} \end{bmatrix} = \begin{bmatrix} \widehat{\mathbf{I}} & 0 & 0 & 0 & 0 & 0 & 0 \\ 0 & \mathbf{I} & 0 & 0 & 0 & 0 & 0 \\ 0 & 0 & \mathbf{I} & 0 & 0 & 0 & 0 \\ 0 & 0 & 0 & 1 & 0 & 0 & 0 \\ 0 & 0 & 0 & 0 & 1 & 0 & 0 \\ 0 & 0 & 0 & 0 & 0 & \frac{1}{\mathrm{T}_0}\mathbf{I} & \frac{\mu_\infty}{\mathrm{T}_0}\mathbf{I} \\ 0 & 0 & 0 & 0 & 0 & 0 & \frac{\mu_\infty}{\mathrm{C}_\infty}\mathbf{I} \end{bmatrix} \begin{bmatrix} \boldsymbol{\sigma}^{(k)} \\ \mathbf{D}^{(k)} \\ \mathbf{B}^{(k)} \\ \eta^{(k)} \\ \mu^{(k)} \\ \mathbf{h}^{(k)} \\ \mathbf{c}^{(k)} \end{bmatrix} \tag{42}$$

$\widehat{\mathbf{I}}$ is the identity matrix of size 6×6, whereas $\mathbf{I}$ denotes the identity matrix of size 3×3. Introducing the generalized definition equations (26) into Eqn.(42), one gets:

$$\delta Y = \sum_{k=1}^{l} \int_{\alpha_1} \int_{\alpha_2} \int_{\zeta_k}^{\zeta_{k+1}} \left(\sum_{\tau=0}^{N+1} \sum_{i=1}^{7} \mathbf{Z}^{(k\tau)\alpha_i} \delta \overline{\boldsymbol{\pi}}^{(\tau)\alpha_i} \right)^T \mathbf{B} \boldsymbol{\chi}^{(k)} A_1 A_2 H_1 H_2 d\zeta d\alpha_1 d\alpha_2 =$$
$$= \sum_{\tau=0}^{N+1} \sum_{i=1}^{7} \int_{\alpha_1} \int_{\alpha_2} \left(\delta \overline{\boldsymbol{\pi}}^{(\tau)\alpha_i}\right)^T \overline{\mathbf{B}} \left(\sum_{k=1}^{l} \int_{\zeta_k}^{\zeta_{k+1}} \left(\mathbf{Z}^{(k\tau)\alpha_i}\right)^T \boldsymbol{\chi}^{(k)} H_1 H_2 d\zeta \right) A_1 A_2 d\alpha_1 d\alpha_2 =$$
$$= \sum_{\tau=0}^{N+1} \sum_{i=1}^{7} \int_{\alpha_1} \int_{\alpha_2} \left(\delta \overline{\boldsymbol{\pi}}^{(\tau)\alpha_i}\right)^T \overline{\mathbf{B}} \boldsymbol{\Sigma}^{(\tau)\alpha_i} A_1 A_2 d\alpha_1 d\alpha_2 = \sum_{\tau=0}^{N+1} \sum_{i=1}^{7} \int_{\alpha_1} \int_{\alpha_2} \left(\delta \overline{\boldsymbol{\pi}}^{(\tau)\alpha_i}\right)^T \overline{\boldsymbol{\Sigma}}^{(\tau)\alpha_i} A_1 A_2 d\alpha_1 d\alpha_2 \tag{43}$$

As can be seen, in the previous relation the generalized stress resultant vector $\boldsymbol{\Sigma}^{(\tau)\alpha_i}$ has been introduced for each τ-th kinematic expansion order and $i = 1, \ldots, 7$, and it can be computed in each point of the physical domain as follows:

$$\boldsymbol{\Sigma}^{(\tau)\alpha_i} = \sum_{k=1}^{l} \int_{\zeta_k}^{\zeta_{k+1}} \left(\mathbf{Z}^{(k\tau)\alpha_i}\right)^T \boldsymbol{\chi}^{(k)} H_1 H_2 d\zeta \tag{44}$$

In a condensed matrix form, $\boldsymbol{\Sigma}^{(\tau)\alpha_i}$ assumes the following aspect [45]:

$$\boldsymbol{\Sigma}^{(\tau)\alpha_i} = \begin{bmatrix} \mathbf{S}^{(\tau)\alpha_i T} & \mathbf{D}^{(\tau)\alpha_i T} & \mathbf{B}^{(\tau)\alpha_i T} & E^{(\tau)\alpha_i} & M^{(\tau)\alpha_i} & \mathbf{H}^{(\tau)\alpha_i T} & \mathbf{C}^{(\tau)\alpha_i T} \end{bmatrix}^T \tag{45}$$

On the other hand, the vectors $\mathbf{S}^{(\tau)\alpha_i}, \mathbf{D}^{(\tau)\alpha_i}, \mathbf{B}^{(\tau)\alpha_i}, \mathbf{H}^{(\tau)\alpha_i}, \mathbf{C}^{(\tau)\alpha_i}$ are expressed as:

$$\begin{aligned}
\mathbf{S}^{(\tau)\alpha_i} &= \left[N_1^{(\tau)\alpha_i} \;\; N_2^{(\tau)\alpha_i} \;\; N_{12}^{(\tau)\alpha_i} \;\; N_{21}^{(\tau)\alpha_i} \;\; T_1^{(\tau)\alpha_i} \;\; T_2^{(\tau)\alpha_i} \;\; P_1^{(\tau)\alpha_i} \;\; P_2^{(\tau)\alpha_i} \;\; S_3^{(\tau)\alpha_i}\right]^T \\
\mathbf{D}^{(\tau)\alpha_i} &= \left[D_1^{(\tau)\alpha_i} \;\; D_2^{(\tau)\alpha_i} \;\; D_3^{(\tau)\alpha_i}\right]^T, \quad \mathbf{B}^{(\tau)\alpha_i} = \left[B_1^{(\tau)\alpha_i} \;\; B_2^{(\tau)\alpha_i} \;\; B_3^{(\tau)\alpha_i}\right]^T \\
\mathbf{H}^{(\tau)\alpha_i} &= \left[H_1^{(\tau)\alpha_i} \;\; H_2^{(\tau)\alpha_i} \;\; H_3^{(\tau)\alpha_i}\right]^T, \quad \mathbf{C}^{(\tau)\alpha_i} = \left[C_1^{(\tau)\alpha_i} \;\; C_2^{(\tau)\alpha_i} \;\; C_3^{(\tau)\alpha_i}\right]^T
\end{aligned} \tag{46}$$

As demonstrated in Eqn. (44), the generalized stress resultant vector $\boldsymbol{\Sigma}^{(\tau)\alpha_i}$ is related to the vector $\overline{\boldsymbol{\Sigma}}^{(\tau)\alpha_i}$ through the matrix $\overline{\mathbf{B}}$. To this end, the following relation is adopted, with $\breve{\mathbf{I}}$ representing the identity 9 ×9 matrix:

$$\overline{\boldsymbol{\Sigma}}^{(\tau)\alpha_i} = \overline{\mathbf{B}}\boldsymbol{\Sigma}^{(\tau)\alpha_i} \;\Leftrightarrow\; \begin{bmatrix} \mathbf{S}^{(\tau)\alpha_i} \\ \mathbf{D}^{(\tau)\alpha_i} \\ \mathbf{B}^{(\tau)\alpha_i} \\ E^{(\tau)\alpha_i} \\ M^{(\tau)\alpha_i} \\ \overline{\mathbf{H}}^{(\tau)\alpha_i} \\ \overline{\mathbf{C}}^{(\tau)\alpha_i} \end{bmatrix} = \begin{bmatrix} \breve{\mathbf{I}} & \mathbf{0} & \mathbf{0} & \mathbf{0} & \mathbf{0} & \mathbf{0} & \mathbf{0} \\ \mathbf{0} & \mathbf{I} & \mathbf{0} & \mathbf{0} & \mathbf{0} & \mathbf{0} & \mathbf{0} \\ \mathbf{0} & \mathbf{0} & \mathbf{I} & \mathbf{0} & \mathbf{0} & \mathbf{0} & \mathbf{0} \\ \mathbf{0} & \mathbf{0} & \mathbf{0} & 1 & 0 & \mathbf{0} & \mathbf{0} \\ \mathbf{0} & \mathbf{0} & \mathbf{0} & 0 & 1 & \mathbf{0} & \mathbf{0} \\ \mathbf{0} & \mathbf{0} & \mathbf{0} & \mathbf{0} & \mathbf{0} & \frac{1}{\mathrm{T}_0}\mathbf{I} & \frac{\mu_\infty}{\mathrm{T}_0}\mathbf{I} \\ \mathbf{0} & \mathbf{0} & \mathbf{0} & \mathbf{0} & \mathbf{0} & \mathbf{0} & \frac{\mu_\infty}{\mathrm{C}_\infty}\mathbf{I} \end{bmatrix} \begin{bmatrix} \mathbf{S}^{(\tau)\alpha_i} \\ \mathbf{D}^{(\tau)\alpha_i} \\ \mathbf{B}^{(\tau)\alpha_i} \\ E^{(\tau)\alpha_i} \\ M^{(\tau)\alpha_i} \\ \mathbf{H}^{(\tau)\alpha_i} \\ \mathbf{C}^{(\tau)\alpha_i} \end{bmatrix} \tag{47}$$

After performing all matrix multiplications, the following definitions [45] can be derived for the generalized stress resultants of Eqn. (47):

$$\begin{aligned}
N_1^{(\tau)\alpha_i} &= \sum_{k=1}^{l}\int_{\zeta_k}^{\zeta_{k+1}} \sigma_1^{(k)} F_\tau^{(k)\alpha_i} H_2 d\zeta, \quad N_2^{(\tau)\alpha_i} = \sum_{k=1}^{l}\int_{\zeta_k}^{\zeta_{k+1}} \sigma_2^{(k)} F_\tau^{(k)\alpha_i} H_1 d\zeta, \quad N_{12}^{(\tau)\alpha_i} = \sum_{k=1}^{l}\int_{\zeta_k}^{\zeta_{k+1}} \tau_{12}^{(k)} F_\tau^{(k)\alpha_i} H_2 d\zeta, \\
N_{21}^{(\tau)\alpha_i} &= \sum_{k=1}^{l}\int_{\zeta_k}^{\zeta_{k+1}} \tau_{12}^{(k)} F_\tau^{(k)\alpha_i} H_1 d\zeta, \quad T_1^{(\tau)\alpha_i} = \sum_{k=1}^{l}\int_{\zeta_k}^{\zeta_{k+1}} \tau_{13}^{(k)} F_\tau^{(k)\alpha_i} H_2 d\zeta, \quad T_2^{(\tau)\alpha_i} = \sum_{k=1}^{l}\int_{\zeta_k}^{\zeta_{k+1}} \tau_{23}^{(k)} F_\tau^{(k)\alpha_i} H_1 d\zeta, \\
P_1^{(\tau)\alpha_i} &= \sum_{k=1}^{l}\int_{\zeta_k}^{\zeta_{k+1}} \tau_{13}^{(k)} \frac{\partial F_\tau^{(k)\alpha_i}}{\partial\zeta} H_1 H_2 d\zeta, \quad P_2^{(\tau)\alpha_i} = \sum_{k=1}^{l}\int_{\zeta_k}^{\zeta_{k+1}} \tau_{23}^{(k)} \frac{\partial F_\tau^{(k)\alpha_i}}{\partial\zeta} H_1 H_2 d\zeta, \quad S_3^{(\tau)\alpha_i} = \sum_{k=1}^{l}\int_{\zeta_k}^{\zeta_{k+1}} \sigma_3^{(k)} \frac{\partial F_\tau^{(k)\alpha_i}}{\partial\zeta} H_1 H_2 d\zeta, \\
D_1^{(\tau)\alpha_i} &= \sum_{k=1}^{l}\int_{\zeta_k}^{\zeta_{k+1}} D_1^{(k)} F_\tau^{(k)\alpha_i} H_2 d\zeta, \quad D_2^{(\tau)\alpha_i} = \sum_{k=1}^{l}\int_{\zeta_k}^{\zeta_{k+1}} D_2^{(k)} F_\tau^{(k)\alpha_i} H_1 d\zeta, \quad D_3^{(\tau)\alpha_i} = \sum_{k=1}^{l}\int_{\zeta_k}^{\zeta_{k+1}} D_3^{(k)} \frac{\partial F_\tau^{(k)\alpha_i}}{\partial\zeta} H_1 H_2 d\zeta, \\
B_1^{(\tau)\alpha_i} &= \sum_{k=1}^{l}\int_{\zeta_k}^{\zeta_{k+1}} B_1^{(k)} F_\tau^{(k)\alpha_i} H_2 d\zeta, \quad B_2^{(\tau)\alpha_i} = \sum_{k=1}^{l}\int_{\zeta_k}^{\zeta_{k+1}} B_2^{(k)} F_\tau^{(k)\alpha_i} H_1 d\zeta, \quad B_3^{(\tau)\alpha_i} = \sum_{k=1}^{l}\int_{\zeta_k}^{\zeta_{k+1}} B_3^{(k)} \frac{\partial F_\tau^{(k)\alpha_i}}{\partial\zeta} H_1 H_2 d\zeta, \\
H_1^{(\tau)\alpha_i} &= \sum_{k=1}^{l}\int_{\zeta_k}^{\zeta_{k+1}} h_1^{(k)} F_\tau^{(k)\alpha_i} H_2 d\zeta, \quad H_2^{(\tau)\alpha_i} = \sum_{k=1}^{l}\int_{\zeta_k}^{\zeta_{k+1}} h_2^{(k)} F_\tau^{(k)\alpha_i} H_1 d\zeta, \quad H_3^{(\tau)\alpha_i} = \sum_{k=1}^{l}\int_{\zeta_k}^{\zeta_{k+1}} h_3^{(k)} \frac{\partial F_\tau^{(k)\alpha_i}}{\partial\zeta} H_1 H_2 d\zeta, \\
C_1^{(\tau)\alpha_i} &= \sum_{k=1}^{l}\int_{\zeta_k}^{\zeta_{k+1}} c_1^{(k)} F_\tau^{(k)\alpha_i} H_2 d\zeta, \quad C_2^{(\tau)\alpha_i} = \sum_{k=1}^{l}\int_{\zeta_k}^{\zeta_{k+1}} c_2^{(k)} F_\tau^{(k)\alpha_i} H_1 d\zeta, \quad C_3^{(\tau)\alpha_i} = \sum_{k=1}^{l}\int_{\zeta_k}^{\zeta_{k+1}} h_3^{(k)} \frac{\partial F_\tau^{(k)\alpha_i}}{\partial\zeta} H_1 H_2 d\zeta, \\
E^{(\tau)\alpha_i} &= \sum_{k=1}^{l}\int_{\zeta_k}^{\zeta_{k+1}} \eta^{(k)} F_\tau^{(k)\alpha_i} H_1 H_2 d\zeta, \quad M^{(\tau)\alpha_i} = \sum_{k=1}^{l}\int_{\zeta_k}^{\zeta_{k+1}} \mu^{(k)} F_\tau^{(k)\alpha_i} H_1 H_2 d\zeta
\end{aligned} \tag{48}$$

Substituting the three-dimensional elastic constitutive relation (28) into the definition (45) and recalling the generalized ESL version of the definition equations as reported in Eqn. (24), the generalized ESL constitutive relationship can be derived [45]:

$$\boldsymbol{\Sigma}^{(\tau)\alpha_i} = \sum_{\eta=0}^{N+1}\sum_{j=1}^{7}\left(\sum_{k=1}^{l}\int_{\zeta_k}^{\zeta_{k+1}} \left(\mathbf{Z}^{(k\tau)\alpha_i}\right)^T \overline{\boldsymbol{\Gamma}}^{(k)} \mathbf{Z}^{(k\eta)\alpha_j} H_1 H_2 d\zeta\right)\boldsymbol{\pi}^{(\eta)\alpha_j} = \sum_{\eta=0}^{N+1}\sum_{j=1}^{7} \mathbf{A}^{(\tau\eta)\alpha_i\alpha_j}\boldsymbol{\pi}^{(\eta)\alpha_j} \tag{49}$$

In the previous equation, the quantity $\mathbf{A}^{(\tau\eta)\alpha_i\alpha_j}$ represents the generalized stiffness matrix of the multifield problem associated with each $\tau,\eta = 0,...,N+1$ and $i,j = 1,...,7$. Starting from the expression (26) of matrix $\mathbf{Z}^{(k\tau)\alpha_i}$ and the extended version of $\overline{\Gamma}^{(k)}$ adopted in Eqn. (28), an extended version of the generalized stiffness matrix $\mathbf{A}^{(\tau\eta)\alpha_i\alpha_j}$ can be provided:

$$\mathbf{A}^{(\tau\eta)\alpha_i\alpha_j} = \begin{bmatrix} \mathbf{A}_{\varepsilon\varepsilon}^{(\tau\eta)\alpha_i\alpha_j} & \mathbf{A}_{\varepsilon\phi}^{(\tau\eta)\alpha_i\alpha_j} & \mathbf{A}_{\varepsilon\psi}^{(\tau\eta)\alpha_i\alpha_j} & \mathbf{A}_{\varepsilon\mathrm{T}}^{(\tau\eta)\alpha_i\alpha_j} & \mathbf{A}_{\varepsilon\mathrm{C}}^{(\tau\eta)\alpha_i\alpha_j} & \mathbf{0} & \mathbf{0} \\ \mathbf{A}_{\phi\varepsilon}^{(\tau\eta)\alpha_i\alpha_j} & \mathbf{A}_{\phi\phi}^{(\tau\eta)\alpha_i\alpha_j} & \mathbf{A}_{\phi\psi}^{(\tau\eta)\alpha_i\alpha_j} & \mathbf{A}_{\phi\mathrm{T}}^{(\tau\eta)\alpha_i\alpha_j} & \mathbf{A}_{\phi\mathrm{C}}^{(\tau\eta)\alpha_i\alpha_j} & \mathbf{0} & \mathbf{0} \\ \mathbf{A}_{\psi\varepsilon}^{(\tau\eta)\alpha_i\alpha_j} & \mathbf{A}_{\psi\phi}^{(\tau\eta)\alpha_i\alpha_j} & \mathbf{A}_{\psi\psi}^{(\tau\eta)\alpha_i\alpha_j} & \mathbf{A}_{\psi\mathrm{T}}^{(\tau\eta)\alpha_i\alpha_j} & \mathbf{A}_{\psi\mathrm{C}}^{(\tau\eta)\alpha_i\alpha_j} & \mathbf{0} & \mathbf{0} \\ \mathbf{A}_{\mathrm{T}\varepsilon}^{(\tau\eta)\alpha_i\alpha_j} & \mathbf{A}_{\mathrm{T}\phi}^{(\tau\eta)\alpha_i\alpha_j} & \mathbf{A}_{\mathrm{T}\psi}^{(\tau\eta)\alpha_i\alpha_j} & \mathbf{A}_{\mathrm{TT}}^{(\tau\eta)\alpha_i\alpha_j} & \mathbf{A}_{\mathrm{TC}}^{(\tau\eta)\alpha_i\alpha_j} & \mathbf{0} & \mathbf{0} \\ \mathbf{A}_{\mathrm{C}\varepsilon}^{(\tau\eta)\alpha_i\alpha_j} & \mathbf{A}_{\mathrm{C}\phi}^{(\tau\eta)\alpha_i\alpha_j} & \mathbf{A}_{\mathrm{C}\psi}^{(\tau\eta)\alpha_i\alpha_j} & \mathbf{A}_{\mathrm{CT}}^{(\tau\eta)\alpha_i\alpha_j} & \mathbf{A}_{\mathrm{CC}}^{(\tau\eta)\alpha_i\alpha_j} & \mathbf{0} & \mathbf{0} \\ \mathbf{0} & \mathbf{0} & \mathbf{0} & \mathbf{0} & \mathbf{0} & \mathbf{A}_{\theta\theta}^{(\tau\eta)\alpha_i\alpha_j} & \mathbf{A}_{\theta\lambda}^{(\tau\eta)\alpha_i\alpha_j} \\ \mathbf{0} & \mathbf{0} & \mathbf{0} & \mathbf{0} & \mathbf{0} & \mathbf{A}_{\lambda\theta}^{(\tau\eta)\alpha_i\alpha_j} & \mathbf{A}_{\lambda\lambda}^{(\tau\eta)\alpha_i\alpha_j} \end{bmatrix} \tag{50}$$

The generic element of the matrix $\mathbf{A}^{(\tau\eta)\alpha_i\alpha_j}$, denoted by $A_{rsnm\,(pq)}^{(\tau\eta)[fg]\,\alpha_i\alpha_j}$, can be calculated using the following condensed relation [45]:

$$A_{rs\,nm\,(pq)}^{(\tau\eta)[fg]\,\alpha_i\alpha_j} = \sum_{k=1}^{l} \int_{\zeta_k}^{\zeta_{k+1}} \overline{\mathrm{Y}}_{nm}^{(k)} \frac{\partial^f F_\tau^{(k)\alpha_i}}{\partial \zeta^f} \frac{\partial^g F_\eta^{(k)\alpha_j}}{\partial \zeta^g} \frac{H_1 H_2}{H_1^p H_2^q} d\zeta \qquad \begin{array}{ll} \text{for} & \tau,\eta = 0,...,N+1 \\ \text{for} & n,m = 1,...,6 \\ \text{for} & p,q = 0,1,2 \\ \text{for} & i,j = 1,...,7 \end{array} \tag{51}$$

Introducing in Eqn. (50) the expression (24) of the generalized higher order strain vector $\boldsymbol{\pi}^{(\eta)\alpha_j}$ in terms of the higher order vector $\boldsymbol{\delta}^{(\eta)}$, the vector $\boldsymbol{\Sigma}^{(\tau)\alpha_i}$ is expressed in terms of the quantities $\boldsymbol{\delta}^{(\eta)}$ with $\eta = 0,...,N+1$ [45]:

$$\boldsymbol{\Sigma}^{(\tau)\alpha_i} = \sum_{\eta=0}^{N+1} \sum_{j=1}^{7} \mathbf{A}^{(\tau\eta)\alpha_i\alpha_j} \mathbf{D}_\Omega^{\alpha_j} \boldsymbol{\delta}^{(\eta)} = \sum_{\eta=0}^{N+1} \mathbf{O}^{(\tau\eta)\alpha_i} \boldsymbol{\delta}^{(\eta)} \tag{52}$$

Note that when the ESL kinematic model of Eqn. (10) cannot predict the stretching effect along the thickness direction, the three-dimensional elastic constants $\overline{\mathrm{Y}}_{nm}^{(k)}$ of Eqn. (52) are adjusted by means of the well-known shear correction factor $\kappa(\zeta) = 5/6$, as shown in the following relationship:

$$\overline{\mathrm{Y}}_{nm}^{(k)} = \kappa(\zeta)\overline{\Gamma}_{nm}^{(k)} \tag{53}$$

$$\begin{aligned} &\overline{C}_{\mathrm{R}nm}^{(k)} = \overline{C}_{nm}^{(k)} - \frac{\overline{C}_{m3}^{(k)}\overline{C}_{n3}^{(k)}}{\overline{C}_{33}^{(k)}},\ \overline{p}_{\mathrm{R}nm}^{(k)} = \overline{p}_{nm}^{(k)} - \frac{\overline{C}_{m3}^{(k)}\overline{p}_{n3}^{(k)}}{\overline{C}_{33}^{(k)}},\ \overline{q}_{\mathrm{R}nm}^{(k)} = \overline{q}_{nm}^{(k)} - \frac{\overline{C}_{m3}^{(k)}\overline{q}_{n3}^{(k)}}{\overline{C}_{33}^{(k)}} \\ &\overline{z}_{\mathrm{R}nm}^{(k)} = \overline{z}_{nm}^{(k)} - \frac{\overline{C}_{m3}^{(k)}\overline{z}_{33}^{(k)}}{\overline{C}_{33}^{(k)}},\ \overline{e}_{\mathrm{R}nm}^{(k)} = \overline{e}_{nm}^{(k)} - \frac{\overline{C}_{m3}^{(k)}\overline{e}_{33}^{(k)}}{\overline{C}_{33}^{(k)}},\ \overline{l}_{\mathrm{R}nm}^{(k)} = \overline{l}_{nm}^{(k)} + \frac{\overline{p}_{m3}^{(k)}\overline{p}_{n3}^{(k)}}{\overline{C}_{33}^{(k)}} \\ &\overline{m}_{\mathrm{R}nm}^{(k)} = \overline{m}_{nm}^{(k)} + \frac{\overline{q}_{m3}^{(k)}\overline{q}_{n3}^{(k)}}{\overline{C}_{33}^{(k)}},\ \overline{d}_{\mathrm{R}nm}^{(k)} = \overline{d}_{nm}^{(k)} + \frac{\overline{p}_{m3}^{(k)}\overline{q}_{n3}^{(k)}}{\overline{C}_{33}^{(k)}},\ \overline{o}_{\mathrm{R}nm}^{(k)} = \overline{o}_{nm}^{(k)} + \frac{\overline{z}_{33}^{(k)}\overline{p}_{n3}^{(k)}}{\overline{C}_{33}^{(k)}} \\ &\overline{g}_{\mathrm{R}nm}^{(k)} = \overline{g}_{nm}^{(k)} + \frac{\overline{e}_{33}^{(k)}\overline{p}_{n3}^{(k)}}{\overline{C}_{33}^{(k)}},\ \overline{w}_{\mathrm{R}nm}^{(k)} = \overline{w}_{nm}^{(k)} + \frac{\overline{z}_{33}^{(k)}\overline{q}_{n3}^{(k)}}{\overline{C}_{33}^{(k)}},\ \overline{f}_{\mathrm{R}nm}^{(k)} = \overline{f}_{nm}^{(k)} + \frac{\overline{e}_{33}^{(k)}\overline{q}_{n3}^{(k)}}{\overline{C}_{33}^{(k)}} \end{aligned} \tag{54}$$

5. Balance equations and external actions

At this point, the governing equations of the multifield problem for a doubly-curved shell structure are derived for the equilibrium thermodynamic condition, neglecting the irreversible processes. According to the Master Balance principle, the time integral of the virtual variation of the total energy of the system E or Hamiltonian Action restricted to an arbitrary time interval $[t_1,t_2]$ with $t_1 < t_2$ is equal to zero [45]:

$$\int_{t_1}^{t_2} \delta E\, dt = \int_{t_1}^{t_2} (\delta L - \delta Y) dt = 0 \tag{55}$$

where δL is the energy of generalized external actions, which is obtained from the sum of the energetic contributions $\delta L_{\mathrm{T}}, \delta L_{\mathrm{C}}$ associated with the reference entropy density and the reference chemical potential, respectively, and the quantityδL_s coming from the virtual work of the generalized external actions acting on the system and the energy associated with heat transfer processes. Furthermore, Y denotes the total free energy of the doubly-curved shell solid. More specifically, the generalized external surface actions are applied at the top (+) and the bottom (-) surfaces of the shell, located at $\zeta = h/2$ and $\zeta = -h/2$, respectively. Volumetric actions are neglected. In this way, δL_s can be written as the sum of the virtual work δL_{es} of the external mechanical loads $q_1^{(-)}$, $q_2^{(-)}$, $q_3^{(-)}$, $q_1^{(+)}$, $q_2^{(+)}$, $q_3^{(+)}$, the generalized virtual works $\delta L_{\phi s}, \delta L_{\psi s}$ of the electric and magnetic fluxes $q_{\mathrm{D}}^{(-)}$, $q_{\mathrm{D}}^{(+)}$ and $q_{\mathrm{B}}^{(-)}$, $q_{\mathrm{B}}^{(+)}$, and the generalized virtual works $\delta L_{\mathrm{T}s}$ and $\delta L_{\mathrm{C}s}$ associated with heat and mass transfer fluxes $q_{\mathrm{T}}^{(-)}$, $q_{\mathrm{T}}^{(+)}$ and $q_{\mathrm{C}}^{(-)}$, $q_{\mathrm{C}}^{(+)}$. If $\delta U_1^{(\pm)}, \delta U_2^{(\pm)}, \delta U_3^{(\pm)}, \delta\Delta\phi^{(\pm)}, \delta\Delta\psi^{(\pm)}, \delta\Delta\mathrm{T}^{(\pm)}, \delta\Delta\mathrm{C}^{(\pm)}$ denote the virtual variations of the three-dimensional configuration variables introduced in Eqn. (9) evaluated at the top and bottom surfaces of the solid, one gets the following relation [45]:

$$\begin{aligned} \delta L_s = \delta L_{es} + \delta L_{\phi s} + \delta L_{\psi s} + \delta Q_{\mathrm{T}s} + \delta Q_{\mathrm{C}s} = \int_{\alpha_1}\int_{\alpha_2} \Big(\Big(q_{1s}^{(-)}\delta U_1^{(-)} + q_{2s}^{(-)}\delta U_2^{(-)} + q_{3s}^{(-)}\delta U_3^{(-)} + \\ + q_{\mathrm{D}}^{(-)}\delta\Delta\phi^{(-)} + q_{\mathrm{B}}^{(-)}\delta\Delta\psi^{(-)} + \frac{q_{\mathrm{T}}^{(-)}}{\mathrm{T}_0}\delta\Delta\mathrm{T}^{(-)} + \frac{\mu_\infty q_{\mathrm{C}}^{(-)}}{\mathrm{C}_\infty}\delta\Delta\mathrm{C}^{(-)} \Big) H_1^{(-)} H_2^{(-)} + \Big(q_{1s}^{(+)}\delta U_1^{(+)} + q_{2s}^{(+)}\delta U_2^{(+)} + q_{3s}^{(+)}\delta U_3^{(+)} + \\ + \Big(q_{\mathrm{D}}^{(+)}\delta\Delta\phi^{(+)} + q_{\mathrm{B}}^{(+)}\delta\Delta\psi^{(+)} + \frac{q_{\mathrm{T}}^{(+)}}{\mathrm{T}_0}\delta\Delta\mathrm{T}^{(+)} + \frac{\mu_\infty q_{\mathrm{C}}^{(+)}}{\mathrm{C}_\infty}\delta\Delta\mathrm{C}^{(+)} \Big) H_1^{(+)} H_2^{(+)} \Big) A_1 A_2 d\alpha_1 d\alpha_2 \end{aligned} \tag{56}$$

where $\overline{\Gamma}_{nm}^{(k)} = \overline{C}_{nm}^{(k)}, \pm\overline{p}_{nm}^{(k)}, \pm\overline{q}_{nm}^{(k)}, \pm\overline{z}_{nm}^{(k)}, \pm\overline{e}_{nm}^{(k)}$. In addition, when the formulation in hand adopts the reduced multifield elastic coefficients, the following definitions are derived from the three-dimensional constitutive relation (28), setting $\sigma_3^{(k)} = 0$:

Note that the computation of δL_s is carried out as a generalization of the virtual work of mechanical elasticity because the secondary variables of each field are multiplied by the virtual variation of the corresponding configuration variables. To this end, generalized secondary variables are introduced for the heat and mass transfer equations so that

the dimensions of δL_{Ts} and δL_{Cs} are consistent with those of the other fields. In this way, it is correct to state that δL_s is written as the sum of the virtual works of the generalized multifield external actions of the problem under consideration. Note that the quantities $H_i^{(-)} = H_1^{(-)}, H_2^{(-)}$ and $H_i^{(+)} = H_1^{(+)}, H_2^{(+)}$ adopted in Eqn. (57) denote the geometric scaling parameters evaluated for $\zeta = -h/2$ and $\zeta = h/2$, respectively. These quantities are calculated as $H_i^{(-)} = 1 - h/(2R_i)$ and $H_i^{(+)} = 1 + h/(2R_i)$.

At this point, the generalized loads $q_{1s}^{(\tau)}$, $q_{2s}^{(\tau)}$, $q_{3s}^{(\tau)}$, $q_{Ds}^{(\tau)}$, $q_{Bs}^{(\tau)}$, $q_{Ts}^{(\tau)}$, $q_{Cs}^{(\tau)}$ are introduced for each τ-th kinematic expansion order, which act on the reference surface of the shell, following the ESL model. The generalized virtual work of these actions can be evaluated as follows:

$$\delta L_{is} = \int_{\alpha_1}\int_{\alpha_2}\sum_{\tau=0}^{N+1}\left(q_{1s}^{(\tau)}\delta u_1^{(\tau)} + q_{2s}^{(\tau)}\delta u_2^{(\tau)} + q_{3s}^{(\tau)}\delta u_3^{(\tau)} + q_{Ds}^{(\tau)}\delta\phi^{(\tau)} + q_{Bs}^{(\tau)}\delta\psi^{(\tau)} + \frac{q_{Ts}^{(\tau)}}{T_0}\delta\xi^{(\tau)} + \frac{\mu_\infty q_{Cs}^{(\tau)}}{C_\infty}\delta\kappa^{(\tau)}\right) A_1 A_2 d\alpha_1 d\alpha_2 \tag{57}$$

where $\delta u_1^{(\tau)}, \delta u_2^{(\tau)}, \delta u_3^{(\tau)}, \delta\phi^{(\tau)}, \delta\psi^{(\tau)}, \delta\xi^{(\tau)}$ and $\delta\kappa^{(\tau)}$ represent the virtual variations of the generalized configuration variables introduced in Eqn. (10). According to the static equivalence principle, the virtual work of Eqn. (57) of the external surface actions is taken to be equal to that of the generalized external actions, as reported in Eqn. (59). By introducing the kinematic model (10) into Eqn. (57), an expression can be derived for each $\tau = 0, ..., N+1$, representing the generalized multifield external actions in terms of the magnitudes of the external loads acting on the three-dimensional solid [45]:

$$\begin{aligned}
q_{1s}^{(\tau)} &= q_{1s}^{(-)} F_\tau^{(1)\alpha_1(-)} H_1^{(-)} H_2^{(-)} + q_{1s}^{(+)} F_\tau^{(l)\alpha_1(+)} H_1^{(+)} H_2^{(+)} \\
q_{2s}^{(\tau)} &= q_{2s}^{(-)} F_\tau^{(1)\alpha_2(-)} H_1^{(-)} H_2^{(-)} + q_{2s}^{(+)} F_\tau^{(l)\alpha_2(+)} H_1^{(+)} H_2^{(+)} \\
q_{3s}^{(\tau)} &= q_{3s}^{(-)} F_\tau^{(1)\alpha_3(-)} H_1^{(-)} H_2^{(-)} + q_{3s}^{(+)} F_\tau^{(l)\alpha_3(+)} H_1^{(+)} H_2^{(+)} \\
q_{Ds}^{(\tau)} &= q_{D}^{(-)} F_\tau^{(1)\alpha_4(-)} H_1^{(-)} H_2^{(-)} + q_{D}^{(+)} F_\tau^{(l)\alpha_4(+)} H_1^{(+)} H_2^{(+)} \\
q_{Bs}^{(\tau)} &= q_{B}^{(-)} F_\tau^{(1)\alpha_5(-)} H_1^{(-)} H_2^{(-)} + q_{B}^{(+)} F_\tau^{(l)\alpha_5(+)} H_1^{(+)} H_2^{(+)} \\
q_{Ts}^{(\tau)} &= q_{T}^{(-)} F_\tau^{(1)\alpha_6(-)} H_1^{(-)} H_2^{(-)} + q_{T}^{(+)} F_\tau^{(l)\alpha_6(+)} H_1^{(+)} H_2^{(+)} \\
q_{Cs}^{(\tau)} &= q_{C}^{(-)} F_\tau^{(1)\alpha_7(-)} H_1^{(-)} H_2^{(-)} + q_{C}^{(+)} F_\tau^{(l)\alpha_7(+)} H_1^{(+)} H_2^{(+)}
\end{aligned} \tag{58}$$

Finally, it is convenient to collect the generalized external actions of Eqn. (60) in the algebraic vector $\mathbf{q}^{(\tau)}$, defined for each $\tau = 0, ..., N+1$:

$$\mathbf{q}^{(\tau)} = \begin{bmatrix} q_{1s}^{(\tau)} & q_{2s}^{(\tau)} & q_{3s}^{(\tau)} & q_{Ds}^{(\tau)} & q_{Bs}^{(\tau)} & q_{Ts}^{(\tau)} & q_{Cs}^{(\tau)} \end{bmatrix}^T \tag{59}$$

If the quantities $\overline{\eta}^{(k)}$ and $\overline{\mu}^{(k)}$ represent the values of the reference entropy density and the reference specific chemical potential of the system at an arbitrary point in a k-th layer, respectively, the virtual works δL_T and δL_C introduced previously can be calculated as follows:

$$\begin{aligned}
\delta L_T &= -\sum_{k=1}^{l}\int_{\zeta_k}^{\zeta_{k+1}}\int_{\alpha_1}\int_{\alpha_2}\overline{\eta}^{(k)}\delta\Delta T^{(k)} H_1 H_2 A_1 A_2 d\alpha_1 d\alpha_2 d\zeta \\
\delta L_C &= -\sum_{k=1}^{l}\int_{\zeta_k}^{\zeta_{k+1}}\int_{\alpha_1}\int_{\alpha_2}\overline{\mu}^{(k)}\delta\Delta C^{(k)} H_1 H_2 A_1 A_2 d\alpha_1 d\alpha_2 d\zeta
\end{aligned} \tag{60}$$

For irreversible processes, it is assumed that the time integral of the quantities introduced in the previous equation assumes a null value.

The virtual variation δY of the total free energy, as presented in Eqn. (56), is expressed in terms of the virtual variation $\delta\overline{\pi}^{(k)}$ of the generalized strain characteristics as reported in Eqn. (44). It gives:

$$\begin{aligned}
&\delta Y = \delta K - \delta E_Q = \\
&= \sum_{k=1}^{l}\int_{\alpha_1}\int_{\alpha_2}\int_{\zeta_k}^{\zeta_{k+1}}\delta\overline{\boldsymbol{\pi}}^{(k)T}\overline{\boldsymbol{\chi}}^{(k)} A_1 A_2 H_1 H_2 d\zeta d\alpha_1 d\alpha_2 = \sum_{\tau=0}^{N+1}\sum_{i=1}^{7}\int_{\alpha_1}\int_{\alpha_2}\left(\delta\boldsymbol{\pi}^{(\tau)\alpha_i}\right)^T\widetilde{\boldsymbol{\Sigma}}^{(\tau)\alpha_i} A_1 A_2 d\alpha_1 d\alpha_2 = \\
&= \sum_{\tau=0}^{N+1}\sum_{i=1}^{7}\int_{\alpha_1}\int_{\alpha_2}\left(\delta\boldsymbol{\varepsilon}^{(\tau)\alpha_i}\right)^T\mathbf{S}^{(\tau)\alpha_i} A_1 A_2 d\alpha_1 d\alpha_2 - \sum_{\tau=0}^{N+1}\sum_{i=1}^{7}\int_{\alpha_1}\int_{\alpha_2}\left(\delta\mathbf{E}^{(\tau)\alpha_i}\right)^T\mathbf{D}^{(\tau)\alpha_i} A_1 A_2 d\alpha_1 d\alpha_2 + \\
&- \sum_{\tau=0}^{N+1}\sum_{i=1}^{7}\int_{\alpha_1}\int_{\alpha_2}\left(\delta\mathbf{H}^{(\tau)\alpha_i}\right)^T\mathbf{B}^{(\tau)\alpha_i} A_1 A_2 d\alpha_1 d\alpha_2 - \sum_{\tau=0}^{N+1}\sum_{i=1}^{7}\int_{\alpha_1}\int_{\alpha_2}\left(\delta\boldsymbol{\theta}^{(\tau)\alpha_i}\right)^T\left(\frac{1}{T_0}\mathbf{H}^{(\tau)\alpha_i} + \frac{\mu_\infty}{T_0}\mathbf{C}^{(\tau)\alpha_i}\right) A_1 A_2 d\alpha_1 d\alpha_2 + \\
&- \sum_{\tau=0}^{N+1}\sum_{i=1}^{7}\int_{\alpha_1}\int_{\alpha_2}\left(\delta\boldsymbol{\lambda}^{(\tau)\alpha_i}\right)^T\left(\frac{\mu_\infty}{C_\infty}\mathbf{C}^{(\tau)\alpha_i}\right) A_1 A_2 d\alpha_1 d\alpha_2 + \\
&- \sum_{\tau=0}^{N+1}\sum_{i=1}^{7}\int_{\alpha_1}\int_{\alpha_2}E^{(\tau)\alpha_i}\delta\widehat{\Delta T}^{(\tau)\alpha_i} A_1 A_2 d\alpha_1 d\alpha_2 - \sum_{\tau=0}^{N+1}\sum_{i=1}^{7}\int_{\alpha_1}\int_{\alpha_2}M^{(\tau)\alpha_i}\delta\widehat{\Delta C}^{(\tau)\alpha_i} A_1 A_2 d\alpha_1 d\alpha_2
\end{aligned} \tag{61}$$

At this point, the definition of the generalized strain characteristics is introduced into the previous equation, and the integration by parts rule is applied. Then, Eqn. (59) and Eqn. (63) are integrated in the time interval $[t_1, t_2]$ and substituted into Eqn. (56).Recalling that the time integral in hand is set equal to zero, the balance equations of the multifield problem are obtained [45]:

$$
\begin{aligned}
&\frac{1}{A_1}\frac{\partial N_1^{(\tau)\alpha_1}}{\partial \alpha_1} + \frac{N_1^{(\tau)\alpha_1}}{A_1 A_2}\frac{\partial A_2}{\partial \alpha_1} + \frac{1}{A_2}\frac{\partial N_{21}^{(\tau)\alpha_1}}{\partial \alpha_2} + \frac{N_{21}^{(\tau)\alpha_1}}{A_1 A_2}\frac{\partial A_1}{\partial \alpha_2} + \frac{N_{12}^{(\tau)\alpha_1}}{A_1 A_2}\frac{\partial A_1}{\partial \alpha_2} \\
&\quad - \frac{N_2^{(\tau)\alpha_1}}{A_1 A_2}\frac{\partial A_2}{\partial \alpha_1} + \frac{T_1^{(\tau)\alpha_1}}{R_1} - P_1^{(\tau)\alpha_1} + q_{1s}^{(\tau)} \\
&\quad = 0 \\[2ex]
&\frac{1}{A_2}\frac{\partial N_2^{(\tau)\alpha_2}}{\partial \alpha_2} + \frac{N_2^{(\tau)\alpha_2}}{A_1 A_2}\frac{\partial A_1}{\partial \alpha_2} + \frac{1}{A_1}\frac{\partial N_{12}^{(\tau)\alpha_2}}{\partial \alpha_1} + \frac{N_{12}^{(\tau)\alpha_2}}{A_1 A_2}\frac{\partial A_2}{\partial \alpha_1} + \frac{N_{21}^{(\tau)\alpha_2}}{A_1 A_2}\frac{\partial A_2}{\partial \alpha_1} \\
&\quad - \frac{N_1^{(\tau)\alpha_2}}{A_1 A_2}\frac{\partial A_1}{\partial \alpha_2} + \frac{T_2^{(\tau)\alpha_2}}{R_2} - P_2^{(\tau)\alpha_2} + q_{2s}^{(\tau)} \\
&\quad = 0 \\[2ex]
&\frac{1}{A_1}\frac{\partial T_1^{(\tau)\alpha_3}}{\partial \alpha_1} + \frac{T_1^{(\tau)\alpha_3}}{A_1 A_2}\frac{\partial A_2}{\partial \alpha_1} + \frac{1}{A_2}\frac{\partial T_2^{(\tau)\alpha_3}}{\partial \alpha_2} + \frac{T_2^{(\tau)\alpha_3}}{A_1 A_2}\frac{\partial A_1}{\partial \alpha_2} - \frac{N_1^{(\tau)\alpha_3}}{R_1} - \frac{N_2^{(\tau)\alpha_3}}{R_2} - S_3^{(\tau)\alpha_3} \\
&\quad + q_{3s}^{(\tau)} \\
&\quad = 0 \\[2ex]
&\frac{1}{A_1}\frac{\partial D_1^{(\tau)\alpha_4}}{\partial \alpha_1} + \frac{D_1^{(\tau)\alpha_4}}{A_1 A_2}\frac{\partial A_2}{\partial \alpha_1} + \frac{1}{A_2}\frac{\partial D_2^{(\tau)\alpha_4}}{\partial \alpha_2} + \frac{D_2^{(\tau)\alpha_4}}{A_1 A_2}\frac{\partial A_1}{\partial \alpha_2} - D_3^{(\tau)\alpha_4} + q_{\mathrm{D}s}^{(\tau)} = 0 \\[2ex]
&\frac{1}{A_1}\frac{\partial B_1^{(\tau)\alpha_5}}{\partial \alpha_1} + \frac{B_1^{(\tau)\alpha_5}}{A_1 A_2}\frac{\partial A_2}{\partial \alpha_1} + \frac{1}{A_2}\frac{\partial B_2^{(\tau)\alpha_5}}{\partial \alpha_2} + \frac{B_2^{(\tau)\alpha_5}}{A_1 A_2}\frac{\partial A_1}{\partial \alpha_2} - B_3^{(\tau)\alpha_5} + q_{\mathrm{B}s}^{(\tau)} = 0 \\[2ex]
&\frac{1}{A_1}\frac{\partial H_1^{(\tau)\alpha_6}}{\partial \alpha_1} + \frac{H_1^{(\tau)\alpha_6}}{A_1 A_2}\frac{\partial A_2}{\partial \alpha_1} + \frac{1}{A_2}\frac{\partial H_2^{(\tau)\alpha_6}}{\partial \alpha_2} + \frac{H_2^{(\tau)\alpha_6}}{A_1 A_2}\frac{\partial A_1}{\partial \alpha_2} - H_3^{(\tau)\alpha_6} + q_{\mathrm{T}s}^{(\tau)} = 0 \\[2ex]
&\frac{1}{A_1}\frac{\partial C_1^{(\tau)\alpha_7}}{\partial \alpha_1} + \frac{C_1^{(\tau)\alpha_7}}{A_1 A_2}\frac{\partial A_2}{\partial \alpha_1} + \frac{1}{A_2}\frac{\partial C_2^{(\tau)\alpha_7}}{\partial \alpha_2} + \frac{C_2^{(\tau)\alpha_7}}{A_1 A_2}\frac{\partial A_1}{\partial \alpha_2} - C_3^{(\tau)\alpha_7} + q_{\mathrm{C}s}^{(\tau)} = 0
\end{aligned}
\tag{62}
$$

As can be seen, in the previous relation it is assumed that the external loads come from generalized surface actions applied at the top and the bottom surfaces of the panel, whereas volumetric actions are neglected. In a more compact matrix form, Eqn. (64) can be expressed as follows:

$$
\sum_{i=1}^{7} \mathbf{D}_{\Omega}^{*\alpha_i} \boldsymbol{\Sigma}^{(\tau)\alpha_i} + \mathbf{q}^{(\tau)} = \mathbf{0} \tag{63}
$$

for $\tau = 0, \ldots, N+1$. In the previous equation, the matrices $\mathbf{D}_{\Omega}^{*\alpha_i}$ with $i = 1, \ldots, 7$ denote the equilibrium operators, whose definition is reported in the following:

$$
\mathbf{D}_{\Omega}^{*\alpha_1} = \begin{bmatrix}
\overline{\mathbf{D}}_{\Omega}^{*\alpha_1} & \mathbf{0} & \mathbf{0} & \mathbf{0} & \mathbf{0} & \mathbf{0} & \mathbf{0} \\
\mathbf{0} & \mathbf{0} & \mathbf{0} & \mathbf{0} & \mathbf{0} & \mathbf{0} & \mathbf{0} \\
\mathbf{0} & \mathbf{0} & \mathbf{0} & \mathbf{0} & \mathbf{0} & \mathbf{0} & \mathbf{0} \\
\mathbf{0} & \mathbf{0} & \mathbf{0} & \mathbf{0} & \mathbf{0} & \mathbf{0} & \mathbf{0} \\
\mathbf{0} & \mathbf{0} & \mathbf{0} & \mathbf{0} & \mathbf{0} & \mathbf{0} & \mathbf{0} \\
\mathbf{0} & \mathbf{0} & \mathbf{0} & \mathbf{0} & \mathbf{0} & \mathbf{0} & \mathbf{0} \\
\mathbf{0} & \mathbf{0} & \mathbf{0} & \mathbf{0} & \mathbf{0} & \mathbf{0} & \mathbf{0}
\end{bmatrix}, \quad
\mathbf{D}_{\Omega}^{*\alpha_2} = \begin{bmatrix}
\mathbf{0} & \mathbf{0} & \mathbf{0} & \mathbf{0} & \mathbf{0} & \mathbf{0} & \mathbf{0} \\
\overline{\mathbf{D}}_{\Omega}^{*\alpha_2} & \mathbf{0} & \mathbf{0} & \mathbf{0} & \mathbf{0} & \mathbf{0} & \mathbf{0} \\
\mathbf{0} & \mathbf{0} & \mathbf{0} & \mathbf{0} & \mathbf{0} & \mathbf{0} & \mathbf{0} \\
\mathbf{0} & \mathbf{0} & \mathbf{0} & \mathbf{0} & \mathbf{0} & \mathbf{0} & \mathbf{0} \\
\mathbf{0} & \mathbf{0} & \mathbf{0} & \mathbf{0} & \mathbf{0} & \mathbf{0} & \mathbf{0} \\
\mathbf{0} & \mathbf{0} & \mathbf{0} & \mathbf{0} & \mathbf{0} & \mathbf{0} & \mathbf{0} \\
\mathbf{0} & \mathbf{0} & \mathbf{0} & \mathbf{0} & \mathbf{0} & \mathbf{0} & \mathbf{0}
\end{bmatrix}, \quad
\mathbf{D}_{\Omega}^{*\alpha_3} = \begin{bmatrix}
\mathbf{0} & \mathbf{0} & \mathbf{0} & \mathbf{0} & \mathbf{0} & \mathbf{0} & \mathbf{0} \\
\mathbf{0} & \mathbf{0} & \mathbf{0} & \mathbf{0} & \mathbf{0} & \mathbf{0} & \mathbf{0} \\
\overline{\mathbf{D}}_{\Omega}^{*\alpha_3} & \mathbf{0} & \mathbf{0} & \mathbf{0} & \mathbf{0} & \mathbf{0} & \mathbf{0} \\
\mathbf{0} & \mathbf{0} & \mathbf{0} & \mathbf{0} & \mathbf{0} & \mathbf{0} & \mathbf{0} \\
\mathbf{0} & \mathbf{0} & \mathbf{0} & \mathbf{0} & \mathbf{0} & \mathbf{0} & \mathbf{0} \\
\mathbf{0} & \mathbf{0} & \mathbf{0} & \mathbf{0} & \mathbf{0} & \mathbf{0} & \mathbf{0} \\
\mathbf{0} & \mathbf{0} & \mathbf{0} & \mathbf{0} & \mathbf{0} & \mathbf{0} & \mathbf{0}
\end{bmatrix},
$$

$$
\mathbf{D}_{\Omega}^{*\alpha_4} = \begin{bmatrix}
\mathbf{0} & \mathbf{0} & \mathbf{0} & \mathbf{0} & \mathbf{0} & \mathbf{0} & \mathbf{0} \\
\mathbf{0} & \mathbf{0} & \mathbf{0} & \mathbf{0} & \mathbf{0} & \mathbf{0} & \mathbf{0} \\
\mathbf{0} & \mathbf{0} & \mathbf{0} & \mathbf{0} & \mathbf{0} & \mathbf{0} & \mathbf{0} \\
\mathbf{0} & \overline{\mathbf{D}}_{\Omega}^{*\alpha_4} & \mathbf{0} & \mathbf{0} & \mathbf{0} & \mathbf{0} & \mathbf{0} \\
\mathbf{0} & \mathbf{0} & \mathbf{0} & \mathbf{0} & \mathbf{0} & \mathbf{0} & \mathbf{0} \\
\mathbf{0} & \mathbf{0} & \mathbf{0} & \mathbf{0} & \mathbf{0} & \mathbf{0} & \mathbf{0} \\
\mathbf{0} & \mathbf{0} & \mathbf{0} & \mathbf{0} & \mathbf{0} & \mathbf{0} & \mathbf{0}
\end{bmatrix}, \quad
\mathbf{D}_{\Omega}^{*\alpha_5} = \begin{bmatrix}
\mathbf{0} & \mathbf{0} & \mathbf{0} & \mathbf{0} & \mathbf{0} & \mathbf{0} & \mathbf{0} \\
\mathbf{0} & \mathbf{0} & \mathbf{0} & \mathbf{0} & \mathbf{0} & \mathbf{0} & \mathbf{0} \\
\mathbf{0} & \mathbf{0} & \mathbf{0} & \mathbf{0} & \mathbf{0} & \mathbf{0} & \mathbf{0} \\
\mathbf{0} & \mathbf{0} & \mathbf{0} & \mathbf{0} & \mathbf{0} & \mathbf{0} & \mathbf{0} \\
\mathbf{0} & \mathbf{0} & \overline{\mathbf{D}}_{\Omega}^{*\alpha_5} & \mathbf{0} & \mathbf{0} & \mathbf{0} & \mathbf{0} \\
\mathbf{0} & \mathbf{0} & \mathbf{0} & \mathbf{0} & \mathbf{0} & \mathbf{0} & \mathbf{0} \\
\mathbf{0} & \mathbf{0} & \mathbf{0} & \mathbf{0} & \mathbf{0} & \mathbf{0} & \mathbf{0}
\end{bmatrix}, \quad
\mathbf{D}_{\Omega}^{*\alpha_6} = \begin{bmatrix}
\mathbf{0} & \mathbf{0} & \mathbf{0} & \mathbf{0} & \mathbf{0} & \mathbf{0} & \mathbf{0} \\
\mathbf{0} & \mathbf{0} & \mathbf{0} & \mathbf{0} & \mathbf{0} & \mathbf{0} & \mathbf{0} \\
\mathbf{0} & \mathbf{0} & \mathbf{0} & \mathbf{0} & \mathbf{0} & \mathbf{0} & \mathbf{0} \\
\mathbf{0} & \mathbf{0} & \mathbf{0} & \mathbf{0} & \mathbf{0} & \mathbf{0} & \mathbf{0} \\
\mathbf{0} & \mathbf{0} & \mathbf{0} & \mathbf{0} & \mathbf{0} & \mathbf{0} & \mathbf{0} \\
\mathbf{0} & \mathbf{0} & \mathbf{0} & \mathbf{0} & \mathbf{0} & \overline{\mathbf{D}}_{\Omega}^{*\alpha_6} & \mathbf{0} \\
\mathbf{0} & \mathbf{0} & \mathbf{0} & \mathbf{0} & \mathbf{0} & \mathbf{0} & \mathbf{0}
\end{bmatrix},
$$

$$
\mathbf{D}_{\Omega}^{*\alpha_7} = \begin{bmatrix} \mathbf{0} & \mathbf{0} & \mathbf{0} & \mathbf{0} & \mathbf{0} & \mathbf{0} & \mathbf{0} \\ \mathbf{0} & \mathbf{0} & \mathbf{0} & \mathbf{0} & \mathbf{0} & \mathbf{0} & \mathbf{0} \\ \mathbf{0} & \mathbf{0} & \mathbf{0} & \mathbf{0} & \mathbf{0} & \mathbf{0} & \mathbf{0} \\ \mathbf{0} & \mathbf{0} & \mathbf{0} & \mathbf{0} & \mathbf{0} & \mathbf{0} & \mathbf{0} \\ \mathbf{0} & \mathbf{0} & \mathbf{0} & \mathbf{0} & \mathbf{0} & \mathbf{0} & \mathbf{0} \\ \mathbf{0} & \mathbf{0} & \mathbf{0} & \mathbf{0} & \mathbf{0} & \mathbf{0} & \mathbf{0} \\ \mathbf{0} & \mathbf{0} & \mathbf{0} & \mathbf{0} & \mathbf{0} & \mathbf{0} & \overline{\mathbf{D}}_{\Omega}^{*\alpha_7} \end{bmatrix} \tag{64}
$$

where the sub-matrices $\overline{\mathbf{D}}_{\Omega}^{*\alpha_i}$ assume the following aspect:

$$
\begin{aligned}
\overline{\mathbf{D}}_{\Omega}^{*\alpha_1} &= \left[\frac{1}{A_1}\frac{\partial}{\partial\alpha_1} + \frac{1}{A_1A_2}\frac{\partial A_2}{\partial\alpha_1} \quad -\frac{1}{A_1A_2}\frac{\partial A_2}{\partial\alpha_1} \quad \frac{1}{A_1A_2}\frac{\partial A_1}{\partial\alpha_2} \quad \frac{1}{A_2}\frac{\partial}{\partial\alpha_2} + \frac{1}{A_1A_2}\frac{\partial A_1}{\partial\alpha_2} \quad \frac{1}{R_1} \quad 0 \quad -1 \quad 0 \quad 0 \right] \\
\overline{\mathbf{D}}_{\Omega}^{*\alpha_2} &= \left[-\frac{1}{A_1A_2}\frac{\partial A_1}{\partial\alpha_2} \quad \frac{1}{A_2}\frac{\partial}{\partial\alpha_2} + \frac{1}{A_1A_2}\frac{\partial A_1}{\partial\alpha_2} \quad \frac{1}{A_1}\frac{\partial}{\partial\alpha_1} + \frac{1}{A_1A_2}\frac{\partial A_2}{\partial\alpha_1} \quad \frac{1}{A_1A_2}\frac{\partial A_2}{\partial\alpha_1} \quad 0 \quad \frac{1}{R_2} \quad 0 \quad -1 \quad 0 \right] \\
\overline{\mathbf{D}}_{\Omega}^{*\alpha_3} &= \left[-\frac{1}{R_1} \quad -\frac{1}{R_2} \quad 0 \quad 0 \quad \frac{1}{A_1}\frac{\partial}{\partial\alpha_1} + \frac{1}{A_1A_2}\frac{\partial A_2}{\partial\alpha_1} \quad \frac{1}{A_2}\frac{\partial}{\partial\alpha_2} + \frac{1}{A_1A_2}\frac{\partial A_1}{\partial\alpha_2} \quad 0 \quad 0 \quad -1 \right] \\
\overline{\mathbf{D}}_{\Omega}^{*\alpha_4} &= \overline{\mathbf{D}}_{\Omega}^{*\alpha_5} = \overline{\mathbf{D}}_{\Omega}^{*\alpha_6} = \overline{\mathbf{D}}_{\Omega}^{*\alpha_7} = \left[\frac{1}{A_1}\frac{\partial}{\partial\alpha_1} + \frac{1}{A_1A_2}\frac{\partial A_2}{\partial\alpha_1} \quad \frac{1}{A_2}\frac{\partial}{\partial\alpha_2} + \frac{1}{A_1A_2}\frac{\partial A_1}{\partial\alpha_2} \quad -1 \right]
\end{aligned} \tag{65}
$$

The Master Balance principle, as defined in Eqn. (56), also yields the following boundary conditions along the edges of the two-dimensional physical domain:

$$
\begin{aligned}
&\left(\overline{N}_1^{(\tau)\alpha_1} - N_1^{(\tau)\alpha_1}\right)\delta u_1^{(\tau)} = 0 \quad &&\left(\overline{N}_{21}^{(\tau)\alpha_1} - N_{21}^{(\tau)\alpha_1}\right)\delta u_1^{(\tau)} = 0 \\
&\left(\overline{N}_{12}^{(\tau)\alpha_2} - N_{12}^{(\tau)\alpha_2}\right)\delta u_2^{(\tau)} = 0 \quad &&\left(\overline{N}_2^{(\tau)\alpha_2} - N_2^{(\tau)\alpha_2}\right)\delta u_2^{(\tau)} = 0 \\
&\left(\overline{T}_1^{(\tau)\alpha_3} - T_1^{(\tau)\alpha_3}\right)\delta u_3^{(\tau)} = 0 \quad &&\left(\overline{T}_2^{(\tau)\alpha_3} - T_2^{(\tau)\alpha_3}\right)\delta u_3^{(\tau)} = 0 \\
&\left(\overline{D}_1^{(\tau)\alpha_4} - D_1^{(\tau)\alpha_4}\right)\delta \phi^{(\tau)} = 0 \quad &&\left(\overline{D}_2^{(\tau)\alpha_4} - D_2^{(\tau)\alpha_4}\right)\delta \phi^{(\tau)} = 0 \\
&\left(\overline{B}_1^{(\tau)\alpha_5} - B_1^{(\tau)\alpha_5}\right)\delta \psi^{(\tau)} = 0 \quad &&\left(\overline{B}_2^{(\tau)\alpha_5} - B_2^{(\tau)\alpha_5}\right)\delta \psi^{(\tau)} = 0 \\
&\left(\overline{H}_1^{(\tau)\alpha_6} - H_1^{(\tau)\alpha_6}\right)\delta \xi^{(\tau)} = 0 \quad &&\left(\overline{H}_2^{(\tau)\alpha_6} - H_2^{(\tau)\alpha_6}\right)\delta \xi^{(\tau)} = 0 \\
&\left(\overline{C}_1^{(\tau)\alpha_7} - C_1^{(\tau)\alpha_7}\right)\delta \kappa^{(\tau)} = 0 \quad &&\left(\overline{C}_2^{(\tau)\alpha_7} - C_2^{(\tau)\alpha_7}\right)\delta \kappa^{(\tau)} = 0
\end{aligned} \tag{66}
$$

Introducing the generalized constitutive relationship of Eqn. (50) into the balance multifield relations (65) and taking into account the higher order kinematic relations (24), the fundamental relations of the multifield problem are obtained, in which a relation is provided that links the vector $\boldsymbol{\delta}^{(\eta)}$ of the generalized configuration variables and the vector $\mathbf{q}^{(\tau)}$ of the external loads [45]:

$$
\sum_{\eta=0}^{N+1} \mathbf{L}^{(\tau\eta)}\boldsymbol{\delta}^{(\eta)} + \mathbf{q}^{(\tau)} = \mathbf{0} \tag{67}
$$

for $\tau = 0, ..., N+1$. The matrix $\mathbf{L}^{(\tau\eta)}$ is the higher order fundamental operator, whose elements $L_{ij}^{(\tau\eta)\alpha_i\alpha_j}$ with $i, j = 1, ..., 7$ are evaluated according to the following relations:

$$
\mathbf{L}^{(\tau\eta)} = \begin{bmatrix}
L_{11}^{(\tau\eta)\alpha_1\alpha_1} & L_{12}^{(\tau\eta)\alpha_1\alpha_2} & L_{13}^{(\tau\eta)\alpha_1\alpha_3} & L_{14}^{(\tau\eta)\alpha_1\alpha_4} & L_{15}^{(\tau\eta)\alpha_1\alpha_5} & L_{16}^{(\tau\eta)\alpha_1\alpha_6} & L_{17}^{(\tau\eta)\alpha_1\alpha_7} \\
L_{21}^{(\tau\eta)\alpha_2\alpha_1} & L_{22}^{(\tau\eta)\alpha_2\alpha_2} & L_{23}^{(\tau\eta)\alpha_2\alpha_3} & L_{24}^{(\tau\eta)\alpha_2\alpha_4} & L_{25}^{(\tau\eta)\alpha_2\alpha_5} & L_{26}^{(\tau\eta)\alpha_2\alpha_6} & L_{27}^{(\tau\eta)\alpha_2\alpha_7} \\
L_{31}^{(\tau\eta)\alpha_3\alpha_1} & L_{32}^{(\tau\eta)\alpha_3\alpha_2} & L_{33}^{(\tau\eta)\alpha_3\alpha_3} & L_{34}^{(\tau\eta)\alpha_3\alpha_4} & L_{35}^{(\tau\eta)\alpha_3\alpha_5} & L_{36}^{(\tau\eta)\alpha_3\alpha_6} & L_{37}^{(\tau\eta)\alpha_3\alpha_7} \\
L_{41}^{(\tau\eta)\alpha_4\alpha_1} & L_{42}^{(\tau\eta)\alpha_4\alpha_2} & L_{43}^{(\tau\eta)\alpha_4\alpha_3} & L_{44}^{(\tau\eta)\alpha_4\alpha_4} & L_{45}^{(\tau\eta)\alpha_4\alpha_5} & L_{46}^{(\tau\eta)\alpha_4\alpha_6} & L_{47}^{(\tau\eta)\alpha_4\alpha_7} \\
L_{51}^{(\tau\eta)\alpha_5\alpha_1} & L_{52}^{(\tau\eta)\alpha_5\alpha_2} & L_{53}^{(\tau\eta)\alpha_5\alpha_3} & L_{54}^{(\tau\eta)\alpha_5\alpha_4} & L_{55}^{(\tau\eta)\alpha_5\alpha_5} & L_{56}^{(\tau\eta)\alpha_5\alpha_6} & L_{57}^{(\tau\eta)\alpha_5\alpha_7} \\
L_{61}^{(\tau\eta)\alpha_6\alpha_1} & L_{62}^{(\tau\eta)\alpha_6\alpha_2} & L_{63}^{(\tau\eta)\alpha_6\alpha_3} & L_{64}^{(\tau\eta)\alpha_6\alpha_4} & L_{65}^{(\tau\eta)\alpha_6\alpha_5} & L_{66}^{(\tau\eta)\alpha_6\alpha_6} & L_{67}^{(\tau\eta)\alpha_6\alpha_7} \\
L_{71}^{(\tau\eta)\alpha_7\alpha_1} & L_{72}^{(\tau\eta)\alpha_7\alpha_2} & L_{73}^{(\tau\eta)\alpha_7\alpha_3} & L_{74}^{(\tau\eta)\alpha_7\alpha_4} & L_{75}^{(\tau\eta)\alpha_7\alpha_5} & L_{76}^{(\tau\eta)\alpha_7\alpha_6} & L_{77}^{(\tau\eta)\alpha_7\alpha_7}
\end{bmatrix} =
$$

$$
= \begin{bmatrix}
\overline{\mathbf{D}}_{\Omega}^{*\alpha_1}\mathbf{A}_{uu}^{(\tau\eta)\alpha_1\alpha_1}\overline{\mathbf{D}}_{\Omega}^{\alpha_1} & \overline{\mathbf{D}}_{\Omega}^{*\alpha_1}\mathbf{A}_{uu}^{(\tau\eta)\alpha_1\alpha_2}\overline{\mathbf{D}}_{\Omega}^{\alpha_2} & \overline{\mathbf{D}}_{\Omega}^{*\alpha_1}\mathbf{A}_{uu}^{(\tau\eta)\alpha_1\alpha_3}\overline{\mathbf{D}}_{\Omega}^{\alpha_3} & \overline{\mathbf{D}}_{\Omega}^{*\alpha_1}\mathbf{A}_{u\phi}^{(\tau\eta)\alpha_1\alpha_4}\overline{\mathbf{D}}_{\Omega}^{\alpha_4} & \overline{\mathbf{D}}_{\Omega}^{*\alpha_1}\mathbf{A}_{u\psi}^{(\tau\eta)\alpha_1\alpha_5}\overline{\mathbf{D}}_{\Omega}^{\alpha_5} & \overline{\mathbf{D}}_{\Omega}^{*\alpha_1}\mathbf{A}_{u\vartheta}^{(\tau\eta)\alpha_1\alpha_6}\overline{\mathbf{D}}_{\Omega}^{\alpha_6} & \overline{\mathbf{D}}_{\Omega}^{*\alpha_1}\mathbf{A}_{uC}^{(\tau\eta)\alpha_1\alpha_7}\overline{\mathbf{D}}_{\Omega}^{\alpha_7} \\
\overline{\mathbf{D}}_{\Omega}^{*\alpha_2}\mathbf{A}_{uu}^{(\tau\eta)\alpha_2\alpha_1}\overline{\mathbf{D}}_{\Omega}^{\alpha_1} & \overline{\mathbf{D}}_{\Omega}^{*\alpha_2}\mathbf{A}_{uu}^{(\tau\eta)\alpha_2\alpha_2}\overline{\mathbf{D}}_{\Omega}^{\alpha_2} & \overline{\mathbf{D}}_{\Omega}^{*\alpha_2}\mathbf{A}_{uu}^{(\tau\eta)\alpha_2\alpha_3}\overline{\mathbf{D}}_{\Omega}^{\alpha_3} & \overline{\mathbf{D}}_{\Omega}^{*\alpha_2}\mathbf{A}_{u\phi}^{(\tau\eta)\alpha_2\alpha_4}\overline{\mathbf{D}}_{\Omega}^{\alpha_4} & \overline{\mathbf{D}}_{\Omega}^{*\alpha_2}\mathbf{A}_{u\psi}^{(\tau\eta)\alpha_2\alpha_5}\overline{\mathbf{D}}_{\Omega}^{\alpha_5} & \overline{\mathbf{D}}_{\Omega}^{*\alpha_2}\mathbf{A}_{u\vartheta}^{(\tau\eta)\alpha_2\alpha_6}\overline{\mathbf{D}}_{\Omega}^{\alpha_6} & \overline{\mathbf{D}}_{\Omega}^{*\alpha_2}\mathbf{A}_{uC}^{(\tau\eta)\alpha_2\alpha_7}\overline{\mathbf{D}}_{\Omega}^{\alpha_7} \\
\overline{\mathbf{D}}_{\Omega}^{*\alpha_3}\mathbf{A}_{uu}^{(\tau\eta)\alpha_3\alpha_1}\overline{\mathbf{D}}_{\Omega}^{\alpha_1} & \overline{\mathbf{D}}_{\Omega}^{*\alpha_3}\mathbf{A}_{uu}^{(\tau\eta)\alpha_3\alpha_2}\overline{\mathbf{D}}_{\Omega}^{\alpha_2} & \overline{\mathbf{D}}_{\Omega}^{*\alpha_3}\mathbf{A}_{uu}^{(\tau\eta)\alpha_3\alpha_3}\overline{\mathbf{D}}_{\Omega}^{\alpha_3} & \overline{\mathbf{D}}_{\Omega}^{*\alpha_3}\mathbf{A}_{u\phi}^{(\tau\eta)\alpha_3\alpha_4}\overline{\mathbf{D}}_{\Omega}^{\alpha_4} & \overline{\mathbf{D}}_{\Omega}^{*\alpha_3}\mathbf{A}_{u\psi}^{(\tau\eta)\alpha_3\alpha_5}\overline{\mathbf{D}}_{\Omega}^{\alpha_5} & \overline{\mathbf{D}}_{\Omega}^{*\alpha_3}\mathbf{A}_{u\vartheta}^{(\tau\eta)\alpha_3\alpha_6}\overline{\mathbf{D}}_{\Omega}^{\alpha_6} & \overline{\mathbf{D}}_{\Omega}^{*\alpha_3}\mathbf{A}_{uC}^{(\tau\eta)\alpha_3\alpha_7}\overline{\mathbf{D}}_{\Omega}^{\alpha_7} \\
\overline{\mathbf{D}}_{\Omega}^{*\alpha_4}\mathbf{A}_{\phi u}^{(\tau\eta)\alpha_4\alpha_1}\overline{\mathbf{D}}_{\Omega}^{\alpha_1} & \overline{\mathbf{D}}_{\Omega}^{*\alpha_4}\mathbf{A}_{\phi u}^{(\tau\eta)\alpha_4\alpha_2}\overline{\mathbf{D}}_{\Omega}^{\alpha_2} & \overline{\mathbf{D}}_{\Omega}^{*\alpha_4}\mathbf{A}_{\phi u}^{(\tau\eta)\alpha_4\alpha_3}\overline{\mathbf{D}}_{\Omega}^{\alpha_3} & \overline{\mathbf{D}}_{\Omega}^{*\alpha_4}\mathbf{A}_{\phi\phi}^{(\tau\eta)\alpha_4\alpha_4}\overline{\mathbf{D}}_{\Omega}^{\alpha_4} & \overline{\mathbf{D}}_{\Omega}^{*\alpha_4}\mathbf{A}_{\phi\psi}^{(\tau\eta)\alpha_4\alpha_5}\overline{\mathbf{D}}_{\Omega}^{\alpha_5} & \overline{\mathbf{D}}_{\Omega}^{*\alpha_4}\mathbf{A}_{\phi\vartheta}^{(\tau\eta)\alpha_4\alpha_6}\overline{\mathbf{D}}_{\Omega}^{\alpha_6} & \overline{\mathbf{D}}_{\Omega}^{*\alpha_4}\mathbf{A}_{\phi C}^{(\tau\eta)\alpha_4\alpha_7}\overline{\mathbf{D}}_{\Omega}^{\alpha_7} \\
\overline{\mathbf{D}}_{\Omega}^{*\alpha_5}\mathbf{A}_{\psi u}^{(\tau\eta)\alpha_5\alpha_1}\overline{\mathbf{D}}_{\Omega}^{\alpha_1} & \overline{\mathbf{D}}_{\Omega}^{*\alpha_5}\mathbf{A}_{\psi u}^{(\tau\eta)\alpha_5\alpha_2}\overline{\mathbf{D}}_{\Omega}^{\alpha_2} & \overline{\mathbf{D}}_{\Omega}^{*\alpha_5}\mathbf{A}_{\psi u}^{(\tau\eta)\alpha_5\alpha_3}\overline{\mathbf{D}}_{\Omega}^{\alpha_3} & \overline{\mathbf{D}}_{\Omega}^{*\alpha_5}\mathbf{A}_{\psi\phi}^{(\tau\eta)\alpha_5\alpha_4}\overline{\mathbf{D}}_{\Omega}^{\alpha_4} & \overline{\mathbf{D}}_{\Omega}^{*\alpha_5}\mathbf{A}_{\psi\psi}^{(\tau\eta)\alpha_5\alpha_5}\overline{\mathbf{D}}_{\Omega}^{\alpha_5} & \overline{\mathbf{D}}_{\Omega}^{*\alpha_5}\mathbf{A}_{\psi\vartheta}^{(\tau\eta)\alpha_5\alpha_6}\overline{\mathbf{D}}_{\Omega}^{\alpha_6} & \overline{\mathbf{D}}_{\Omega}^{*\alpha_5}\mathbf{A}_{\psi C}^{(\tau\eta)\alpha_5\alpha_7}\overline{\mathbf{D}}_{\Omega}^{\alpha_7} \\
0 & 0 & 0 & 0 & 0 & \overline{\mathbf{D}}_{\Omega}^{*\alpha_6}\mathbf{A}_{\vartheta\vartheta}^{(\tau\eta)\alpha_6\alpha_6}\overline{\mathbf{D}}_{\Omega}^{\alpha_6} & \overline{\mathbf{D}}_{\Omega}^{*\alpha_6}\mathbf{A}_{\vartheta C}^{(\tau\eta)\alpha_6\alpha_7}\overline{\mathbf{D}}_{\Omega}^{\alpha_7} \\
0 & 0 & 0 & 0 & 0 & \overline{\mathbf{D}}_{\Omega}^{*\alpha_7}\mathbf{A}_{C\vartheta}^{(\tau\eta)\alpha_7\alpha_6}\overline{\mathbf{D}}_{\Omega}^{\alpha_6} & \overline{\mathbf{D}}_{\Omega}^{*\alpha_7}\mathbf{A}_{CC}^{(\tau\eta)\alpha_7\alpha_7}\overline{\mathbf{D}}_{\Omega}^{\alpha_7}
\end{bmatrix} \tag{68}
$$

Starting from Eqn. (68), the boundary conditions for the differential

Table 1
Nomenclature for multifield simulations. Each letter refers to a specific field of the present formulation. In particular, "D" is the mechanical elasticity, "E" and "M" stand for electrostatic and magnetostatic fields, respectively. Finally, "T" and "C" refers to heat transfer and hygrometric simulations.

Nomenclature	Multifield simulation
	One field
D	Displacement field or mechanical analysis
	Two fields coupled
T-D	Thermo-elastic or thermo-mechanical analysis
H-D	Hygro- elastic or hygro-mechanical analysis
E-D	Electro-elastic or electro-mechanical analysis
M-D	Magneto-elastic or magneto-mechanical analysis
	Three fields coupled
T-E-D	Thermo-electro-elastic or thermo-electro-mechanical analysis
T-M-D	Thermo-magneto-elastic or thermo-magneto-mechanical analysis
H-E-D	Hygro-electro-elastic or hygro-electro-mechanical analysis
H-M-D	Hygro-magneto-elastic or hygro-magneto-mechanical analysis
M-E-D	Magneto-electro-elastic or magneto-electro-mechanical analysis
H-T-D	Hygro-thermo-elastic or hygro-thermo-mechanical analysis
	All fields coupled
H-T-M-E-D	Hygro-thermo-magneto-electro-elastic or hygro-thermo-magneto-electro-mechanical analysis

problem (69) are derived by setting a null value for the generalized configuration and secondary variables along the edges of the rectangular physical domain. More specifically, in this study the Simply-supported (S) boundary condition is represented by the following relation:

$$\begin{aligned} &N_1^{(\tau)\alpha_1}=0,\ \ u_2^{(\tau)}=u_3^{(\tau)}=\phi^{(\tau)}=\psi^{(\tau)}=\xi^{(\tau)}=\kappa^{(\tau)}=0 \ \ \text{at} \ \ \alpha_1=\alpha_1^0 \ \text{or} \ \alpha_1=\alpha_1^1 \\ &N_2^{(\tau)\alpha_2}=0,\ \ u_1^{(\tau)}=u_3^{(\tau)}=\phi^{(\tau)}=\psi^{(\tau)}=\xi^{(\tau)}=\kappa^{(\tau)}=0 \ \ \text{at} \ \ \alpha_2=\alpha_2^0 \ \text{or} \ \alpha_2=\alpha_2^1 \end{aligned} \tag{69}$$

6. Semi-analytical navier solution

In this section, a semi-analytical solution is derived for the higher order fundamental relations (69) of the multifield problem in hand. To this end, some geometric and mechanical assumptions are made, and the Navier method is employed to solve the fundamental equations set. The solution presented here is valid under the assumption of uniform principal radii of curvature R_1, R_2 and constant Lamè parameters A_1, A_2 throughout the rectangular physical domain, as detailed in Ref. [45]. As a consequence, the following relations are considered:

$$\begin{aligned} &A_1=\text{cost} \Rightarrow \frac{\partial^{n+m}A_1}{\partial s_1^n \partial s_2^m}=0, \quad A_2=\text{cost} \Rightarrow \frac{\partial^{n+m}A_2}{\partial s_1^n \partial s_2^m}=0, \\ &R_1=\text{cost} \Rightarrow \frac{\partial^{n+m}R_1}{\partial s_1^n \partial s_2^m}=0, \quad R_2=\text{cost} \Rightarrow \frac{\partial^{n+m}R_2}{\partial s_1^n \partial s_2^m}=0 \end{aligned} \tag{70}$$

In this way, the lengths of the curvilinear parametric lines along the principal directions α_1, α_2, denoted by L_1 and L_2, respectively, can be computed as follows:

$$\begin{aligned} L_1&=s_1^1-s_1^0=(\alpha_1^1-\alpha_1^0)R_1 \\ L_2&=s_2^1-s_2^0=(\alpha_2^1-\alpha_2^0)R_2 \end{aligned} \tag{71}$$

Here, α_1^0, α_1^1 and α_2^0, α_2^1 represent the extremes of the physical domain along α_1 and α_2, respectively, whereas s_1^0, s_1^1 and s_2^0, s_2^1 are evaluated as $s_i^j = \alpha_i^j R_i$ with $i = 1, 2$ and $j = 0, 1$. As a particular case of Eqn. (73), in the case of a cylindrical surface with $k_{n1} = 0$ and $R_2 = R$, the quantities L_1, L_2 are determined as:

$$\begin{aligned} L_1&=s_1^1-s_1^0=\alpha_1^1-\alpha_1^0 \\ L_2&=s_2^1-s_2^0=(\alpha_2^1-\alpha_2^0)R \end{aligned} \tag{72}$$

Note that in this case the extremes α_1^0, α_1^1 correspond to lengths, whereas the quantities α_2^0, α_2^1 are angles expressed in radians. On the other hand, when $k_{n1} = k_{n2} = 0$ as happens in a rectangular plate, it can be demonstrated that the lengths L_1, L_2 of the parametric lines are evaluated as:

$$\begin{aligned} L_1&=s_1^1-s_1^0=\alpha_1^1-\alpha_1^0 \\ L_2&=s_2^1-s_2^0=\alpha_2^1-\alpha_2^0 \end{aligned} \tag{73}$$

Following the Navier approach, an harmonic solution of the differential problem is developed within the physical domain $(s_1, s_2) \in [0, L_1] \times [0, L_2]$. In this way, each element of the vector $\boldsymbol{\delta}^{(\tau)}$ of the generalized configuration variables is expanded, for each $\tau = 0, ..., N+1$, in terms of a two-dimensional harmonic distribution as shown below [45]:

$$\begin{aligned} u_1^{(\tau)}(s_1,s_2)&=\sum_{n=1}^{\infty}\sum_{m=1}^{\infty}\mathrm{U}_{1nm}^{(\tau)}\cos\left(\frac{n\pi}{L_1}s_1\right)sin\left(\frac{m\pi}{L_2}s_2\right) \\ u_2^{(\tau)}(s_1,s_2)&=\sum_{n=1}^{\infty}\sum_{m=1}^{\infty}\mathrm{U}_{2nm}^{(\tau)}\sin\left(\frac{n\pi}{L_1}s_1\right)\cos\left(\frac{m\pi}{L_2}s_2\right) \\ u_3^{(\tau)}(s_1,s_2)&=\sum_{n=1}^{\infty}\sum_{m=1}^{\infty}\mathrm{U}_{3nm}^{(\tau)}\sin\left(\frac{n\pi}{L_1}s_1\right)sin\left(\frac{m\pi}{L_2}s_2\right) \\ \phi^{(\tau)}(s_1,s_2)&=\sum_{n=1}^{\infty}\sum_{m=1}^{\infty}\Phi_{nm}^{(\tau)}\sin\left(\frac{n\pi}{L_1}s_1\right)sin\left(\frac{m\pi}{L_2}s_2\right) \\ \psi^{(\tau)}(s_1,s_2)&=\sum_{n=1}^{\infty}\sum_{m=1}^{\infty}\Psi_{nm}^{(\tau)}\sin\left(\frac{n\pi}{L_1}s_1\right)sin\left(\frac{m\pi}{L_2}s_2\right) \\ \xi^{(\tau)}(s_1,s_2)&=\sum_{n=1}^{\infty}\sum_{m=1}^{\infty}\Xi_{nm}^{(\tau)}\sin\left(\frac{n\pi}{L_1}s_1\right)sin\left(\frac{m\pi}{L_2}s_2\right) \\ \kappa^{(\tau)}(s_1,s_2)&=\sum_{n=1}^{\infty}\sum_{m=1}^{\infty}\mathrm{K}_{nm}^{(\tau)}\sin\left(\frac{n\pi}{L_1}s_1\right)sin\left(\frac{m\pi}{L_2}s_2\right) \end{aligned} \tag{74}$$

In the previous equation, the quantities $\mathrm{U}_{1nm}^{(\tau)}, \mathrm{U}_{2nm}^{(\tau)}, \mathrm{U}_{3nm}^{(\tau)}, \Phi_{nm}^{(\tau)}, \Psi_{nm}^{(\tau)}, \Xi_{nm}^{(\tau)}, \mathrm{K}_{nm}^{(\tau)}$ denote the wave amplitudes of the generalized configuration variables. If the relations presented in Eqn. (76) are assumed for the unknown field variables, the simply-supported boundary conditions described in Eqn. (71) are implicitly enforced along the edges of the physical domain. In the same way, the generalized external loads of Eqn. (60) are expanded using trigonometric functions according to the following expressions [45]:

$$\begin{aligned} q_{1s}^{(\tau)}(s_1,s_2)&=\sum_{n=1}^{\infty}\sum_{m=1}^{\infty}Q_{1snm}^{(\tau)}\cos\left(\frac{n\pi}{L_1}s_1\right)sin\left(\frac{m\pi}{L_2}s_2\right) \\ q_{2s}^{(\tau)}(s_1,s_2)&=\sum_{n=1}^{\infty}\sum_{m=1}^{\infty}Q_{2snm}^{(\tau)}\sin\left(\frac{n\pi}{L_1}s_1\right)\cos\left(\frac{m\pi}{L_2}s_2\right) \\ q_{3s}^{(\tau)}(s_1,s_2)&=\sum_{n=1}^{\infty}\sum_{m=1}^{\infty}Q_{3snm}^{(\tau)}\sin\left(\frac{n\pi}{L_1}s_1\right)sin\left(\frac{m\pi}{L_2}s_2\right) \\ q_{\mathrm{D}s}^{(\tau)}(s_1,s_2)&=\sum_{n=1}^{\infty}\sum_{m=1}^{\infty}Q_{\mathrm{D}snm}^{(\tau)}\sin\left(\frac{n\pi}{L_1}s_1\right)sin\left(\frac{m\pi}{L_2}s_2\right) \\ q_{\mathrm{B}s}^{(\tau)}(s_1,s_2)&=\sum_{n=1}^{\infty}\sum_{m=1}^{\infty}Q_{\mathrm{B}snm}^{(\tau)}\sin\left(\frac{n\pi}{L_1}s_1\right)sin\left(\frac{m\pi}{L_2}s_2\right) \\ q_{\mathrm{T}s}^{(\tau)}(s_1,s_2)&=\sum_{n=1}^{\infty}\sum_{m=1}^{\infty}Q_{\mathrm{T}snm}^{(\tau)}\sin\left(\frac{n\pi}{L_1}s_1\right)sin\left(\frac{m\pi}{L_2}s_2\right) \\ q_{\mathrm{C}s}^{(\tau)}(s_1,s_2)&=\sum_{n=1}^{\infty}\sum_{m=1}^{\infty}Q_{\mathrm{C}snm}^{(\tau)}\sin\left(\frac{n\pi}{L_1}s_1\right)sin\left(\frac{m\pi}{L_2}s_2\right) \end{aligned} \tag{75}$$

where $Q_{1snm}^{(\tau)}, Q_{2snm}^{(\tau)}, Q_{3snm}^{(\tau)}, Q_{\mathrm{D}snm}^{(\tau)}, Q_{\mathrm{B}snm}^{(\tau)}, Q_{\mathrm{T}snm}^{(\tau)}, Q_{\mathrm{C}snm}^{(\tau)}$ represents the wave amplitudes of the generalized external loads for each n,m. By comparing the previous relation to Eqn. (60), the following definition of these quantities can be derived for each $\tau = 0, ..., N+1$:

$$
\begin{aligned}
Q^{(\tau)}_{1snm} &= Q^{(-)}_{1snm} F^{(1)\alpha_1(-)}_{\tau} H^{(-)}_{1} H^{(-)}_{2} + Q^{(+)}_{1snm} F^{(l)\alpha_1(+)}_{\tau} H^{(+)}_{1} H^{(+)}_{2} \\
Q^{(\tau)}_{2snm} &= Q^{(-)}_{2snm} F^{(1)\alpha_2(-)}_{\tau} H^{(-)}_{1} H^{(-)}_{2} + Q^{(+)}_{2snm} F^{(l)\alpha_2(+)}_{\tau} H^{(+)}_{1} H^{(+)}_{2} \\
Q^{(\tau)}_{3snm} &= Q^{(-)}_{3snm} F^{(1)\alpha_3(-)}_{\tau} H^{(-)}_{1} H^{(-)}_{2} + Q^{(+)}_{3snm} F^{(l)\alpha_3(+)}_{\tau} H^{(+)}_{1} H^{(+)}_{2} \\
Q^{(\tau)}_{\mathrm{D}snm} &= Q^{(-)}_{\mathrm{D}snm} F^{(1)\alpha_4(-)}_{\tau} H^{(-)}_{1} H^{(-)}_{2} + Q^{(+)}_{\mathrm{D}snm} F^{(l)\alpha_4(+)}_{\tau} H^{(+)}_{1} H^{(+)}_{2} \\
Q^{(\tau)}_{\mathrm{B}snm} &= Q^{(-)}_{\mathrm{B}snm} F^{(1)\alpha_5(-)}_{\tau} H^{(-)}_{1} H^{(-)}_{2} + Q^{(+)}_{\mathrm{B}snm} F^{(l)\alpha_5(+)}_{\tau} H^{(+)}_{1} H^{(+)}_{2} \\
Q^{(\tau)}_{\mathrm{T}snm} &= Q^{(-)}_{\mathrm{T}snm} F^{(1)\alpha_6(-)}_{\tau} H^{(-)}_{1} H^{(-)}_{2} + Q^{(+)}_{\mathrm{T}snm} F^{(l)\alpha_6(+)}_{\tau} H^{(+)}_{1} H^{(+)}_{2} \\
Q^{(\tau)}_{\mathrm{C}snm} &= Q^{(-)}_{\mathrm{C}snm} F^{(1)\alpha_7(-)}_{\tau} H^{(-)}_{1} H^{(-)}_{2} + Q^{(+)}_{\mathrm{C}snm} F^{(l)\alpha_7(+)}_{\tau} H^{(+)}_{1} H^{(+)}_{2}
\end{aligned}
\tag{76}
$$

The Navier semi-analytical solution can be derived under the assumptions of Eqn. (76) and of Eqn. (77) for cross-ply lamination schemes. As a consequence, the following expression of the three-dimensional constitutive relation of Eqn. (29) of each k-th layer is considered written in the geometric reference system:

$$
\begin{bmatrix}
\sigma_1^{(k)} \\ \sigma_2^{(k)} \\ \tau_{12}^{(k)} \\ \tau_{13}^{(k)} \\ \tau_{23}^{(k)} \\ \sigma_3^{(k)} \\ \hline
D_1^{(k)} \\ D_2^{(k)} \\ D_3^{(k)} \\ \hline
B_1^{(k)} \\ B_2^{(k)} \\ B_3^{(k)} \\ \hline
\eta^{(k)} \\ \hline
\mu^{(k)} \\ \hline
h_1^{(k)} \\ h_2^{(k)} \\ h_3^{(k)} \\ \hline
c_1^{(k)} \\ c_2^{(k)} \\ c_3^{(k)}
\end{bmatrix}
=
\left[\begin{array}{cccccc|ccc|ccc|cc|ccc|ccc}
\overline{C}_{11}^{(k)} & \overline{C}_{12}^{(k)} & 0 & 0 & 0 & \overline{C}_{13}^{(k)} & 0 & 0 & -\overline{p}_{31}^{(k)} & 0 & 0 & -\overline{q}_{31}^{(k)} & -\overline{\varepsilon}_{11}^{(k)} & -\overline{e}_{11}^{(k)} & 0 & 0 & 0 & 0 & 0 & 0 \\
\overline{C}_{12}^{(k)} & \overline{C}_{22}^{(k)} & 0 & 0 & 0 & \overline{C}_{23}^{(k)} & 0 & 0 & -\overline{p}_{32}^{(k)} & 0 & 0 & -\overline{q}_{32}^{(k)} & -\overline{\varepsilon}_{22}^{(k)} & -\overline{e}_{22}^{(k)} & 0 & 0 & 0 & 0 & 0 & 0 \\
0 & 0 & \overline{C}_{66}^{(k)} & 0 & 0 & 0 & 0 & 0 & 0 & 0 & 0 & 0 & 0 & 0 & 0 & 0 & 0 & 0 & 0 & 0 \\
0 & 0 & 0 & \overline{C}_{44}^{(k)} & 0 & 0 & -\overline{p}_{14}^{(k)} & 0 & 0 & -\overline{q}_{14}^{(k)} & 0 & 0 & 0 & 0 & 0 & 0 & 0 & 0 & 0 & 0 \\
0 & 0 & 0 & 0 & \overline{C}_{55}^{(k)} & 0 & 0 & -\overline{p}_{25}^{(k)} & 0 & 0 & -\overline{q}_{25}^{(k)} & 0 & 0 & 0 & 0 & 0 & 0 & 0 & 0 & 0 \\
\overline{C}_{13}^{(k)} & \overline{C}_{23}^{(k)} & 0 & 0 & 0 & \overline{C}_{33}^{(k)} & 0 & 0 & -\overline{p}_{33}^{(k)} & 0 & 0 & -\overline{q}_{33}^{(k)} & -\overline{\varepsilon}_{33}^{(k)} & -\overline{e}_{33}^{(k)} & 0 & 0 & 0 & 0 & 0 & 0 \\ \hline
0 & 0 & 0 & \overline{p}_{14}^{(k)} & 0 & 0 & \overline{\Gamma}_{11}^{(k)} & 0 & 0 & \overline{d}_{11}^{(k)} & 0 & 0 & 0 & 0 & 0 & 0 & 0 & 0 & 0 & 0 \\
0 & 0 & 0 & 0 & \overline{p}_{25}^{(k)} & 0 & 0 & \overline{\Gamma}_{22}^{(k)} & 0 & 0 & \overline{d}_{22}^{(k)} & 0 & 0 & 0 & 0 & 0 & 0 & 0 & 0 & 0 \\
\overline{p}_{31}^{(k)} & \overline{p}_{32}^{(k)} & 0 & 0 & 0 & \overline{p}_{33}^{(k)} & 0 & 0 & \overline{\Gamma}_{33}^{(k)} & 0 & 0 & \overline{d}_{33}^{(k)} & \overline{\sigma}_{33}^{(k)} & \overline{g}_{33}^{(k)} & 0 & 0 & 0 & 0 & 0 & 0 \\ \hline
0 & 0 & 0 & \overline{q}_{14}^{(k)} & 0 & 0 & \overline{d}_{11}^{(k)} & 0 & 0 & \overline{m}_{11}^{(k)} & 0 & 0 & 0 & 0 & 0 & 0 & 0 & 0 & 0 & 0 \\
0 & 0 & 0 & 0 & \overline{q}_{25}^{(k)} & 0 & 0 & \overline{d}_{22}^{(k)} & 0 & 0 & \overline{m}_{22}^{(k)} & 0 & 0 & 0 & 0 & 0 & 0 & 0 & 0 & 0 \\
\overline{q}_{31}^{(k)} & \overline{q}_{32}^{(k)} & 0 & 0 & 0 & \overline{q}_{33}^{(k)} & 0 & 0 & \overline{d}_{33}^{(k)} & 0 & 0 & \overline{m}_{33}^{(k)} & \overline{w}_{33}^{(k)} & \overline{f}_{33}^{(k)} & 0 & 0 & 0 & 0 & 0 & 0 \\ \hline
\overline{\varkappa}_{11}^{(k)} & \overline{\varkappa}_{22}^{(k)} & 0 & 0 & 0 & \overline{\varkappa}_{33}^{(k)} & 0 & 0 & \overline{o}_{33}^{(k)} & 0 & 0 & \overline{w}_{33}^{(k)} & \overline{\varphi}_{11}^{(k)} & \overline{\varphi}_{12}^{(k)} & 0 & 0 & 0 & 0 & 0 & 0 \\ \hline
\overline{e}_{31}^{(k)} & \overline{e}_{32}^{(k)} & 0 & 0 & 0 & \overline{e}_{33}^{(k)} & 0 & 0 & \overline{g}_{33}^{(k)} & 0 & 0 & \overline{f}_{33}^{(k)} & \overline{\varphi}_{12}^{(k)} & \overline{\varphi}_{22}^{(k)} & 0 & 0 & 0 & 0 & 0 & 0 \\ \hline
0 & 0 & 0 & 0 & 0 & 0 & 0 & 0 & 0 & 0 & 0 & 0 & 0 & 0 & \overline{k}_{11}^{(k)} & 0 & 0 & \overline{y}_{11}^{(k)} & 0 & 0 \\
0 & 0 & 0 & 0 & 0 & 0 & 0 & 0 & 0 & 0 & 0 & 0 & 0 & 0 & 0 & \overline{k}_{22}^{(k)} & 0 & 0 & \overline{y}_{22}^{(k)} & 0 \\
0 & 0 & 0 & 0 & 0 & 0 & 0 & 0 & 0 & 0 & 0 & 0 & 0 & 0 & 0 & 0 & \overline{k}_{33}^{(k)} & 0 & 0 & \overline{y}_{33}^{(k)} \\ \hline
0 & 0 & 0 & 0 & 0 & 0 & 0 & 0 & 0 & 0 & 0 & 0 & 0 & 0 & \overline{x}_{11}^{(k)} & 0 & 0 & \overline{z}_{11}^{(k)} & 0 & 0 \\
0 & 0 & 0 & 0 & 0 & 0 & 0 & 0 & 0 & 0 & 0 & 0 & 0 & 0 & 0 & \overline{x}_{22}^{(k)} & 0 & 0 & \overline{z}_{22}^{(k)} & 0 \\
0 & 0 & 0 & 0 & 0 & 0 & 0 & 0 & 0 & 0 & 0 & 0 & 0 & 0 & 0 & 0 & \overline{x}_{33}^{(k)} & 0 & 0 & \overline{z}_{33}^{(k)}
\end{array}\right]
\begin{bmatrix}
\varepsilon_1^{(k)} \\ \varepsilon_2^{(k)} \\ \gamma_{12}^{(k)} \\ \gamma_{13}^{(k)} \\ \gamma_{23}^{(k)} \\ \varepsilon_3^{(k)} \\ \hline
E_1^{(k)} \\ E_2^{(k)} \\ E_3^{(k)} \\ \hline
H_1^{(k)} \\ H_2^{(k)} \\ H_3^{(k)} \\ \hline
\widehat{\Delta T}^{(k)} \\ \hline
\widehat{\Delta C}^{(k)} \\ \hline
\theta_1^{(k)} \\ \theta_2^{(k)} \\ \theta_3^{(k)} \\ \hline
\lambda_1^{(k)} \\ \lambda_2^{(k)} \\ \lambda_3^{(k)}
\end{bmatrix}
\tag{77}
$$

The constitutive relation in Eqn. (79) can be derived for a lamination scheme involving orthotropic materials with an orientation angle $\vartheta^{(k)}$ equal to $\pm\pi/2$ or 0. Substituting the harmonic expressions of the unknown field variables and the generalized surface actions of Eqn. (76) and Eqn. (77), respectively, into the fundamental relations of Eqn. (69), the governing equations are simplified into a linear system, leading to the following expression [45]:

$$
\sum_{n=1}^{\infty}\sum_{m=1}^{\infty}\left(\sum_{\eta=0}^{N+1}\widetilde{\mathbf{L}}_{nm}^{(\eta\eta)}\mathbf{U}_{nm}^{(\eta)} + \mathbf{Q}_{snm}^{(\tau)}\right) = \mathbf{0}
\tag{78}
$$

As can be seen, the unknown variables are the wave amplitudes introduced in Eqn. (76) which are arranged into the algebraic vector $\mathbf{U}_{nm}^{(\tau)}$. In the same way, the vector $\mathbf{Q}_{snm}^{(\tau)}$ contains the wave amplitudes of the external surface actions, written for each wave number n, m in accordance with Eqn. (77). In a more expanded form, the previous equation can be written as:

$$
\sum_{n=1}^{\infty}\sum_{m=1}^{\infty}\left(\sum_{\eta=0}^{N+1}
\begin{bmatrix}
\widetilde{L}_{11nm}^{(\tau\eta)\alpha_1\alpha_1} & \widetilde{L}_{12nm}^{(\tau\eta)\alpha_1\alpha_2} & \widetilde{L}_{13nm}^{(\tau\eta)\alpha_1\alpha_3} & \widetilde{L}_{14nm}^{(\tau\eta)\alpha_1\alpha_4} & \widetilde{L}_{15nm}^{(\tau\eta)\alpha_1\alpha_5} & \widetilde{L}_{16nm}^{(\tau\eta)\alpha_1\alpha_6} & \widetilde{L}_{17nm}^{(\tau\eta)\alpha_1\alpha_7} \\
\widetilde{L}_{21nm}^{(\tau\eta)\alpha_2\alpha_1} & \widetilde{L}_{22nm}^{(\tau\eta)\alpha_2\alpha_2} & \widetilde{L}_{23nm}^{(\tau\eta)\alpha_2\alpha_3} & \widetilde{L}_{24nm}^{(\tau\eta)\alpha_2\alpha_4} & \widetilde{L}_{25nm}^{(\tau\eta)\alpha_2\alpha_5} & \widetilde{L}_{26nm}^{(\tau\eta)\alpha_2\alpha_6} & \widetilde{L}_{27nm}^{(\tau\eta)\alpha_2\alpha_7} \\
\widetilde{L}_{31nm}^{(\tau\eta)\alpha_3\alpha_1} & \widetilde{L}_{32nm}^{(\tau\eta)\alpha_3\alpha_2} & \widetilde{L}_{33nm}^{(\tau\eta)\alpha_3\alpha_3} & \widetilde{L}_{34nm}^{(\tau\eta)\alpha_3\alpha_4} & \widetilde{L}_{35nm}^{(\tau\eta)\alpha_3\alpha_5} & \widetilde{L}_{36nm}^{(\tau\eta)\alpha_3\alpha_6} & \widetilde{L}_{37nm}^{(\tau\eta)\alpha_3\alpha_7} \\
\widetilde{L}_{41nm}^{(\tau\eta)\alpha_4\alpha_1} & \widetilde{L}_{42nm}^{(\tau\eta)\alpha_4\alpha_2} & \widetilde{L}_{43nm}^{(\tau\eta)\alpha_4\alpha_3} & \widetilde{L}_{44nm}^{(\tau\eta)\alpha_4\alpha_4} & \widetilde{L}_{45nm}^{(\tau\eta)\alpha_4\alpha_5} & \widetilde{L}_{46nm}^{(\tau\eta)\alpha_4\alpha_6} & \widetilde{L}_{47nm}^{(\tau\eta)\alpha_4\alpha_7} \\
\widetilde{L}_{51nm}^{(\tau\eta)\alpha_5\alpha_1} & \widetilde{L}_{52nm}^{(\tau\eta)\alpha_5\alpha_2} & \widetilde{L}_{53nm}^{(\tau\eta)\alpha_5\alpha_3} & \widetilde{L}_{54nm}^{(\tau\eta)\alpha_5\alpha_4} & \widetilde{L}_{55nm}^{(\tau\eta)\alpha_5\alpha_5} & \widetilde{L}_{56nm}^{(\tau\eta)\alpha_5\alpha_6} & \widetilde{L}_{57nm}^{(\tau\eta)\alpha_5\alpha_7} \\
\widetilde{L}_{61nm}^{(\tau\eta)\alpha_6\alpha_1} & \widetilde{L}_{62nm}^{(\tau\eta)\alpha_6\alpha_2} & \widetilde{L}_{63nm}^{(\tau\eta)\alpha_6\alpha_3} & \widetilde{L}_{64nm}^{(\tau\eta)\alpha_6\alpha_4} & \widetilde{L}_{65nm}^{(\tau\eta)\alpha_6\alpha_5} & \widetilde{L}_{66nm}^{(\tau\eta)\alpha_6\alpha_6} & \widetilde{L}_{67nm}^{(\tau\eta)\alpha_6\alpha_7} \\
\widetilde{L}_{71nm}^{(\tau\eta)\alpha_7\alpha_1} & \widetilde{L}_{72nm}^{(\tau\eta)\alpha_7\alpha_2} & \widetilde{L}_{73nm}^{(\tau\eta)\alpha_7\alpha_3} & \widetilde{L}_{74nm}^{(\tau\eta)\alpha_7\alpha_4} & \widetilde{L}_{75nm}^{(\tau\eta)\alpha_7\alpha_5} & \widetilde{L}_{76nm}^{(\tau\eta)\alpha_7\alpha_6} & \widetilde{L}_{77nm}^{(\tau\eta)\alpha_7\alpha_7}
\end{bmatrix}
\begin{bmatrix}
\mathrm{U}_{1nm}^{(\eta)} \\ \mathrm{U}_{2nm}^{(\eta)} \\ \mathrm{U}_{3nm}^{(\eta)} \\ \Phi_{nm}^{(\eta)} \\ \Psi_{nm}^{(\eta)} \\ \Xi_{nm}^{(\eta)} \\ \mathrm{K}_{nm}^{(\eta)}
\end{bmatrix}
+
\begin{bmatrix}
Q_{1snm}^{(\tau)} \\ Q_{2snm}^{(\tau)} \\ Q_{3snm}^{(\tau)} \\ Q_{\mathrm{D}snm}^{(\tau)} \\ Q_{\mathrm{B}snm}^{(\tau)} \\ Q_{\mathrm{T}snm}^{(\tau)} \\ Q_{\mathrm{C}snm}^{(\tau)}
\end{bmatrix}
\right) =
\begin{bmatrix}
0 \\ 0 \\ 0 \\ 0 \\ 0 \\ 0 \\ 0
\end{bmatrix}
\tag{79}
$$

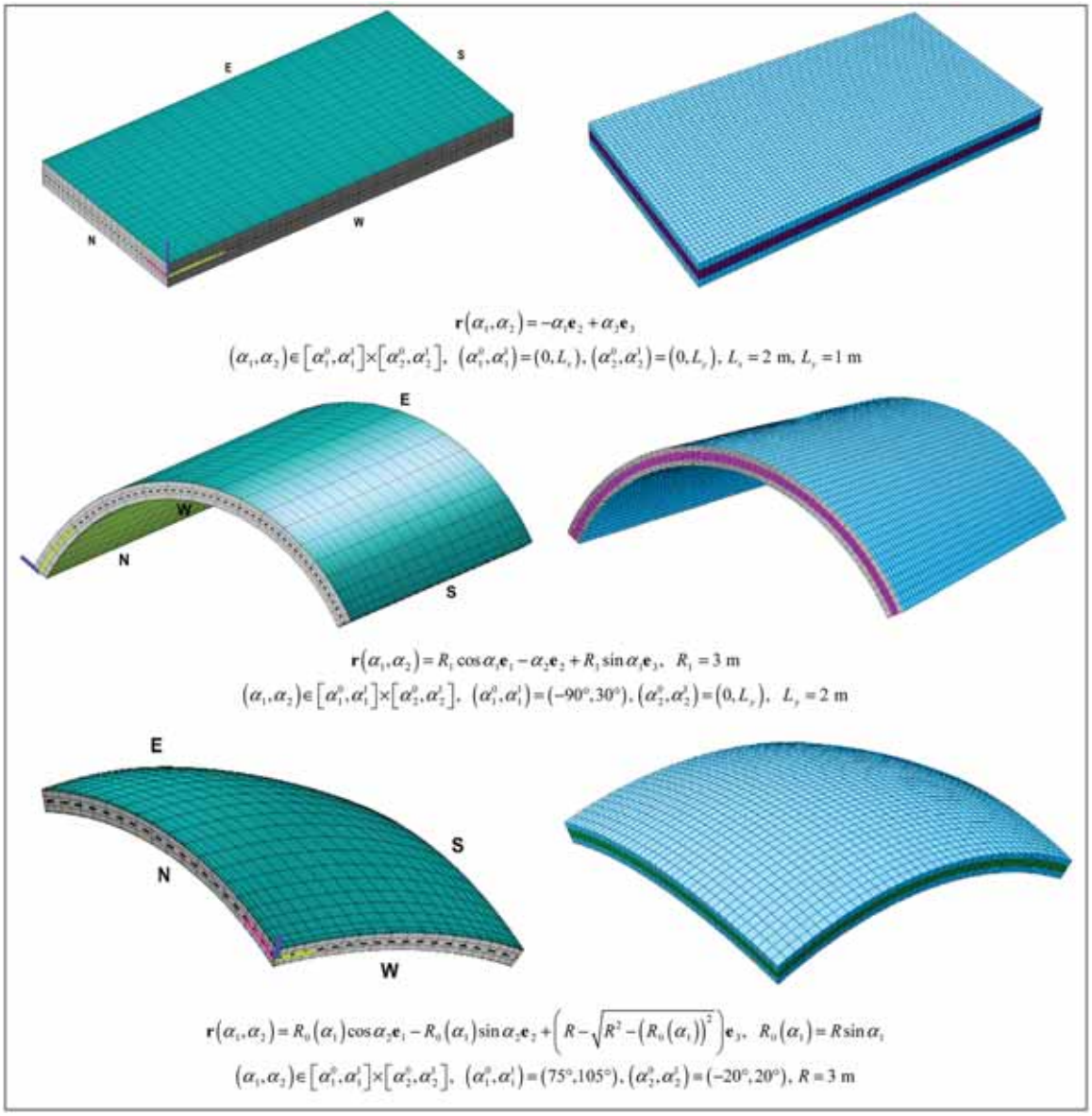

Figure 1. Two-dimensional models developed for the multifield simulations involving a rectangular plate, a cylindrical panel and a spherical panel and three-dimensional mesh discretization for 3D FEM modelling.

7. Generalized differential quadrature

In the previous sections, a semi-analytical solution is derived, according to Eqn. (80), for the two-dimensional multifield formulation of Eqn. (69) using Navier's method. The solution of Eqn. (69) is based on the computation of derivatives and integrals along the thickness direction of the three-dimensional solid to determine the generalized constitutive coefficients described in Eqn. (52). To this end, the GDQ and GIQ method are adopted, which are presented here for the one-dimensional case.

When the GDQ method is adopted, the derivative of an arbitrary n-th order of a univariate smooth function $f=f(x)$ at a discrete point $\overline{x}_i$ defined in a closed interval so that $x_i\in[a,b]$ with $i=1,\ldots,I_Q$ is computed using the following quadrature rule [45]:

$$f^{(n)}(x_i)=\left.\frac{\partial^n f(x)}{\partial x^n}\right|_{x=x_i}\cong\sum_{j=1}^{I_Q}\varsigma_{ij}^{(n)}f(x_j)\qquad i=1,2,\ldots,I_Q \tag{80}$$

In the previous equation, are the values assumed by in an arbitrary discrete grid, whereas $\varsigma_{ij}^{(n)}$ are the GDQ weighting coefficient for the n-th order derivative. It is worth noting that Eqn. (82) does not depend on the particular grid chosen within the definition domain $[a,b]$. The quantities $\varsigma_{ij}^{(n)}$ are computed using the following recursive relationship, which is based on Lagrange polynomials $\mathscr{L}$ for the interpolation of the solution [100]:

$$\begin{aligned}\varsigma_{ij}^{(1)}&=\frac{\mathscr{L}^{(1)}(x_i)}{(x_i-x_j)\mathscr{L}^{(1)}(x_j)},\quad \varsigma_{ij}^{(n)}=n\left(\varsigma_{ij}^{(1)}\varsigma_{ii}^{(n-1)}-\frac{\varsigma_{ij}^{(n-1)}}{x_i-x_j}\right)\qquad i\neq j\\ \varsigma_{ii}^{(n)}&=-\sum_{j=1|j\neq i}^{I_Q}\varsigma_{ij}^{(n)}\qquad i=j\end{aligned} \tag{81}$$

The coefficients $\varsigma_{ij}^{(n)}$ of the n-th order derivative are conveniently assembled into a matrix of size $I_Q\times I_Q$, denoted by $\boldsymbol{\varsigma}^{(n)}$. For the sake of completeness, in the previous relation the terms $\mathscr{L}^{(1)}(x_i)$ and $\mathscr{L}^{(1)}(x_j)$ represent the first order derivatives of the Lagrange polynomials $\mathscr{L}$ evaluated at the sample points x_i,x_j. In addition, the definition $\varsigma_{ij}^{(0)}=\delta_{ij}$

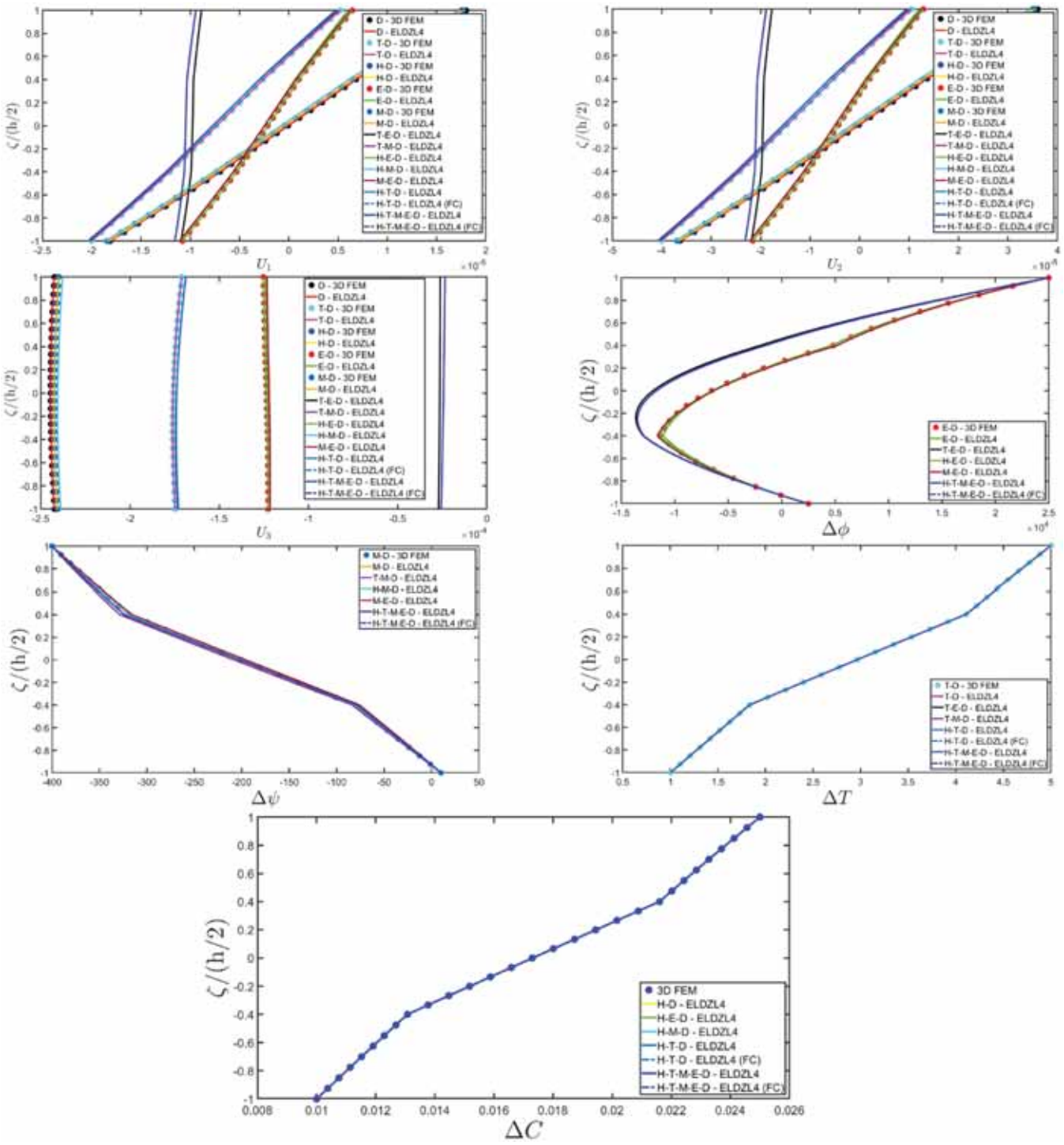

Figure 2. Distribution of the displacement field components, electric potential, magnetostatic potential, temperature variation and concentration variation along the thickness direction of a simply supported rectangular plate subjected to a sinusoidal generalized action. Effect of the coupling in various multifield simulations. Thickness plots are provided at $(0.25{\cdot}L_1, 0.25{\cdot}L_2)$ within the physical domain.

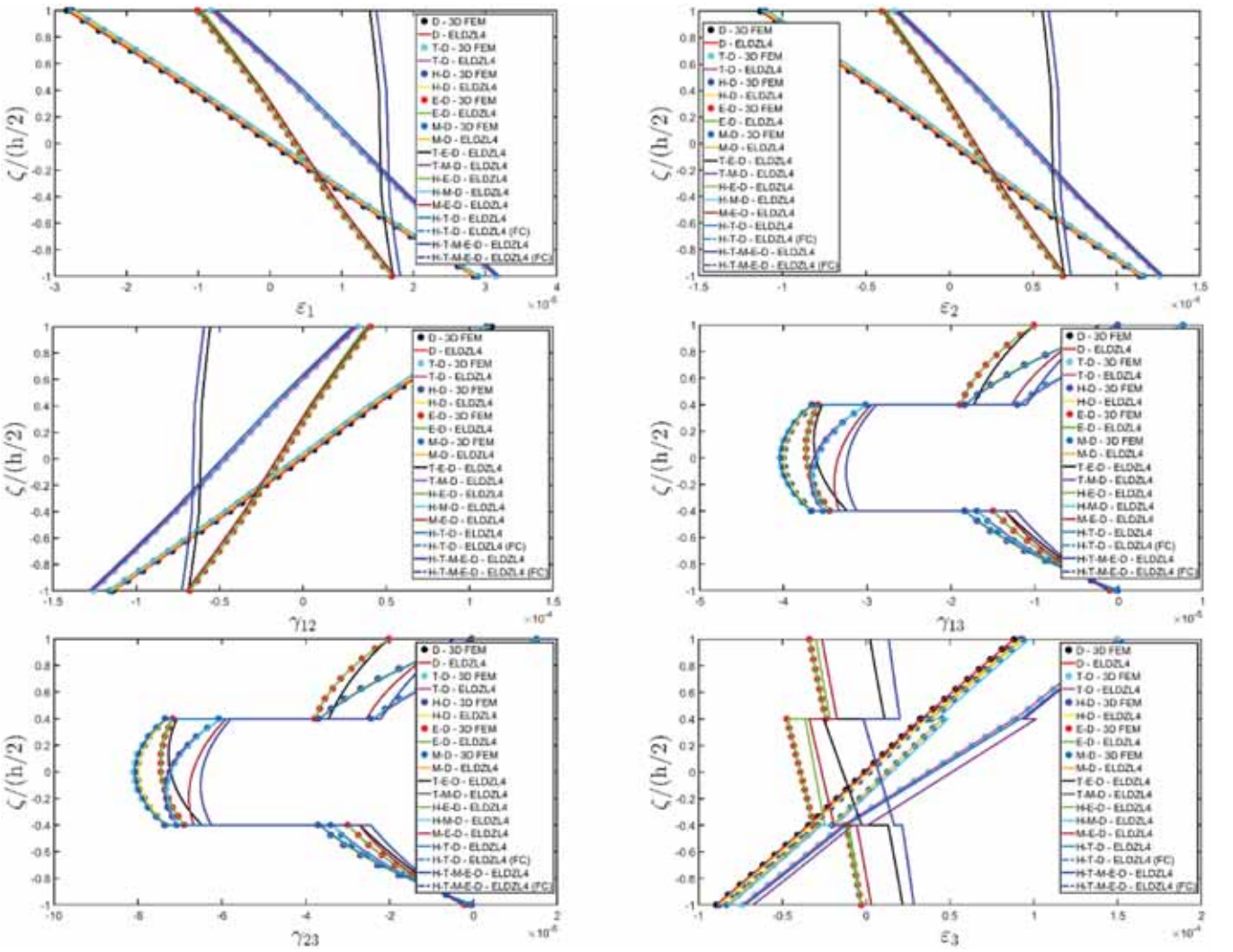

Figure 3. Distribution of the three-dimensional strain components along the thickness direction of a simply supported rectangular plate subjected to a sinusoidal generalized action. Effect of the coupling in various multifield simulations. Thickness plots are provided at $(0.25{\cdot}L_1, 0.25{\cdot}L_2)$ within the physical domain.

is introduced, being δ_{ij} the well-known Kronecker delta function. The discrete points adopted in Eqn. (82) are chosen following the Chebyshev-Gauss-Lobatto (CGL) harmonic distribution. Referring to the interval $[-1, 1]$, the position $\bar{x}_i$ with $i = 1, ..., I_Q$ of an arbitrary CGL sample point can be computed as follows:

$$\bar{x}_i = -\cos\left(\frac{i-1}{I_Q - 1}\pi\right) \tag{82}$$

Recalling the GDQ rule as described in Eqn.(82), it is possible to derive a quadrature procedure, based on Taylor series, for the computation of the integral of a given function $f = f(x)$, where $[a, b]$ represents the definition domain. If this domain is discretized using the sample points x_i, x_j with $i, j = 1, ..., I_Q$ according to the distribution of Eqn. (84), the integral of f reduced to $[x_i, x_j]$ with $x_i, x_j \in [a, b]$ can be expressed as follows, with $m \leq I_Q$:

$$\int_{x_i}^{x_j} f(x)dx = \sum_{r=0}^{m-1} \frac{(x_j - x_i)^{r+1}}{(r+1)!} \frac{d^r f}{dx^r}\bigg|_{x_i} \tag{83}$$

In the previous relation, it is important to note that the Taylor series expansion of the function f to the m-th order is applied near the discrete point x_i. For a more accurate evaluation of the integral, the interval is divided into smaller ones. As a result, the following expression is obtained [100]:

$$\int_{x_i}^{x_j} f(x)dx = \int_{x_i}^{\frac{x_j+x_i}{2}} f(x)dx + \int_{\frac{x_j+x_i}{2}}^{x_j} f(x)dx = \int_{x_i}^{\frac{x_j+x_i}{2}} f(x)dx - \int_{x_j}^{\frac{x_j+x_i}{2}} f(x)dx \tag{84}$$

Introducing Eqn. (85) in the previous relation and recalling the GDQ rule (82) for the computation derivatives, one gets:

$$\begin{aligned}\int_{x_i}^{x_j} f(x)dx &= \sum_{r=0}^{m-1} \frac{(x_j - x_i)^{r+1}}{2^{r+1}(r+1)!} \sum_{k=1}^{N} \varsigma_{ik}^{(r)} f(x_k) - \sum_{r=0}^{m-1} \frac{(x_i - x_j)^{r+1}}{2^{r+1}(r+1)!} \sum_{k=1}^{N} \varsigma_{jk}^{(r)} f(x_k) = \\ &= \sum_{k=1}^{N} \left(\sum_{r=0}^{m-1} \left(\frac{(x_j - x_i)^{r+1}}{2^{r+1}(r+1)!} \varsigma_{ik}^{(r)} - \frac{(x_i - x_j)^{r+1}}{2^{r+1}(r+1)!} \varsigma_{jk}^{(r)} \right) \right) f(x_k) = \\ &= \sum_{k=1}^{N} \left(\sum_{r=0}^{m-1} \frac{(x_j - x_i)^{r+1}}{2^{r+1}(r+1)!} \left(\varsigma_{ik}^{(r)} + (-1)^{r+2} \varsigma_{jk}^{(r)} \right) \right) f(x_k) = \sum_{k=1}^{N} w_k^{ij} f(x_k)\end{aligned} \tag{85}$$

Finally, the numerical evaluation of the integral of the function f over the entire definition domain $[a = x_1, b = x_N]$ is carried out using the GTIQ method as follows:

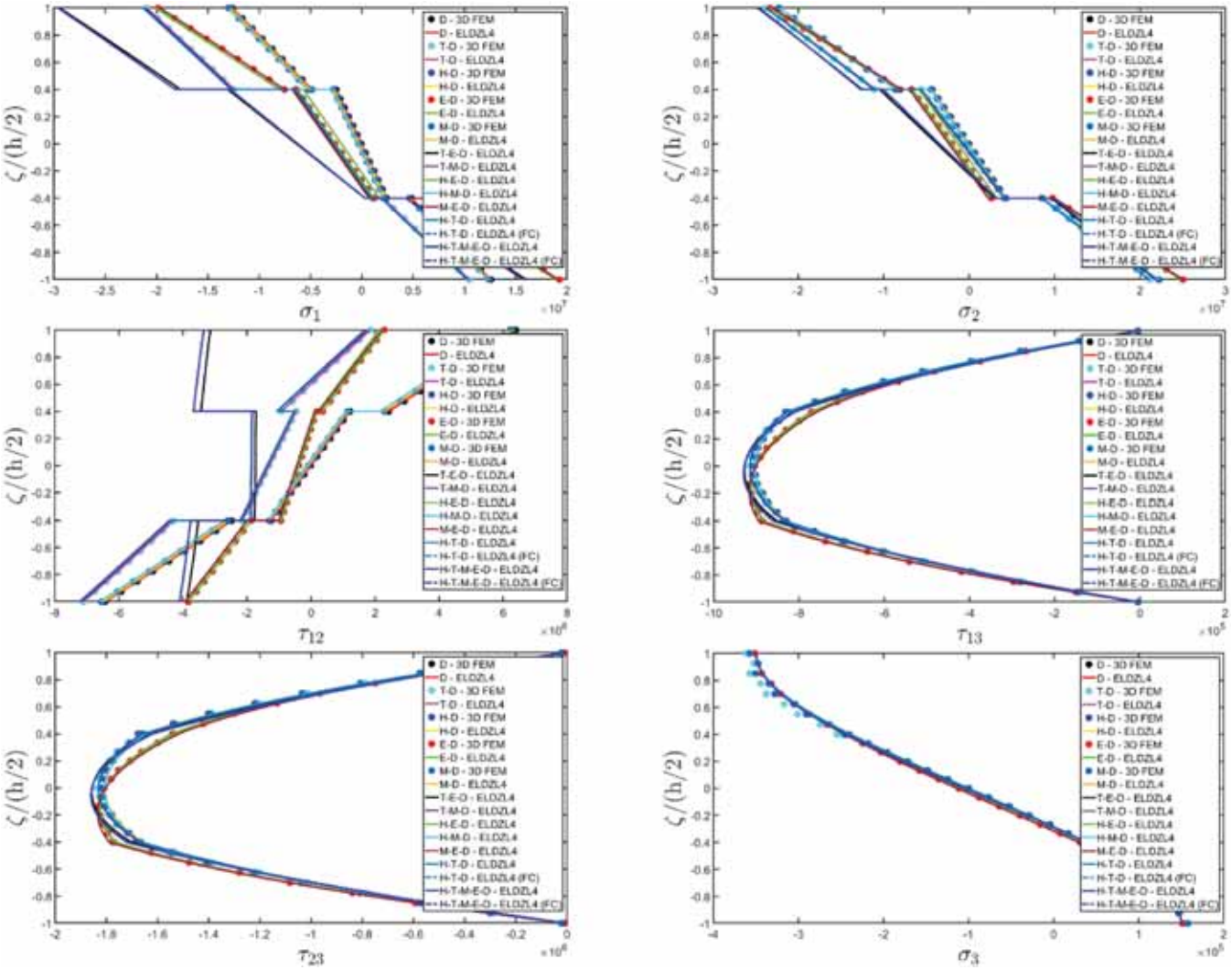

Figure 4. Distribution of the three-dimensional stress components [Pa] along the thickness direction of a simply supported rectangular plate subjected to a sinusoidal generalized action. Effect of the coupling in various multifield simulations. Thickness plots are provided at $(0.25{\cdot}L_1, 0.25{\cdot}L_2)$ within the physical domain.

$$\int_a^b f(x)dx = \sum_{i=1}^{N-1}\int_{x_i}^{x_{i+1}} f(x)dx = \sum_{i=1}^{N-1}\left(\sum_{k=1}^{N} w_k^{i(i+1)} f(x_k)\right) = \sum_{k=1}^{N}\left(\sum_{i=1}^{N-1} w_k^{i(i+1)}\right) f(x_k) = \sum_{k=1}^{N} w_k^{1N} f(x_k) \tag{86}$$

The weighting coefficients w_k^{1N} are thus computed using the following recursive relation:

$$w_k^{1N} = \sum_{i=1}^{N-1} w_k^{i(i+1)} = \sum_{i=1}^{N-1}\sum_{r=0}^{m-1} \frac{(x_{i+1}-x_i)^{r+1}}{2^{r+1}(r+1)!}\left(\varsigma_{ik}^{(r)} + (-1)^{r+2}\varsigma_{(i+1)k}^{(r)}\right) \tag{87}$$

8. Recovery of primary and secondary variablesR

In this section, an accurate reconstruction of the multifield response of the doubly-curved three-dimensional shell solid is performed starting from the two-dimensional solution derived in Eqn. (81) using an higher order two-dimensional model. This procedure is adopted because a higher order two-dimensional model does not implicitly respect the balance of secondary variables in the thickness direction. As a consequence, a correction of the recovered profile of primary and secondary variables is performed using the multifield balance equations written for a three-dimensional solid.

The procedure in hand is based on the definition of a discrete grid of I_Q points in each interval $[\zeta_k, \zeta_{k+1}]$ along the thickness direction in an arbitrary k-th lamina of the stacking sequence. Starting from a dimensionless discrete point $\overline{x}_{\tilde{m}} \in [-1,1]$ with $\tilde{m} = 1,...,I_Q$, as defined in Eqn. (84), a distribution of discrete points $\zeta_{\tilde{m}}^{(k)} \in [\zeta_k, \zeta_{k+1}]$ is established for each layer of the solid, as follows [45]:

$$\zeta_{\tilde{m}}^{(k)} = \frac{\zeta_{k+1}-\zeta_k}{2}\overline{x}_{\tilde{m}} + \frac{\zeta_{k+1}+\zeta_k}{2} = \frac{h_k}{2}\overline{x}_{\tilde{m}} + \frac{\zeta_{k+1}+\zeta_k}{2} \tag{88}$$

The discrete points in Eqn. (90) are, thus, collected in the vector $\boldsymbol{\zeta}^{(k)} = [\zeta_1^{(k)} \ \cdots \ \zeta_{\tilde{m}}^{(k)} \ \cdots \ \zeta_{I_T}^{(k)}]^T$, whose size is $I_Q \times 1$. Furthermore, a new vector of size $lI_Q \times 1$ is introduced, where l represents the total number of layers of the stacking sequence. Each element ζ_m of this vector corresponds to a discrete point belonging to the interval $[-h/2, h/2]$. This vector is constructed in terms of the index $m = (k-1)I_Q + \tilde{m}$ for each $k = 1,...,l$:

$$[\zeta_1 \ \cdots \ \zeta_m \ \cdots \ \zeta_{lI_T}]^T = [\boldsymbol{\zeta}^{(1)T} \ \cdots \ \boldsymbol{\zeta}^{(k)T} \ \cdots \ \boldsymbol{\zeta}^{(l)T}] \tag{89}$$

This allows the through-the-thickness profile of the elements of the vector $\boldsymbol{\Delta}^{(k)}$ of the three-dimensional configuration variables to be determined for an arbitrary point (s_{1i}, s_{2j}) within the physical domain using the following relation, which is derived from Eqn. (10) setting $i =$

$1,...,I_N$, $j = 1,...,I_M$ and $m = 1,...,lI_T$:

$$\boldsymbol{\Delta}^{(k)}_{(ijm)} = \sum_{\tau=0}^{N+1} \mathbf{F}^{(k)}_{\tau(ijm)} \boldsymbol{\delta}^{(\tau)}_{(ij)} \tag{90}$$

In the same way, the discrete version of Eqn. (16) is adopted to derive the three-dimensional primary variables $\boldsymbol{\pi}^{(k)}_{(ijm)}$ of the present multifield problem, once the quantity $\boldsymbol{\Delta}^{(k)}_{(ijm)}$ is obtained from Eqn. (92):

$$\boldsymbol{\pi}^{(k)}_{(ijm)} = \sum_{\tau=0}^{N+1} \sum_{i=1}^{7} \mathbf{Z}^{(k\tau)\alpha_i}_{(ij)} \boldsymbol{\pi}^{(\tau)\alpha_i}_{(ij)} \tag{91}$$

At this point, the in-plane secondary variables of the multifield problem are obtained from the multifield constitutive relationship as described in Eqn. (29). These quantities can be calculated using the following matrix relation:

$$\begin{bmatrix} \sigma_1^{(k)} \\ \sigma_2^{(k)} \\ \tau_{12}^{(k)} \\ D_1^{(k)} \\ D_2^{(k)} \\ B_1^{(k)} \\ B_2^{(k)} \end{bmatrix} = \begin{bmatrix} \overline{C}_{11}^{(k)} & \overline{C}_{12}^{(k)} & 0 & 0 & 0 & \overline{C}_{13}^{(k)} & 0 & 0 & -\overline{p}_{31}^{(k)} & 0 & 0 & -\overline{q}_{31}^{(k)} & -\overline{z}_{11}^{(k)} & -\overline{e}_{11}^{(k)} \\ \overline{C}_{12}^{(k)} & \overline{C}_{22}^{(k)} & 0 & 0 & 0 & \overline{C}_{23}^{(k)} & 0 & 0 & -\overline{p}_{32}^{(k)} & 0 & 0 & -\overline{q}_{32}^{(k)} & -\overline{z}_{22}^{(k)} & -\overline{e}_{22}^{(k)} \\ 0 & 0 & \overline{C}_{66}^{(k)} & 0 & 0 & 0 & 0 & 0 & 0 & 0 & 0 & 0 & 0 & 0 \\ 0 & 0 & 0 & \overline{p}_{14}^{(k)} & 0 & 0 & \overline{l}_{11}^{(k)} & 0 & 0 & \overline{d}_{11}^{(k)} & 0 & 0 & 0 & 0 \\ 0 & 0 & 0 & 0 & \overline{p}_{25}^{(k)} & 0 & 0 & \overline{l}_{22}^{(k)} & 0 & 0 & \overline{d}_{22}^{(k)} & 0 & 0 & 0 \\ 0 & 0 & 0 & \overline{q}_{14}^{(k)} & 0 & 0 & \overline{d}_{11}^{(k)} & 0 & 0 & \overline{m}_{11}^{(k)} & 0 & 0 & 0 & 0 \\ 0 & 0 & 0 & 0 & \overline{q}_{25}^{(k)} & 0 & 0 & \overline{d}_{22}^{(k)} & 0 & 0 & \overline{m}_{22}^{(k)} & 0 & 0 & 0 \end{bmatrix} \begin{bmatrix} \varepsilon_1^{(k)} \\ \varepsilon_2^{(k)} \\ \gamma_{12}^{(k)} \\ \gamma_{13}^{(k)} \\ \gamma_{23}^{(k)} \\ \varepsilon_3^{(k)} \\ E_1^{(k)} \\ E_2^{(k)} \\ E_3^{(k)} \\ H_1^{(k)} \\ H_2^{(k)} \\ H_3^{(k)} \\ \widehat{\Delta \mathrm{T}}^{(k)} \\ \widehat{\Delta \mathrm{C}}^{(k)} \end{bmatrix} \tag{92}$$

$$\begin{bmatrix} h_1^{(k)} \\ h_2^{(k)} \\ c_1^{(k)} \\ c_2^{(k)} \end{bmatrix} = \begin{bmatrix} \overline{k}_{11}^{(k)} & 0 & \overline{y}_{11}^{(k)} & 0 \\ 0 & \overline{k}_{22}^{(k)} & 0 & \overline{y}_{22}^{(k)} \\ \overline{x}_{11}^{(k)} & 0 & \overline{s}_{11}^{(k)} & 0 \\ 0 & \overline{x}_{22}^{(k)} & 0 & \overline{s}_{22}^{(k)} \end{bmatrix} \begin{bmatrix} \theta_1^{(k)} \\ \theta_2^{(k)} \\ \lambda_1^{(k)} \\ \lambda_2^{(k)} \end{bmatrix} \tag{93}$$

The out-of-plane secondary variables for the mechanical case are thus derived from the multifield three-dimensional balance equations reported below [45]:

$$\begin{aligned} \frac{\partial \tau_{13}^{(k)}}{\partial \zeta} + \tau_{13}^{(k)} \left(\frac{2}{R_1+\zeta} + \frac{1}{R_2+\zeta} \right) &= -\frac{1}{A_1(1+\zeta/R_1)} \frac{\partial \sigma_1^{(k)}}{\partial \alpha_1} + \\ &+ \frac{\sigma_2^{(k)} - \sigma_1^{(k)}}{A_1 A_2 (1+\zeta/R_2)} \frac{\partial A_2}{\partial \alpha_1} - \frac{1}{A_2(1+\zeta/R_2)} \frac{\partial \tau_{12}^{(k)}}{\partial \alpha_2} - \frac{2\tau_{12}^{(k)}}{A_1 A_2 (1+\zeta/R_1)} \frac{\partial A_1}{\partial \alpha_2} \\ \frac{\partial \tau_{23}^{(k)}}{\partial \zeta} + \tau_{23}^{(k)} \left(\frac{1}{R_1+\zeta} + \frac{2}{R_2+\zeta} \right) &= -\frac{1}{A_2(1+\zeta/R_2)} \frac{\partial \sigma_2^{(k)}}{\partial \alpha_2} + \\ &+ \frac{\sigma_1^{(k)} - \sigma_2^{(k)}}{A_1 A_2 (1+\zeta/R_1)} \frac{\partial A_1}{\partial \alpha_2} - \frac{1}{A_1(1+\zeta/R_1)} \frac{\partial \tau_{12}^{(k)}}{\partial \alpha_1} - \frac{2\tau_{12}^{(k)}}{A_1 A_2 (1+\zeta/R_2)} \frac{\partial A_2}{\partial \alpha_1} \end{aligned} \tag{94}$$

The previous equation can be solved once the derivatives of $\sigma_1^{(k)}, \sigma_2^{(k)}$ and $\tau_{12}^{(k)}$ are performed. The boundary condition of the previous first order differential equation is derived from the loading condition at the bottom surface when $k = 1$. On the other hand, for $k \neq 1$ the boundary conditions are modelled from the equilibrium conditions at the interface between two adjacent laminae:

$$k = 1 \;\Rightarrow\; \begin{cases} \overline{\tau}^{(1)}_{13(ij1)} = q^{(-)}_{1(ij)} \\ \overline{\tau}^{(1)}_{23(ij1)} = q^{(-)}_{2(ij)} \end{cases} \qquad k \neq 1 \;\Rightarrow\; \begin{cases} \overline{\tau}^{(k)}_{13(ij((k-1)I_T+1))} = \overline{\tau}^{(k-1)}_{13(ij((k-1)I_T))} \\ \overline{\tau}^{(k)}_{23(ij((k-1)I_T+1))} = \overline{\tau}^{(k-1)}_{23(ij((k-1)I_T))} \end{cases} \tag{95}$$

In order to assess the loading condition at the top surface of the shell, namely $\overline{\tau}^{(l)}_{13(ij(lI_T))} = q^{(+)}_{1(ij)}$ and $\overline{\tau}^{(l)}_{23(ij(lI_T))} = q^{(+)}_{2(ij)}$, the recovered profiles of the shear stresses $\overline{\tau}^{(k)}_{13(ijm)}$ and $\tau^{(k)}_{23(ijm)}$ are adjusted, for each $m = 1,...,lI_T$, as follows [45]:

$$\begin{aligned} \tau^{(k)}_{13(ijm)} &= \overline{\tau}^{(k)}_{13(ijm)} + \frac{q^{(+)}_{1(ij)} - \overline{\tau}^{(l)}_{13(ij(l\,I_T))}}{h} \left(\zeta_m + \frac{h}{2} \right) \\ \tau^{(k)}_{23(ijm)} &= \overline{\tau}^{(k)}_{23(ijm)} + \frac{q^{(+)}_{2(ij)} - \overline{\tau}^{(l)}_{23(ij(l\,I_T))}}{h} \left(\zeta_m + \frac{h}{2} \right) \end{aligned} \tag{96}$$

$q^{(+)}_{1(ij)}$ and $q^{(+)}_{2(ij)}$ represent the magnitude of the external load applied at

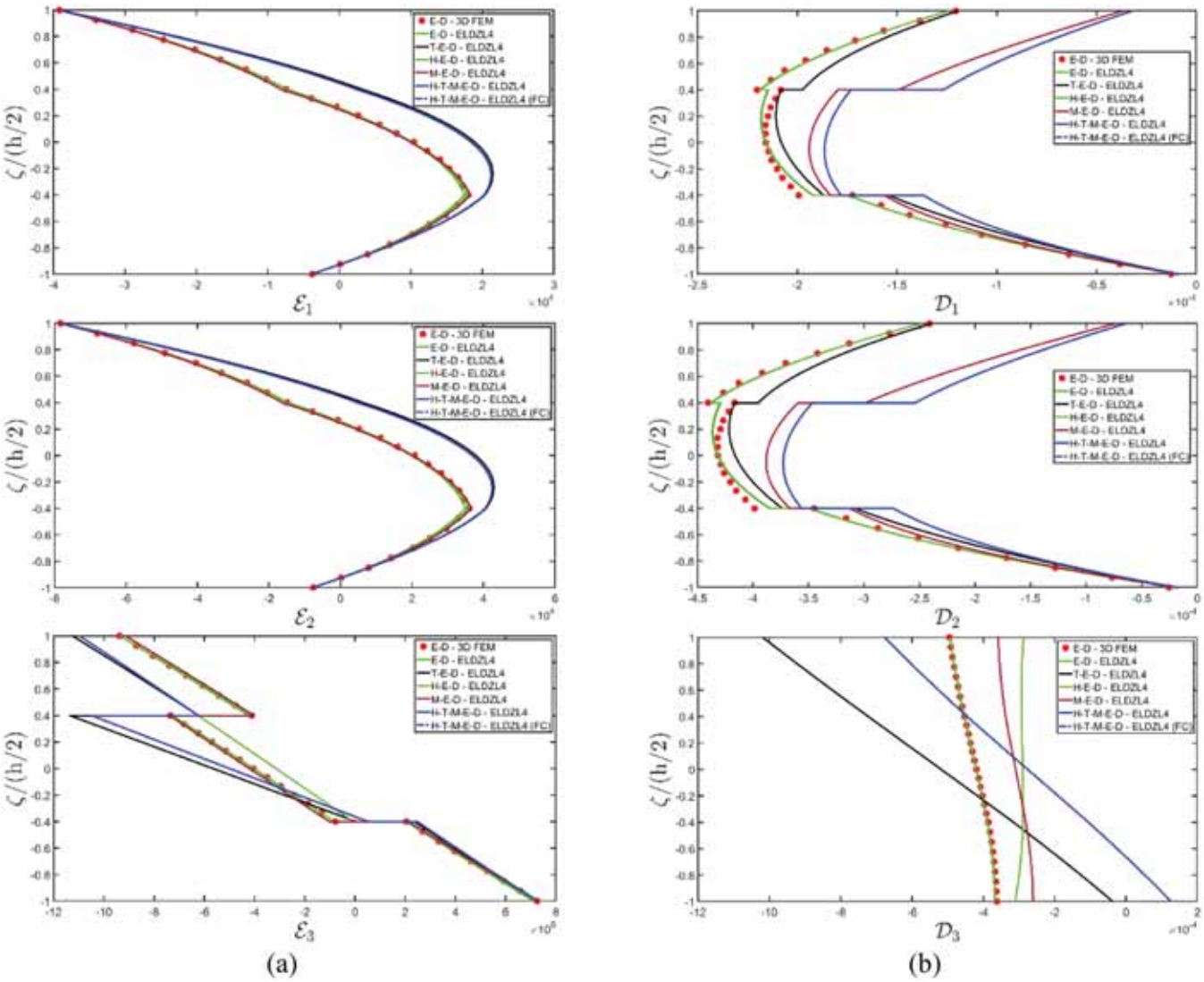

Figure 5. Distribution of the components of the electrostatic field (a) and the magnetostatic field (b) along the thickness direction of a simply supported rectangular plate subjected to a sinusoidal generalized action. Effect of the coupling in various multifield simulations. Thickness plots are provided at $(0.25{\cdot}L_1, 0.25{\cdot}L_2)$ within the physical domain.

$\zeta = h/2$ along α_1 and α_2 directions. As a consequence, the same approach is adopted for the reconstruction of the profile of the out-of-plane normal stress $\sigma_3^{(k)}$. Following a similar procedure, the profiles of the recovered secondary variables, denoted as $D_3^{(k)}, B_3^{(k)}, h_3^{(k)}, c_3^{(k)}$, are derived from the balance equations of the electrostatic, magnetostatic, heat and mass transfer problem, as reported in the following [45]:

$$\frac{\partial \sigma_3^{(k)}}{\partial \zeta}+\sigma_3^{(k)}\left(\frac{1}{R_1+\zeta}+\frac{1}{R_2+\zeta}\right)=-\frac{1}{A_1(1+\zeta/R_1)}\frac{\partial \tau_{13}^{(k)}}{\partial \alpha_1}-\frac{\tau_{13}^{(k)}}{A_1A_2(1+\zeta/R_2)}\frac{\partial A_2}{\partial \alpha_1}+ -\frac{1}{A_2(1+\zeta/R_2)}\frac{\partial \tau_{23}^{(k)}}{\partial \alpha_2}-\frac{\tau_{23}^{(k)}}{A_1A_2(1+\zeta/R_1)}\frac{\partial A_1}{\partial \alpha_2}+\frac{\sigma_1^{(k)}}{R_1+\zeta}+\frac{\sigma_2^{(k)}}{R_2+\zeta}$$

$$\frac{\partial D_3^{(k)}}{\partial \zeta}+D_3^{(k)}\left(\frac{1}{R_1+\zeta}+\frac{1}{R_2+\zeta}\right)=-\frac{1}{A_1(1+\zeta/R_1)}\frac{\partial D_1^{(k)}}{\partial \alpha_1}-\frac{D_1^{(k)}}{A_1A_2(1+\zeta/R_2)}\frac{\partial A_2}{\partial \alpha_1}+ -\frac{1}{A_2(1+\zeta/R_2)}\frac{\partial D_2^{(k)}}{\partial \alpha_2}-\frac{D_2^{(k)}}{A_1A_2(1+\zeta/R_1)}\frac{\partial A_1}{\partial \alpha_2}$$

$$\frac{\partial B_3^{(k)}}{\partial \zeta}+B_3^{(k)}\left(\frac{1}{R_1+\zeta}+\frac{1}{R_2+\zeta}\right)=-\frac{1}{A_1(1+\zeta/R_1)}\frac{\partial B_1^{(k)}}{\partial \alpha_1}-\frac{B_1^{(k)}}{A_1A_2(1+\zeta/R_2)}\frac{\partial A_2}{\partial \alpha_1}+ -\frac{1}{A_2(1+\zeta/R_2)}\frac{\partial B_2^{(k)}}{\partial \alpha_2}-\frac{B_2^{(k)}}{A_1A_2(1+\zeta/R_1)}\frac{\partial A_1}{\partial \alpha_2}$$

$$\frac{\partial h_3^{(k)}}{\partial \zeta}+h_3^{(k)}\left(\frac{1}{R_1+\zeta}+\frac{1}{R_2+\zeta}\right)=-\frac{1}{A_1(1+\zeta/R_1)}\frac{\partial h_1^{(k)}}{\partial \alpha_1}-\frac{h_1^{(k)}}{A_1A_2(1+\zeta/R_2)}\frac{\partial A_2}{\partial \alpha_1}+ -\frac{1}{A_2(1+\zeta/R_2)}\frac{\partial h_2^{(k)}}{\partial \alpha_2}-\frac{h_2^{(k)}}{A_1A_2(1+\zeta/R_1)}\frac{\partial A_1}{\partial \alpha_2}$$

$$\frac{\partial c_3^{(k)}}{\partial \zeta}+c_3^{(k)}\left(\frac{1}{R_1+\zeta}+\frac{1}{R_2+\zeta}\right)=-\frac{1}{A_1(1+\zeta/R_1)}\frac{\partial c_1^{(k)}}{\partial \alpha_1}-\frac{c_1^{(k)}}{A_1A_2(1+\zeta/R_2)}\frac{\partial A_2}{\partial \alpha_1}+ -\frac{1}{A_2(1+\zeta/R_2)}\frac{\partial c_2^{(k)}}{\partial \alpha_2}-\frac{c_2^{(k)}}{A_1A_2(1+\zeta/R_1)}\frac{\partial A_1}{\partial \alpha_2} \tag{97}$$

Following the approach already adopted in Eqns. (96)-(97), a numerical solution can be derived if the boundary conditions and inter-laminar equilibrium conditions are considered:

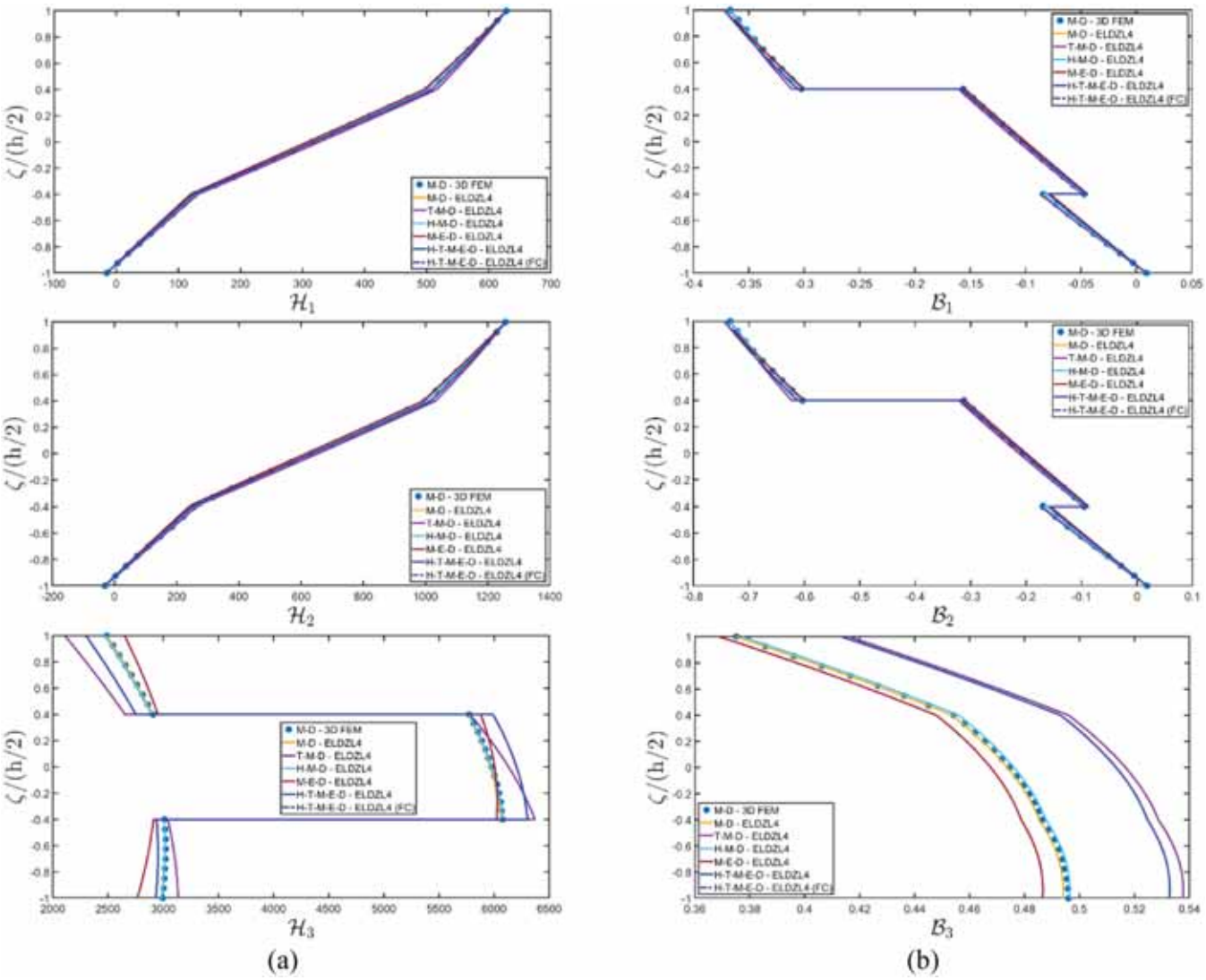

Figure 6. Distribution of the components of the electric displacement (a) and the magnetostatic flux (b) along the thickness direction of a simply supported rectangular plate subjected to a sinusoidal generalized action. Effect of the coupling in various multifield simulations. Thickness plots are provided at $(0.25{\cdot}L_1, 0.25{\cdot}L_2)$ within the physical domain.

$$k=1 \;\Rightarrow\; \begin{cases} \overline{\sigma}^{(1)}_{3(ij1)} = q^{(-)}_{3(ij)} \\ \overline{D}^{(1)}_{3(ij1)} = q^{(-)}_{\mathrm{D}(ij)} \\ \overline{B}^{(1)}_{3(ij1)} = q^{(-)}_{\mathrm{B}(ij)} \\ \overline{h}^{(1)}_{3(ij1)} = q^{(-)}_{\mathrm{T}(ij)} \\ \overline{c}^{(1)}_{3(ij1)} = q^{(-)}_{\mathrm{C}(ij)} \end{cases} \qquad k\neq 1 \;\Rightarrow\; \begin{cases} \overline{\sigma}^{(k)}_{3(ij((k-1)I_T+1))} = \overline{\sigma}^{(k-1)}_{3(ij((k-1)I_T))} \\ \overline{D}^{(k)}_{3(ij((k-1)I_T+1))} = \overline{D}^{(k-1)}_{3(ij((k-1)I_T))} \\ \overline{B}^{(k)}_{3(ij((k-1)I_T+1))} = \overline{B}^{(k-1)}_{3(ij((k-1)I_T))} \\ \overline{h}^{(k)}_{3(ij((k-1)I_T+1))} = \overline{h}^{(k-1)}_{3(ij((k-1)I_T))} \\ \overline{c}^{(k)}_{3(ij((k-1)I_T+1))} = \overline{c}^{(k-1)}_{3(ij((k-1)I_T))} \end{cases} \tag{98}$$

Equilibrium under multifield surface actions is achieved at the top surface through the implementation of the following linear corrections of the solution:

$$\sigma^{(k)}_{3(ijm)} = \overline{\sigma}^{(k)}_{3(ijm)} + \frac{q^{(+)}_{3(ij)} - \overline{\sigma}^{(l)}_{3(ij(l\,I_T))}}{h}\left(\zeta_m + \frac{h}{2}\right)$$

$$D^{(k)}_{3(ijm)} = \overline{D}^{(k)}_{3(ijm)} + \frac{q^{(+)}_{\mathrm{D}(ij)} - \overline{D}^{(l)}_{3(ij(l\,I_T))}}{h}\left(\zeta_m + \frac{h}{2}\right)$$

$$B^{(k)}_{3(ijm)} = \overline{B}^{(k)}_{3(ijm)} + \frac{q^{(+)}_{\mathrm{B}(ij)} - \overline{B}^{(l)}_{3(ij(l\,I_T))}}{h}\left(\zeta_m + \frac{h}{2}\right)$$

$$h^{(k)}_{3(ijm)} = \overline{h}^{(k)}_{3(ijm)} + \frac{q^{(+)}_{\mathrm{T}(ij)} - \overline{h}^{(l)}_{3(ij(l\,I_T))}}{h}\left(\zeta_m + \frac{h}{2}\right)$$

$$c^{(k)}_{3(ijm)} = \overline{c}^{(k)}_{3(ijm)} + \frac{q^{(+)}_{\mathrm{C}(ij)} - \overline{h}^{(l)}_{3(ij(l\,I_T))}}{h}\left(\zeta_m + \frac{h}{2}\right) \tag{99}$$

Starting from the multifield constitutive relations of Eqn. (31), the linear system [45] reported below can be adopted to recover the multifield out-of-plane primary variables, which are collected in the vectors $\mathbf{x}^{(k)}_{1(ijm)} = \left[\gamma^{(k)}_{13(ijm)} \quad \gamma^{(k)}_{23(ijm)} \quad \varepsilon^{(k)}_{3(ijm)} \quad E^{(k)}_{3(ijm)} \quad H^{(k)}_{3(ijm)}\right]^T$ and $\mathbf{x}^{(k)}_{2(ijm)} = \left[\theta^{(k)}_{3(ijm)} \quad \lambda^{(k)}_{3(ijm)}\right]^T$, setting $i = 1,\ldots,I_N$, $j = 1,\ldots,I_M$ and $m = 1,\ldots,lI_T$:

$$\begin{bmatrix} \mathbf{A}^{(k)}_{11(ijm)} & \mathbf{0} \\ \mathbf{0} & \mathbf{A}^{(k)}_{22(ijm)} \end{bmatrix} \begin{bmatrix} \mathbf{x}^{(k)}_{1(ijm)} \\ \mathbf{x}^{(k)}_{2(ijm)} \end{bmatrix} = \begin{bmatrix} \mathbf{B}^{(k)}_{1(ijm)} \\ \mathbf{B}^{(k)}_{2(ijm)} \end{bmatrix} \;\Leftrightarrow\; \mathbf{A}^{(k)}_{(ijm)}\mathbf{x}^{(k)}_{(ijm)} = \mathbf{B}^{(k)}_{(ijm)} \tag{100}$$

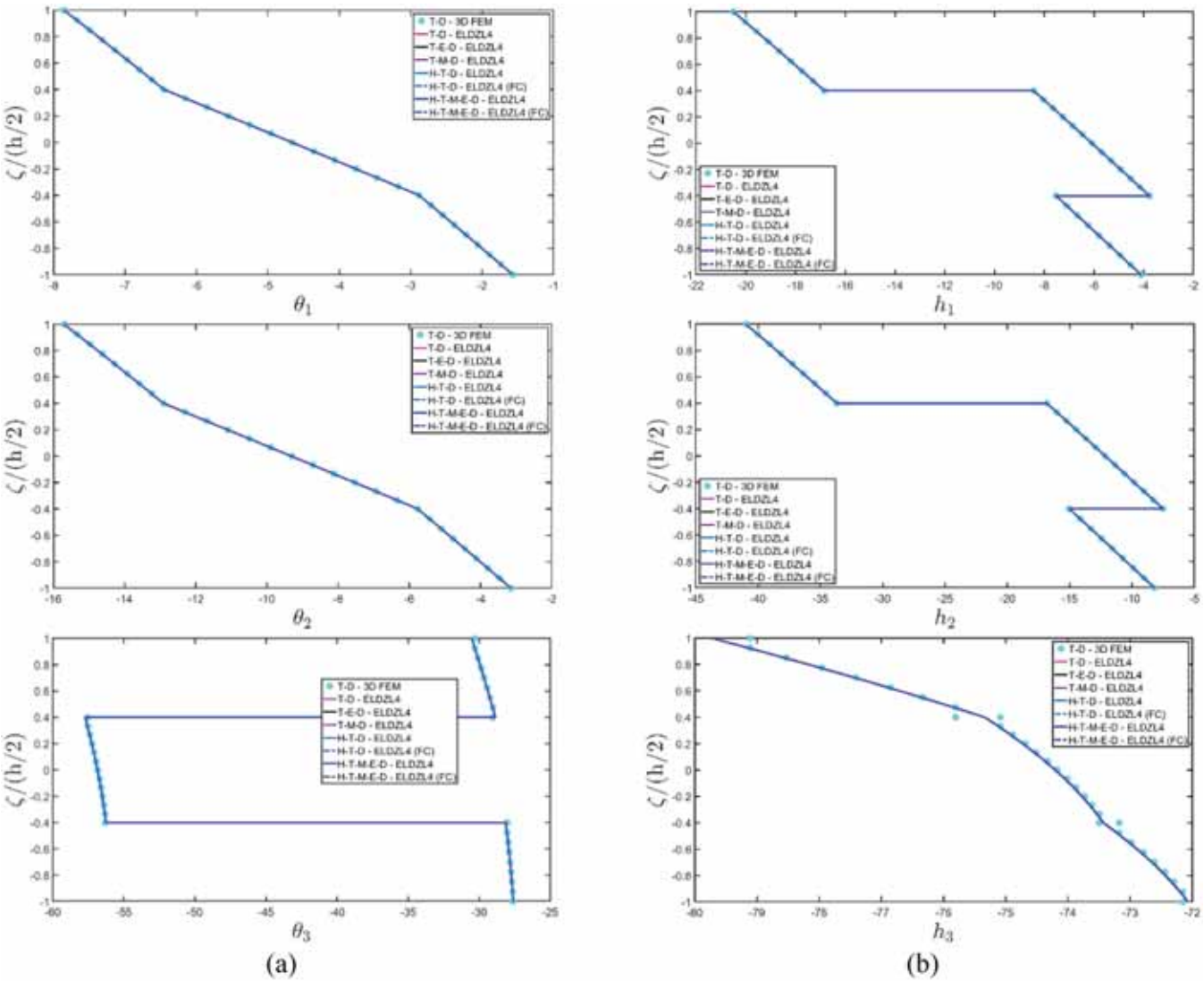

Figure 7. Distribution of the components of the thermal gradient (a) and the thermal flux (b) along the thickness direction of a simply supported rectangular plate subjected to a sinusoidal generalized action. Effect of the coupling in various multifield simulations. Thickness plots are provided at $(0.25{\cdot}L_1, 0.25{\cdot}L_2)$ within the physical domain.

The matrices $\mathbf{A}^{(k)}_{11(ijm)}, \mathbf{A}^{(k)}_{22(ijm)}$ and the vectors $\mathbf{B}^{(k)}_{1(ijm)}, \mathbf{B}^{(k)}_{2(ijm)}$ take the following aspect:

$$\mathbf{A}^{(k)}_{11(ijm)} = \begin{bmatrix} \overline{C}^{(k)}_{44(ijm)} & 0 & 0 & 0 & 0 \\ 0 & \overline{C}^{(k)}_{55(ijm)} & 0 & 0 & 0 \\ 0 & 0 & \overline{C}^{(k)}_{33(ijm)} & -\overline{p}^{(k)}_{33(ijm)} & -\overline{q}^{(k)}_{33(ijm)} \\ 0 & 0 & \overline{p}^{(k)}_{33(ijm)} & \overline{l}^{(k)}_{33(ijm)} & \overline{d}^{(k)}_{33(ijm)} \\ 0 & 0 & \overline{q}^{(k)}_{33(ijm)} & \overline{d}^{(k)}_{33(ijm)} & \overline{m}^{(k)}_{33(ijm)} \end{bmatrix}, \quad \mathbf{A}^{(k)}_{22(ijm)} = \begin{bmatrix} \overline{k}^{(k)}_{33(ijm)} & \overline{y}^{(k)}_{33(ijm)} \\ \overline{x}^{(k)}_{33(ijm)} & \overline{s}^{(k)}_{33(ijm)} \end{bmatrix} \tag{101}$$

$$\mathbf{B}^{(k)}_{1(ijm)} = \begin{bmatrix} b^{(k)}_{1(ijm)} & b^{(k)}_{2(ijm)} & b^{(k)}_{3(ijm)} & b^{(k)}_{4(ijm)} & b^{(k)}_{5(ijm)} \end{bmatrix}^T, \quad \mathbf{B}^{(k)}_{2(ijm)} = \begin{bmatrix} b^{(k)}_{6(ijm)} & b^{(k)}_{7(ijm)} \end{bmatrix}^T \tag{102}$$

The quantities $b^{(k)}_{1(ijm)}, b^{(k)}_{2(ijm)}, b^{(k)}_{3(ijm)}, b^{(k)}_{4(ijm)}, b^{(k)}_{5(ijm)}, b^{(k)}_{6(ijm)}, b^{(k)}_{7(ijm)}$ are written in the following extended form:

$$\begin{aligned}
b^{(k)}_{1(ijm)} &= \tau^{(k)}_{13(ijm)} + \overline{p}^{(k)}_{14(ijm)} E^{(k)}_{1(ijm)} + \overline{q}^{(k)}_{14(ijm)} H^{(k)}_{1(ijm)} \\
b^{(k)}_{2(ijm)} &= \tau^{(k)}_{23(ijm)} + \overline{p}^{(k)}_{25(ijm)} E^{(k)}_{2(ijm)} + \overline{q}^{(k)}_{25(ijm)} H^{(k)}_{2(ijm)} \\
b^{(k)}_{3(ijm)} &= \sigma^{(k)}_{3(ijm)} - \overline{C}^{(k)}_{13(ijm)} \varepsilon^{(k)}_{1(ijm)} - \overline{C}^{(k)}_{23(ijm)} \varepsilon^{(k)}_{2(ijm)} + \overline{\varepsilon}^{(k)}_{33(ijm)} \widehat{\Delta T}^{(k)}_{(ijm)} + \overline{e}^{(k)}_{33(ijm)} \widehat{\Delta C}^{(k)}_{(ijm)} \\
b^{(k)}_{4(ijm)} &= D^{(k)}_{3(ijm)} - \overline{p}^{(k)}_{31(ijm)} \varepsilon^{(k)}_{1(ijm)} - \overline{p}^{(k)}_{32(ijm)} \varepsilon^{(k)}_{2(ijm)} - \overline{o}^{(k)}_{33(ijm)} \widehat{\Delta T}^{(k)}_{(ijm)} - \overline{g}^{(k)}_{33(ijm)} \widehat{\Delta C}^{(k)}_{(ijm)} \\
b^{(k)}_{5(ijm)} &= B^{(k)}_{3(ijm)} - \overline{q}^{(k)}_{31(ijm)} \varepsilon^{(k)}_{1(ijm)} - \overline{q}^{(k)}_{32(ijm)} \varepsilon^{(k)}_{2(ijm)} - \overline{w}^{(k)}_{33(ijm)} \widehat{\Delta T}^{(k)}_{(ijm)} - \overline{f}^{(k)}_{33(ijm)} \widehat{\Delta C}^{(k)}_{(ijm)} \\
b^{(k)}_{6(ijm)} &= h^{(k)}_{3(ijm)} \\
b^{(k)}_{7(ijm)} &= c^{(k)}_{3(ijm)}
\end{aligned} \tag{103}$$

Once the out-of-plane secondary variables are recovered from the three-dimensional balance equations, the multifield constitutive relationship (29) is adopted to derive the recovered values of the in-plane secondary variables. This process takes into account the updated primary variables that have already been recovered. As a consequence, this approach ensures that the profiles, despite being derived from a two-dimensional solution, well match the predictions of a three-dimensional model.

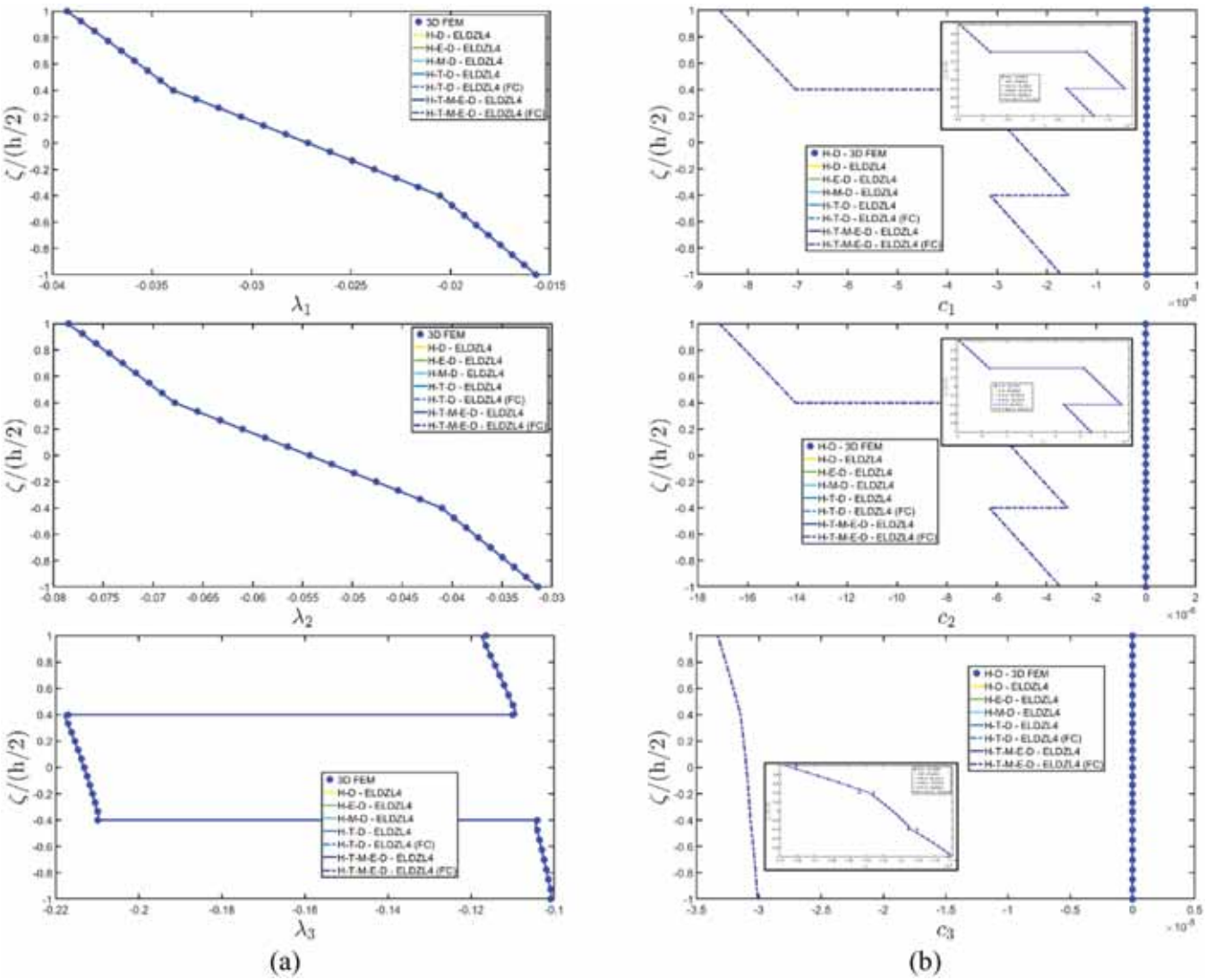

Figure 8. Distribution of the components of the concentration gradient (a) and the hygroscopic flux (b) along the thickness direction of a simply supported rectangular plate subjected to a sinusoidal generalized action. Effect of the coupling in various multifield simulations. Thickness plots are provided at $(0.25{\cdot}L_1, 0.25{\cdot}L_2)$ within the physical domain.

9. Applications and results

Three examples are now presented in which the response of a rectangular plate, a cylindrical panel, and a shallow spherical shell under various multifield loadings is evaluated using the present formulation. For each case, different levels of coupling between the involved fields are considered, and the response of the same structure is predicted under various combinations of loads. A rapid identification of the fields involved in the simulation is achieved through a proper nomenclature. In this context, the mechanical elasticity problem is denoted by the letter "D" because the displacement field vector represents the corresponding configuration variable. On the other hand, the letters "E" and "M" are used when simulating the electric and the magnetic effects, respectively. Furthermore, "T" refers to heat transfer, where the temperature is the unknown field variable, while "C" accounts for the hygrometric problem, with moisture concentration as configuration variable. Finally, the acronym "FC" is employed in simulations involving the Fick diffusion equations and Fourier heat transfer problem, along with Dufour and Soret coupling effects. All the multifield simulations carried out in this study are explained in detail in Table 1. As far as the external loads are concerned, in each simulation two mechanical surface tractions are applied at the top and bottom surfaces of the panel. These loads are distributed with a sinusoidal dispersion with wave numbers along α_1 and α_2 denoted as $n = m = 1$, while $\overline{q}_3^{(+)} = -7{\cdot}10^5$ Pa and $\overline{q}_3^{(-)} = 3{\cdot}10^5$ Pa represent the wave amplitudes of these loads. In addition, a predetermined sinusoidal distribution of the multifield configuration variables is enforced at the top and bottom surfaces of the panel with $n = m = 1$, following the expression given in Eqn. (76). The following reference values of the wave amplitudes are adopted when investigating the rectangular plate:

$$\begin{aligned} \Phi_{nm}^{(0)} &= \phi^{(-)} = 5{\cdot}10^3\,\mathrm{V}, \quad \Phi_{nm}^{(N)} = \phi^{(+)} = 5{\cdot}10^4\,\mathrm{V} \\ \Psi_{nm}^{(0)} &= \psi^{(-)} = 2{\cdot}10^1\,\mathrm{A}, \quad \Psi_{nm}^{(N)} = \psi^{(+)} = -8{\cdot}10^2\,\mathrm{A} \\ \Xi_{nm}^{(0)} &= \Delta\mathrm{T}^{(-)} = 2\,\mathrm{K}, \quad \Xi_{nm}^{(N)} = \Delta\mathrm{T}^{(+)} = 10\,\mathrm{K} \\ \mathrm{K}_{nm}^{(0)} &= \Delta\mathrm{C}^{(-)} = 0.02\,\mathrm{kg/m^3}, \quad \mathrm{K}_{nm}^{(N)} = \Delta\mathrm{C}^{(+)} = 0.05\,\mathrm{kg/m^3} \end{aligned} \tag{104}$$

As can be seen from Eqn. (13), the symbol $(+)$ is used to denote the top surface, while $(-)$ indicates that the configuration variable is applied at the bottom surface. It should be noted that the reference values mentioned in Eqn. (107) are equal to the generalized configuration variables of the kinematic model described in Eqn. (10) corresponding to $\tau = 0$ and $\tau = N$, respectively. These variables are located at the two outer skins of the panel under consideration. On the other hand, the wave amplitudes reported below are enforced for the cylindrical

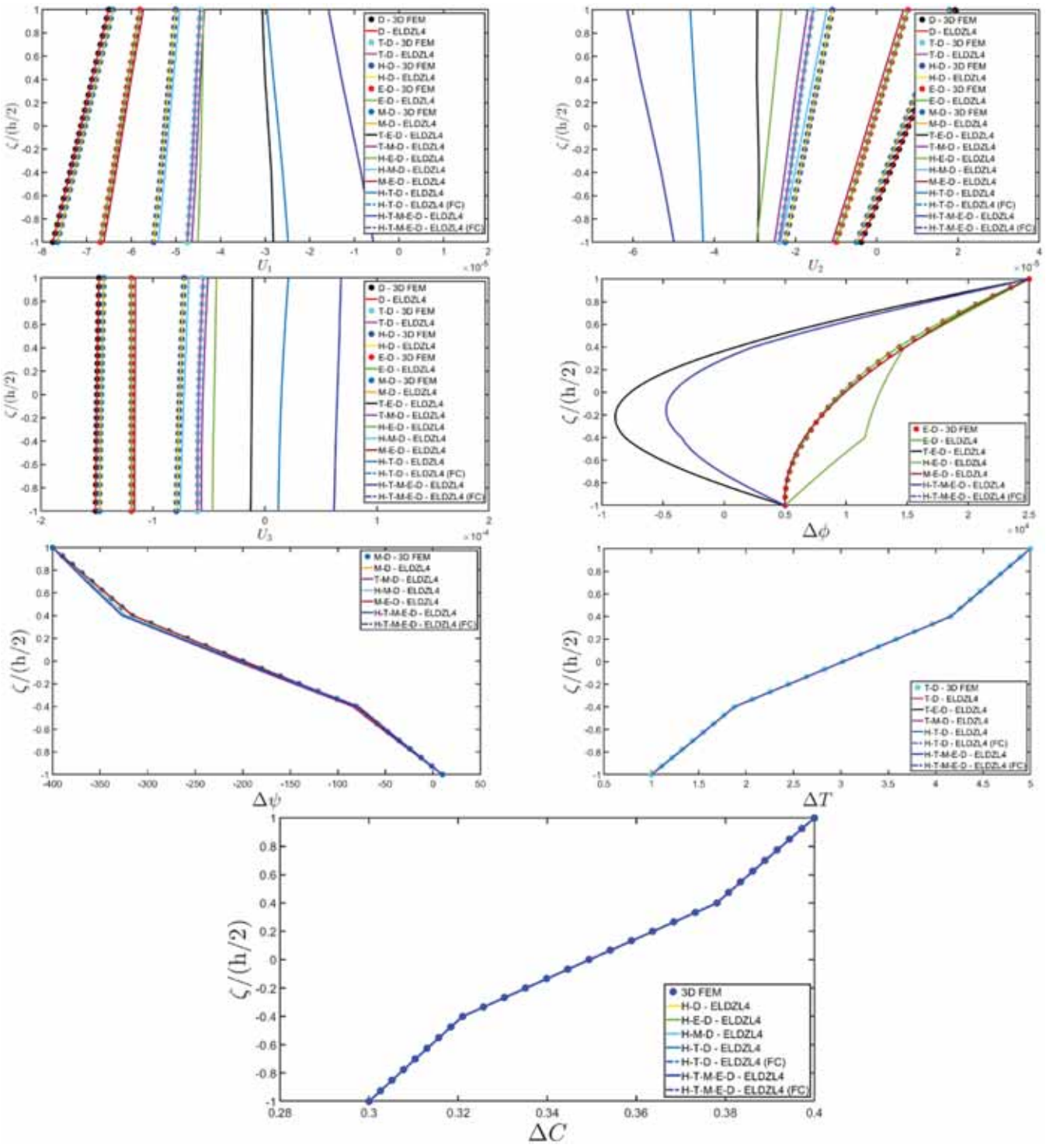

Figure 9. Distribution of the displacement field components, electric potential, magnetostatic potential, temperature variation and concentration variation along the thickness direction of a simply supported cylindrical panel subjected to a sinusoidal generalized action. Effect of the coupling in various multifield simulations. Thickness plots are provided at $(0.25{\cdot}L_1, 0.25{\cdot}L_2)$ within the physical domain.

panel and the shallow spherical shell:

$$\begin{aligned} \Phi_{nm}^{(0)} &= \phi^{(-)} = 1{\cdot}10^4\,\mathrm{V}, \quad \Phi_{nm}^{(N)} = \phi^{(+)} = 5{\cdot}10^4\,\mathrm{V} \\ \Psi_{nm}^{(0)} &= \psi^{(-)} = 1{\cdot}10^4\,\mathrm{A}, \quad \Psi_{nm}^{(N)} = \psi^{(+)} = 5{\cdot}10^4\,\mathrm{A} \\ \Xi_{nm}^{(0)} &= \Delta\mathrm{T}^{(-)} = 2\,\mathrm{K}, \quad \Xi_{nm}^{(N)} = \Delta\mathrm{T}^{(+)} = -10\,\mathrm{K} \\ \mathrm{K}_{nm}^{(0)} &= \Delta\mathrm{C}^{(-)} = 0.6\,\mathrm{kg/m^3}, \quad \mathrm{K}_{nm}^{(N)} = \Delta\mathrm{C}^{(+)} = 0.8\,\mathrm{kg/m^3} \end{aligned} \tag{105}$$

The fundamental relations are solved following Navier's approach, as outlined in Eqn. (76). As a result, the simply-supported boundary conditions are applied along the four edges of the rectangular physical domain, as shown in Eqn. (71). A cross-ply $(0/90/0)$ lamination scheme consisting of three layers is adopted in each panel. More specifically, the two external layers of thickness $h_1 = h_3 = 0.03\,\mathrm{m}$ are composed of adaptive wood, while the central core of thickness $h_2 = 0.04\,\mathrm{m}$ consists of soft adaptive wood. The mechanical properties of the adaptive wood are listed below and taken from Ref. [45], following the notation of Eqn.

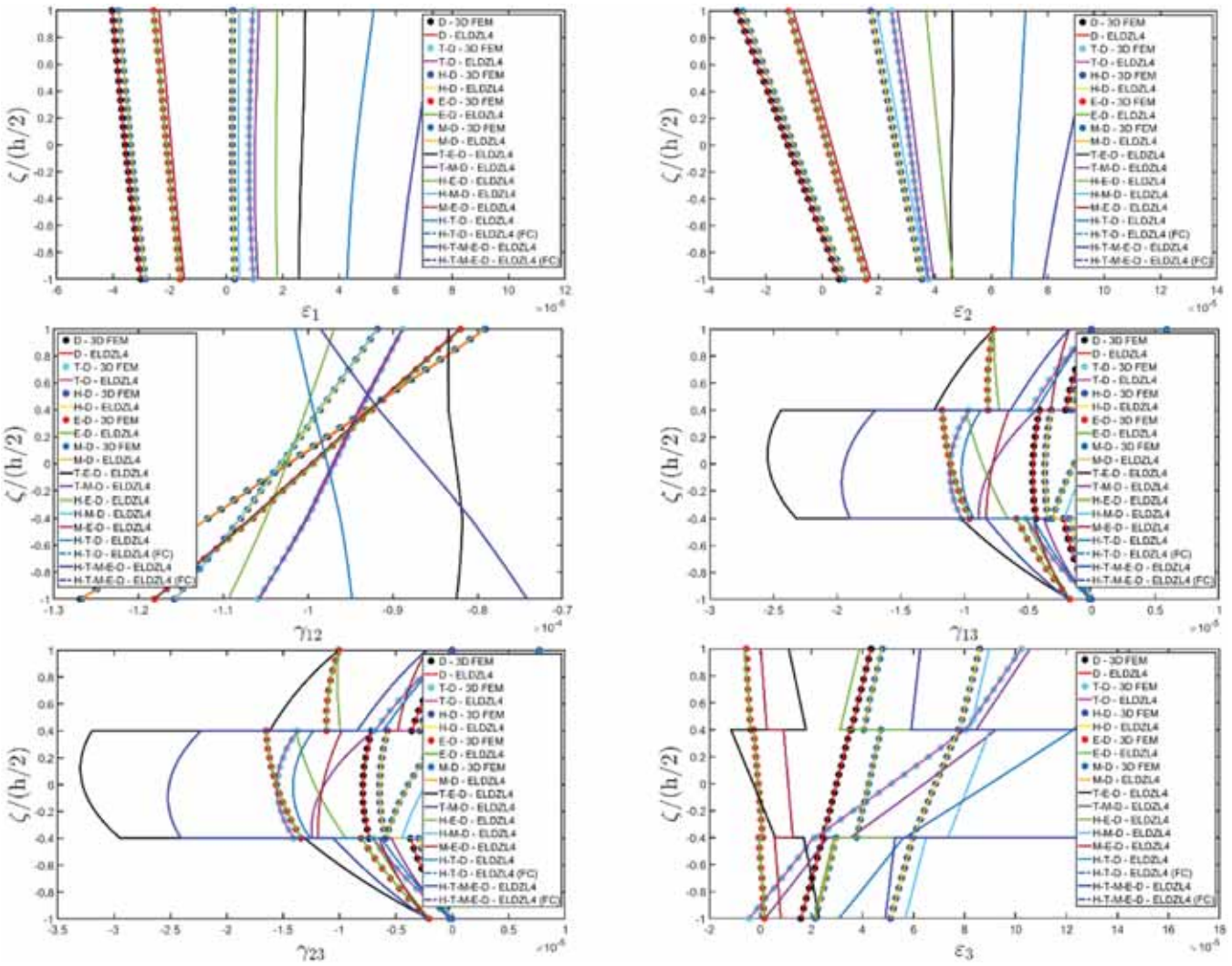

Figure 10. Distribution of the three-dimensional strain components along the thickness direction of a simply supported cylindrical panel subjected to a sinusoidal generalized action. Effect of the coupling in various multifield simulations. Thickness plots are provided at $(0.25{\cdot}L_1, 0.25{\cdot}L_2)$within the physical domain.

(31):

Stiffness matrix

$$\mathbf{\Gamma}_{\mathrm{C}}^{(k)} = \begin{bmatrix} C_{11}^{(k)} & C_{12}^{(k)} & C_{16}^{(k)} & C_{14}^{(k)} & C_{15}^{(k)} & C_{13}^{(k)} \\ C_{12}^{(k)} & C_{22}^{(k)} & C_{26}^{(k)} & C_{24}^{(k)} & C_{25}^{(k)} & C_{23}^{(k)} \\ C_{16}^{(k)} & C_{26}^{(k)} & C_{66}^{(k)} & C_{46}^{(k)} & C_{56}^{(k)} & C_{36}^{(k)} \\ C_{14}^{(k)} & C_{24}^{(k)} & C_{46}^{(k)} & C_{44}^{(k)} & C_{45}^{(k)} & C_{34}^{(k)} \\ C_{15}^{(k)} & C_{25}^{(k)} & C_{56}^{(k)} & C_{45}^{(k)} & C_{55}^{(k)} & C_{35}^{(k)} \\ C_{13}^{(k)} & C_{23}^{(k)} & C_{36}^{(k)} & C_{34}^{(k)} & C_{35}^{(k)} & C_{33}^{(k)} \end{bmatrix} = \begin{bmatrix} 286 & 173 & 0 & 0 & 0 & 170.5 \\ 173 & 286 & 0 & 0 & 0 & 170.5 \\ 0 & 0 & 56.5 & 0 & 0 & 0 \\ 0 & 0 & 0 & 45.3 & 0 & 0 \\ 0 & 0 & 0 & 0 & 45.3 & 0 \\ 170.5 & 170.5 & 0 & 0 & 0 & 269.5 \end{bmatrix} \text{GPa} \tag{106}$$

Piezoelectric matrix

$$\mathbf{\Gamma}_{\mathrm{P}}^{(k)} = \begin{bmatrix} p_{11}^{(k)} & p_{12}^{(k)} & p_{16}^{(k)} & p_{14}^{(k)} & p_{15}^{(k)} & p_{13}^{(k)} \\ p_{21}^{(k)} & p_{22}^{(k)} & p_{26}^{(k)} & p_{24}^{(k)} & p_{25}^{(k)} & p_{23}^{(k)} \\ p_{31}^{(k)} & p_{32}^{(k)} & p_{36}^{(k)} & p_{34}^{(k)} & p_{35}^{(k)} & p_{33}^{(k)} \end{bmatrix} = \begin{bmatrix} 0 & 0 & 0 & 11.6 & 0 & 0 \\ 0 & 0 & 0 & 0 & 11.6 & 0 \\ -4.4 & -4.4 & 0 & 0 & 0 & 18.6 \end{bmatrix} \frac{\mathrm{C}}{\mathrm{m}^2} \tag{107}$$

Piezomagnetic matrix

$$\mathbf{\Gamma}_{\mathrm{Q}}^{(k)} = \begin{bmatrix} q_{11}^{(k)} & q_{12}^{(k)} & q_{16}^{(k)} & q_{14}^{(k)} & q_{15}^{(k)} & q_{13}^{(k)} \\ q_{21}^{(k)} & q_{22}^{(k)} & q_{26}^{(k)} & q_{24}^{(k)} & q_{25}^{(k)} & q_{23}^{(k)} \\ q_{31}^{(k)} & q_{32}^{(k)} & q_{36}^{(k)} & q_{34}^{(k)} & q_{35}^{(k)} & q_{33}^{(k)} \end{bmatrix} = \begin{bmatrix} 0 & 0 & 0 & 560 & 0 & 0 \\ 0 & 0 & 0 & 0 & 560 & 0 \\ 580 & 580 & 0 & 0 & 0 & 700 \end{bmatrix} \frac{\mathrm{N}}{\mathrm{A\,m}} \tag{108}$$

Dielectric matrix

$$\mathbf{\Gamma}_{\mathrm{L}}^{(k)} = \begin{bmatrix} l_{11}^{(k)} & l_{12}^{(k)} & l_{13}^{(k)} \\ l_{21}^{(k)} & l_{22}^{(k)} & l_{23}^{(k)} \\ l_{31}^{(k)} & l_{32}^{(k)} & l_{33}^{(k)} \end{bmatrix} = \begin{bmatrix} 8 & 0 & 0 \\ 0 & 8 & 0 \\ 0 & 0 & 9.3 \end{bmatrix} \cdot 10^{-11} \frac{\mathrm{C}^2}{\mathrm{N\,m}^2} \tag{109}$$

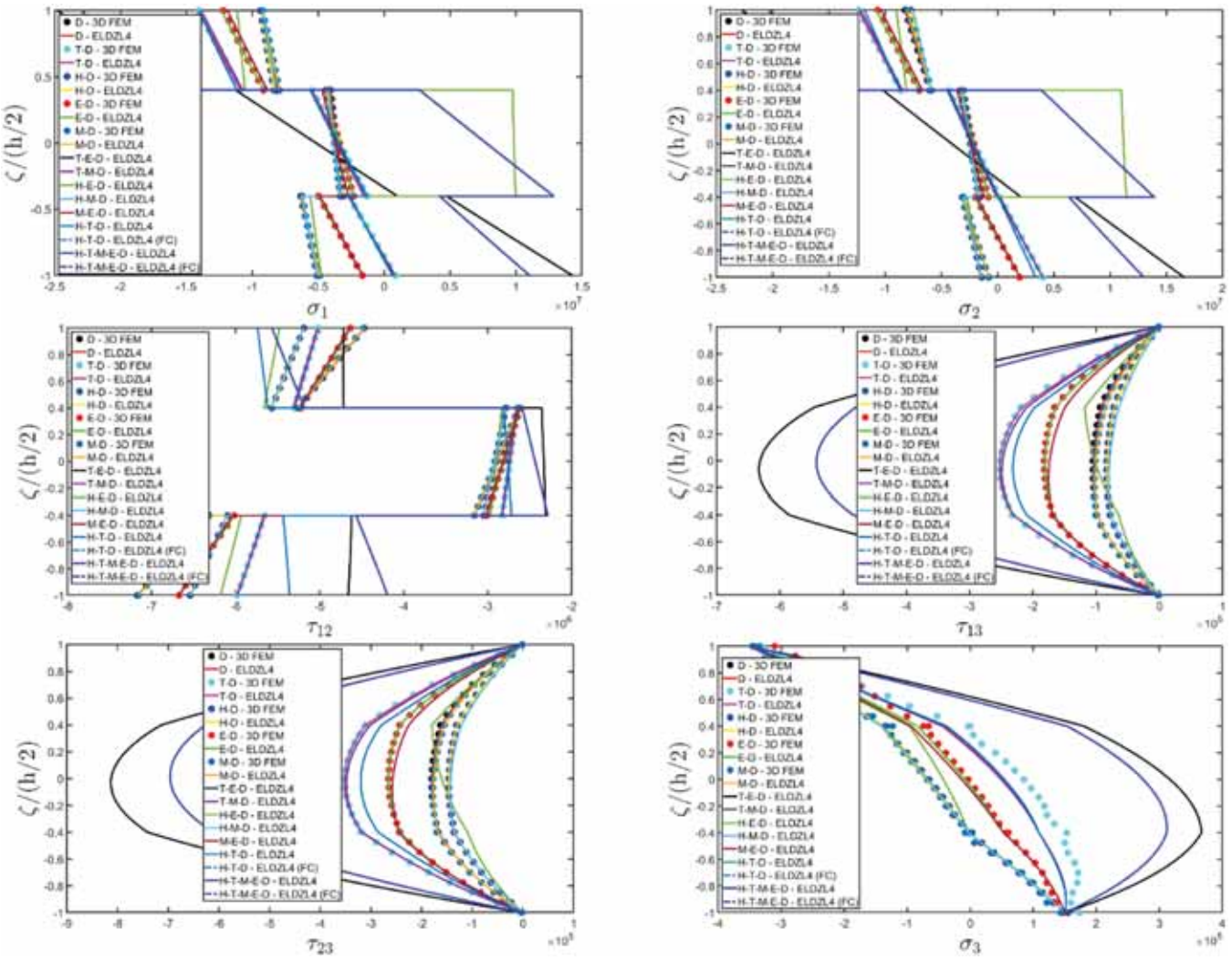

Figure 11. Distribution of the three-dimensional stress components [Pa] along the thickness direction of a simply supported cylindrical panel subjected to a sinusoidal generalized action. Effect of the coupling in various multifield simulations. Thickness plots are provided at $(0.25{\cdot}L_1, 0.25{\cdot}L_2)$ within the physical domain.

Magnetic permittivity matrix

$$\mathbf{\Gamma}_{\mathrm{M}}^{(k)} = \begin{bmatrix} m_{11}^{(k)} & m_{12}^{(k)} & m_{13}^{(k)} \\ m_{21}^{(k)} & m_{22}^{(k)} & m_{23}^{(k)} \\ m_{31}^{(k)} & m_{32}^{(k)} & m_{33}^{(k)} \end{bmatrix} = \begin{bmatrix} -5.9 & 0 & 0 \\ 0 & -5.9 & 0 \\ 0 & 0 & 1.57 \end{bmatrix} \cdot 10^{-4} \, \frac{\mathrm{N\ s^2}}{\mathrm{C^2}} \tag{110}$$

Magnetoelectric matrix

$$\mathbf{\Gamma}_{\mathrm{D}}^{(k)} = \begin{bmatrix} d_{11}^{(k)} & d_{12}^{(k)} & d_{13}^{(k)} \\ d_{21}^{(k)} & d_{22}^{(k)} & d_{23}^{(k)} \\ d_{31}^{(k)} & d_{32}^{(k)} & d_{33}^{(k)} \end{bmatrix} = \begin{bmatrix} 3 & 0 & 0 \\ 0 & 3 & 0 \\ 0 & 0 & 3 \end{bmatrix} \cdot 10^{-12} \, \frac{\mathrm{N\ s}}{\mathrm{V\ C}} \tag{111}$$

Pyroelectric matrix

$$\mathbf{\Gamma}_{\mathrm{o}}^{(k)} = \begin{bmatrix} o_{11}^{(k)} & o_{22}^{(k)} & o_{33}^{(k)} \end{bmatrix} = \begin{bmatrix} 0 & 0 & -1.3 \end{bmatrix} \cdot 10^{-4} \, \frac{\mathrm{C}}{\mathrm{m^2\ K}} \tag{112}$$

Pyromagnetic matrix

$$\mathbf{\Gamma}_{\mathrm{w}}^{(k)} = \begin{bmatrix} w_{11}^{(k)} & w_{22}^{(k)} & w_{33}^{(k)} \end{bmatrix} = \begin{bmatrix} 0 & 0 & 6 \end{bmatrix} \cdot 10^{-3} \, \frac{\mathrm{N}}{\mathrm{A\ m\ K}} \tag{113}$$

Thermal expansion matrix

$$\mathbf{\Gamma}_{\mathrm{a}}^{(k)} = \begin{bmatrix} a_{11}^{(k)} & a_{22}^{(k)} & a_{12}^{(k)} & a_{13}^{(k)} & a_{23}^{(k)} & a_{33}^{(k)} \end{bmatrix} = \begin{bmatrix} 14.1 & 14.1 & 0 & 0 & 0 & 7.2 \end{bmatrix} \cdot 10^{-6} \frac{1}{\mathrm{K}}$$

$$\mathbf{\Gamma}_{\mathrm{z}}^{(k)} = \begin{bmatrix} z_{11}^{(k)} & z_{22}^{(k)} & z_{12}^{(k)} & z_{13}^{(k)} & z_{23}^{(k)} & z_{33}^{(k)} \end{bmatrix} = \begin{bmatrix} 6.9245 & 6.9245 & 0 & 0 & 0 & 6.7155 \end{bmatrix} \cdot 10^{7} \frac{\mathrm{GPa}}{\mathrm{K}} \tag{114}$$

Hygroscopic expansion matrix

$$\mathbf{\Gamma}_{\mathrm{b}}^{(k)} = \begin{bmatrix} b_{11}^{(k)} & b_{22}^{(k)} & b_{12}^{(k)} & b_{13}^{(k)} & b_{23}^{(k)} & b_{33}^{(k)} \end{bmatrix} = \begin{bmatrix} 1.10 & 1.10 & 0 & 0 & 0 & 1.10 \end{bmatrix} \cdot 10^{-4} \frac{\mathrm{m^3}}{\mathrm{kg}}$$

$$\mathbf{\Gamma}_{\mathrm{e}}^{(k)} = \begin{bmatrix} e_{11}^{(k)} & e_{22}^{(k)} & e_{12}^{(k)} & e_{13}^{(k)} & e_{23}^{(k)} & e_{33}^{(k)} \end{bmatrix} = \begin{bmatrix} 7.6995 & 7.6995 & 0 & 0 & 0 & 6.7485 \end{bmatrix} \cdot 10^{6} \frac{\mathrm{m^3\,GPa}}{\mathrm{kg}} \tag{115}$$

Thermal conductivity matrix

$$\mathbf{\Gamma}_{\mathrm{K}}^{(k)} = \begin{bmatrix} k_{11}^{(k)} & k_{12}^{(k)} & k_{13}^{(k)} \\ k_{21}^{(k)} & k_{22}^{(k)} & k_{23}^{(k)} \\ k_{31}^{(k)} & k_{32}^{(k)} & k_{33}^{(k)} \end{bmatrix} = \begin{bmatrix} 2.61 & 0 & 0 \\ 0 & 2.61 & 0 \\ 0 & 0 & 2.61 \end{bmatrix} \frac{\mathrm{J}}{\mathrm{m\ K}} \tag{116}$$

Moisture diffusivity matrix

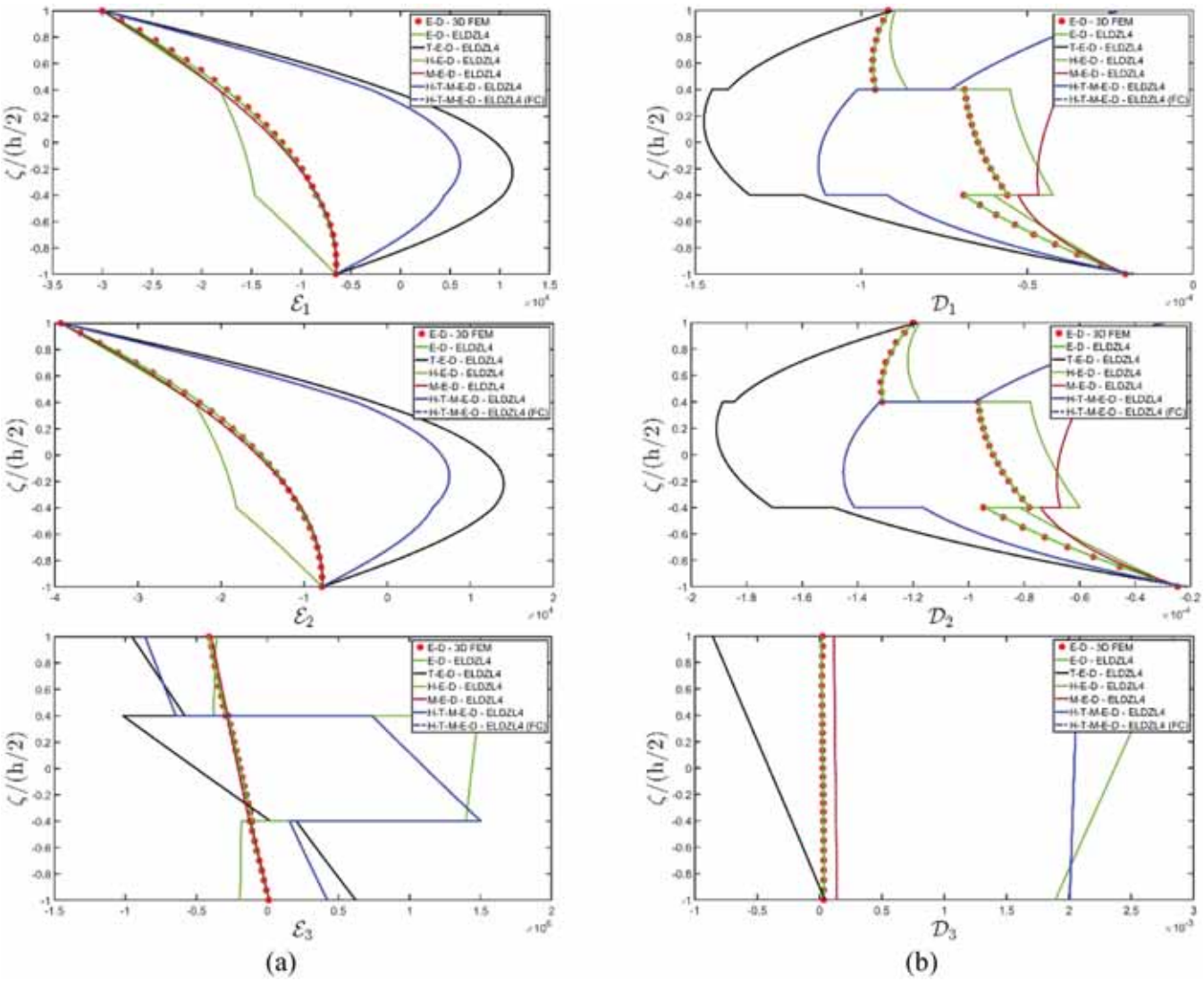

Figure 12. Distribution of the components of the electrostatic field (a) and the magnetostatic field (b) along the thickness direction of a simply supported cylindrical panel subjected to a sinusoidal generalized action. Effect of the coupling in various multifield simulations. Thickness plots are provided at $(0.25{\cdot}L_1, 0.25{\cdot}L_2)$ within the physical domain.

$$\boldsymbol{\Gamma}_{\mathrm{S}}^{(k)} = \begin{bmatrix} s_{11}^{(k)} & s_{12}^{(k)} & s_{13}^{(k)} \\ s_{21}^{(k)} & s_{22}^{(k)} & s_{23}^{(k)} \\ s_{31}^{(k)} & s_{32}^{(k)} & s_{33}^{(k)} \end{bmatrix} = \begin{bmatrix} 1.1347 & 0 & 0 \\ 0 & 1.1347 & 0 \\ 0 & 0 & 1.1347 \end{bmatrix} \cdot 10^{-7}\,\mathrm{m}^2, \;\; u_d^{(k)} = 0.1 \tag{117}$$

Dufour effect matrix and Soret effect matrix

$$\boldsymbol{\Gamma}_{Y}^{(k)} = \begin{bmatrix} y_{11}^{(k)} & y_{12}^{(k)} & y_{13}^{(k)} \\ y_{21}^{(k)} & y_{22}^{(k)} & y_{23}^{(k)} \\ y_{31}^{(k)} & y_{32}^{(k)} & y_{33}^{(k)} \end{bmatrix} = \begin{bmatrix} 0.0679 & 0 & 0 \\ 0 & 0.0679 & 0 \\ 0 & 0 & 0.0679 \end{bmatrix} \frac{\mathrm{J\ m^2}}{\mathrm{kg}}, \quad \nu^{(k)} = 0.26 \frac{\mathrm{m^3\ K}}{\mathrm{kg}}$$

$$\boldsymbol{\Gamma}_{\mathrm{X}}^{(k)} = \begin{bmatrix} x_{11}^{(k)} & x_{12}^{(k)} & x_{13}^{(k)} \\ x_{21}^{(k)} & x_{22}^{(k)} & x_{23}^{(k)} \\ x_{31}^{(k)} & x_{32}^{(k)} & x_{33}^{(k)} \end{bmatrix} = \begin{bmatrix} 1.0902 & 0 & 0 \\ 0 & 1.0902 & 0 \\ 0 & 0 & 1.0902 \end{bmatrix} \cdot 10^{-6} \frac{\mathrm{kg}}{\mathrm{m\ K}}, \; \lambda^{(k)} = 0.9615 \frac{\mathrm{kg}}{\mathrm{m^3\,K}} \tag{118}$$

Specific heat

$$c^{(k)} = 434 \ \frac{\mathrm{J}}{\mathrm{kg\,K}} \tag{119}$$

Density

$$\rho^{(k)} = 5300 \ \frac{\mathrm{kg}}{\mathrm{m^3}} \tag{120}$$

Note that the Soret and Dufour matrices $\boldsymbol{\Gamma}_{\mathrm{X}}^{(k)}$ and $\boldsymbol{\Gamma}_{\mathrm{Y}}^{(k)}$, introduced in Eqn. (39), are derived following to the procedure proposed by Sih. [70], assuming the value $M_\infty = 0.12$ for the reference moisture concentration and $\mathrm{T}_0 = 293\,\mathrm{K}$. In this way, the value $Q_h^{(k)} = 5.9853 \cdot 10^5\,\mathrm{J}$ is easily calculated for the heat of transport, through to Eqn. (41). Finally, the hygrothermal constants $\xi_{11}^{(k)} = 7.8505 \cdot 10^3\,\mathrm{J/m^3K^2}$, $\xi_{22}^{(k)} = 212.6198\,\mathrm{J\,m^3/kg^2}$ and $\xi_{12}^{(k)} = -2.9792 \cdot 10^3\,\mathrm{J/kg\,K}$ are determined from the expression in Eqn. (38). The mechanical properties of the central lamina made of soft adaptive wood are obtained from those of the adaptive wood already presented in Eqns. (109)-(120), with a reduction scaling factor of 50%, except for the thermal expansion coefficients $a_{ij}^{(k)}$ and the hygroscopic expansion coefficients $b_{ij}^{(k)}$ with $i,j = 1, 2, 3$, which remain the same as the original material. For each panel, a

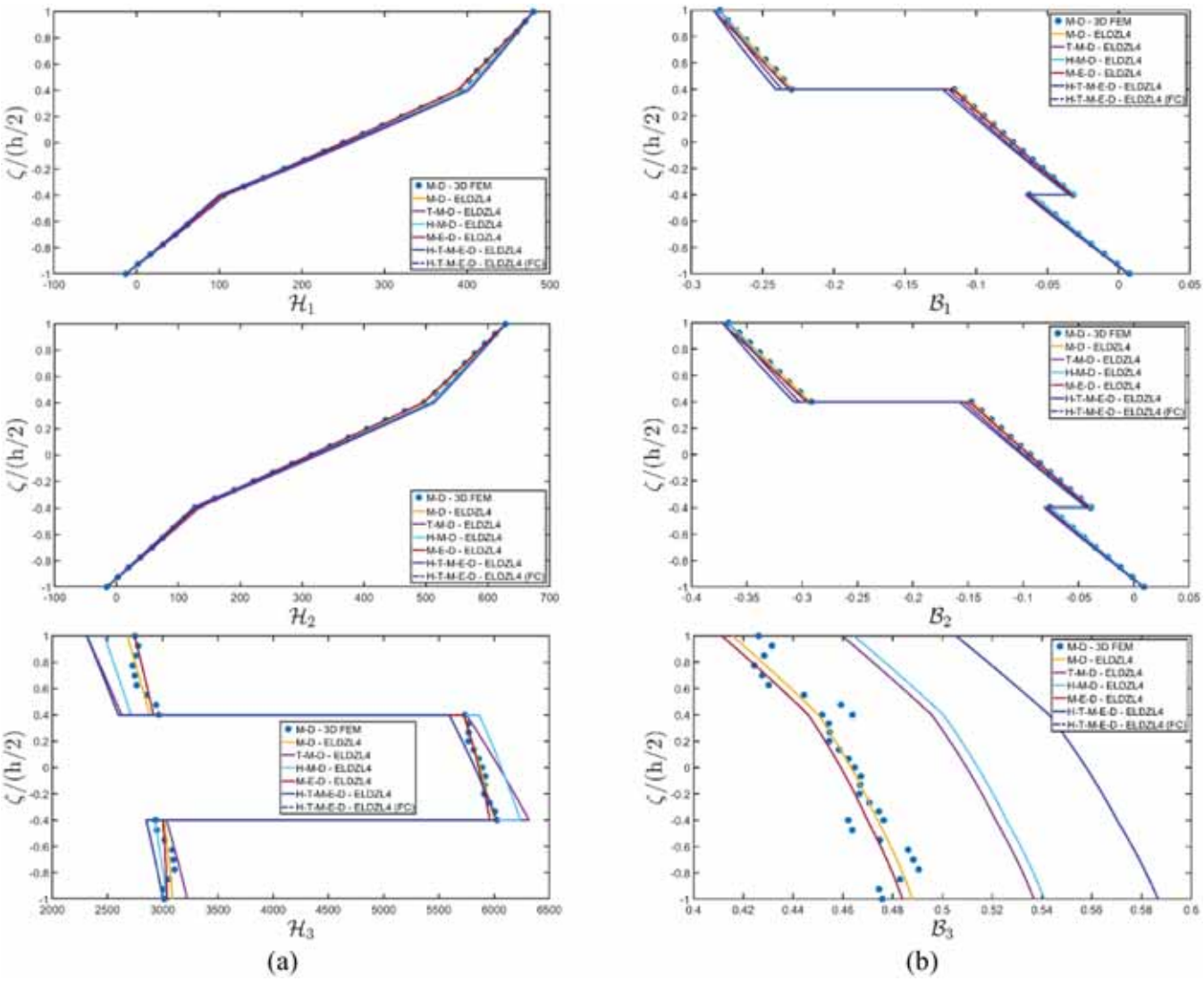

Figure 13. Distribution of the components of the electric displacement (a) and the magnetostatic flux (b) along the thickness direction of a simply supported cylindrical panel subjected to a sinusoidal generalized action. Effect of the coupling in various multifield simulations. Thickness plots are provided at $(0.25{\cdot}L_1, 0.25{\cdot}L_2)$ within the physical domain.

numerical Finite Element model is developed with a commercial software, and the 3D FEM solution is derived for both the mechanical case and simulations involving two coupled fields. The geometric properties of the structures under investigation are reported in Fig. 1, along with a representation of the 3D FEM mesh. The through-the-thickness profiles of all configuration variables, primary variables and secondary variables are determined for the point in the physical domain located at $(0.25(\alpha_1^1 - \alpha_1^0), 0.25(\alpha_2^1 - \alpha_2^0))$. The thickness plots for the rectangular plate are presented in Figs. 2-8, whereas those for the cylindrical surface can be found in Figs. 9-15. Finally, the results of the simulations conducted on a shallow spherical shell are reported in Figs. 16-22. A first preliminary simulation is performed for each structure, where the bending response under sinusoidal mechanical surface tractions is evaluated using the present semi-analytical formulation, and the results are in agreement with those of a refined 3D FEM model. It is worth noting that not only the configuration variables, which are directly derived from the kinematic reconstruction of Eqn. (10), but also the three-dimensional stress and strain components derived from the semi-analytical solution, which are corrected with the GDQ-based recovery procedure in the post-processing, are in agreement with the numerical predictions. Once the model is validated for the mechanical elasticity case, multifield simulations are performed, in which different coupling between the following fields are considered, as outlined in Table 1.

The displacement field components derived for the rectangular plate and presented in Fig. 2 show that in each coupled simulations involving the mechanical elasticity problem and another field, the present analytical solution, based on a two-dimensional model with higher order ELW theories, is in line with those of a refined three-dimensional model. The effect of a prescribed value of an external scalar field is thus accurately predicted. Moreover, the present model can predict the zigzag effect acting between two adjacent laminae even in multifield applications. Furthermore, the three-dimensional strain and stress components shown in Fig. 3 and Fig. 4, respectively, satisfy the equilibrium conditions in the interlaminar region and on the outer surfaces of the panel where the external loads are applied. On the other hand, when a scalar quantity is prescribed at the top and the bottom surfaces of the structure, the ELW kinematic model efficiently evaluates the three-dimensional dispersion of the configuration variables, as demonstrated in Fig. 2. A slight variation in the electric potential and the magnetostatic potential is seen in T-E-D and H-T-M-E-D simulations, highlighting that the present formulation is based on fully-coupled equations. The thickness plots of the primary and secondary variables of the other scalar fields can be found in Figs. 3-8. The recovered profiles of the three-dimensional stress

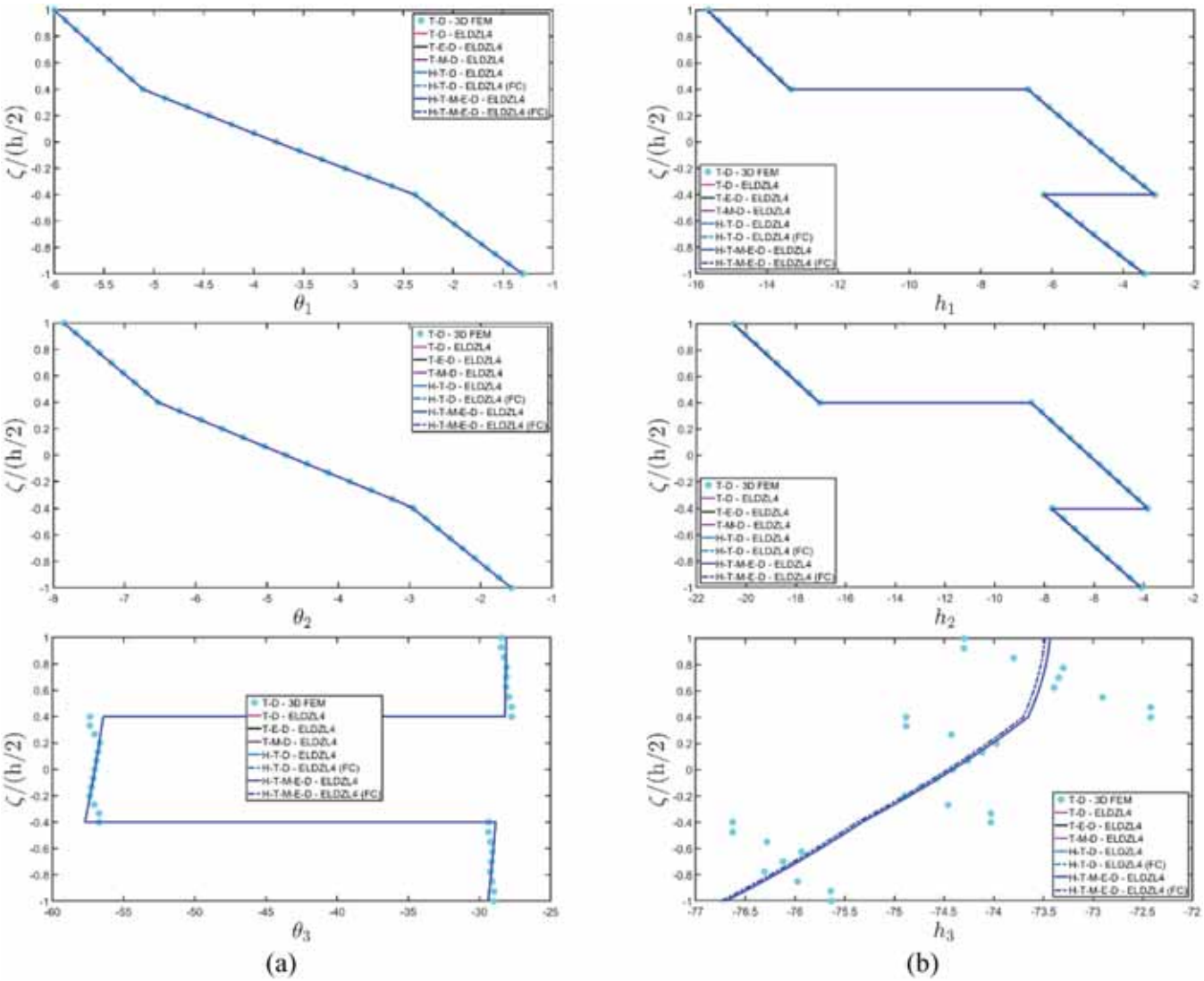

Figure 14. Distribution of the components of the thermal gradient (a) and the thermal flux (b) along the thickness direction of a simply supported cylindrical panel subjected to a sinusoidal generalized action. Effect of the coupling in various multifield simulations. Thickness plots are provided at $(0.25{\cdot}L_1, 0.25{\cdot}L_2)$ within the physical domain.

components from the mechanical case in Fig. 4 satisfy the equilibrium under external mechanical loads even in multifield simulations. However, when the recovery procedure is applied to the electric displacements associated with piezoelectricity (Fig. 5), the boundary condition at the top and bottom surfaces cannot be traced in external loads since a pre-determined distribution of configuration variables was applied. Therefore, the constitutive relation is adopted here for the determination of these quantities. Nevertheless, a perfect alignment with 3D-FEM numerical predictions is seen. Similar considerations can be made for quantities presented in Fig. 6, which are associated with the magnetic field. In multifield simulations involving the heat transfer and moisture concentration, similar profiles of primary and secondary variables are obtained for different multifield couplings (Figs. 7-8). However, when the Dufour effect is considered, along with the coupling between the specific entropy and chemical potential, an additional moisture flux is seen in each direction, even though a similar profile of moisture concentration gradient is obtained, as shown in Fig. 8. Furthermore, in Fig. 7 the flux vector obtained without considering the coupling between heat transfer and mass diffusion is successfully compared to the 3D FEM results.

In the case of a cylindrical panel, the mechanical response in terms of in-plane displacement field components and vertical deflection is significantly influenced by the coupling with other fields. This influence is particularly evident from the deflection profiles shown in Fig. 9, where the deflection direction of mechanical elasticity simulations undergoes a significant variation when the complete multifield solution is considered. Similar observations are made for strain and stress components of Fig. 10 and Fig. 11, respectively. The out-of-plane stresses always satisfy the equilibrium boundary conditions under external surface tractions. Fig. 9 presents also the through-the-thickness distribution of the scalar fields included in the present model. As can be seen, the compatibility conditions with respect to prescribed values of the configuration variables are always respected thanks to the ELW kinematic model. Furthermore, the thickness functions enable the prediction of zigzag effects in each coupled multifield simulation. The components of the three-dimensional electric field vector and the electric displacement vector, whose thickness plots can be found in Fig. 12, are significantly influenced by the coupling between equations. More specifically, when the heat transfer equations are added to the heat transfer problem, the electric field vector undergoes profile changes especially in the central layer of the stacking sequence. Furthermore, the introduction of a prescribed value of the moisture concentration at the two outer surfaces leads to a typical zigzag behavior of the cylindrical surface. Unlike the electric field vector, the components of the magnetostatic field

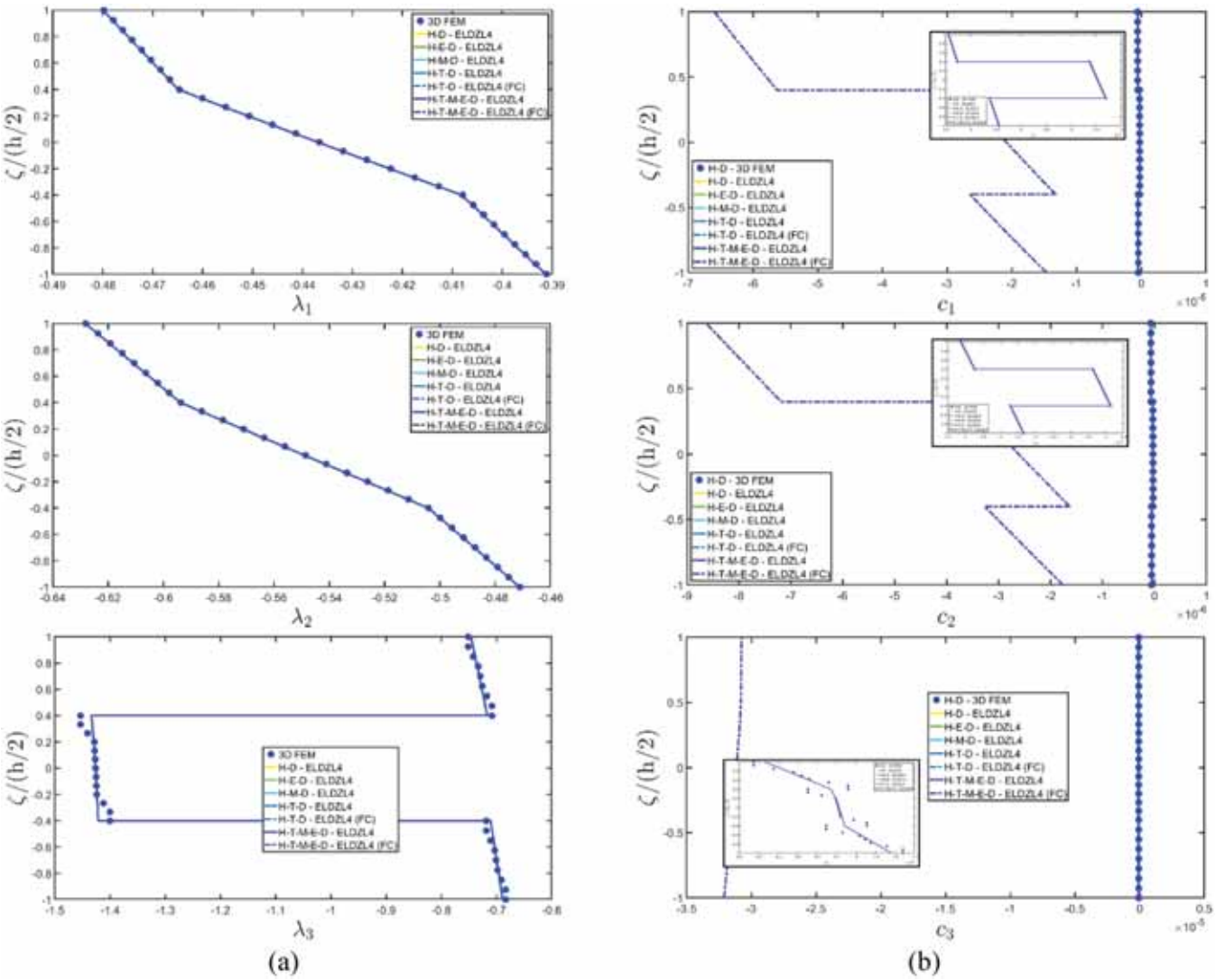

Figure 15. Distribution of the components of the concentration gradient (a) and the hygroscopic flux (b) along the thickness direction of a simply supported cylindrical panel subjected to a sinusoidal generalized action. Effect of the coupling in various multifield simulations. Thickness plots are provided at $(0.25{\cdot}L_1, 0.25{\cdot}L_2)$ within the physical domain.

vector in Fig. 13 are not significantly influenced by multifield loads because the distribution of each component remains similar to that derived in M-D simulations, which are in line with 3D-FEM predictions. On the other hand, variations of the out-of-plane magnetic flux vector are seen using fully-coupled multifield equations. Fig. 14 displays the components of the temperature gradient vector and the heat flux vector. The analytical predictions and numerical outcomes for the T-D simulation exhibit a perfect alignment. A slight variation in the through-the-thickness distribution of the out-of-plane heat flux emerges when the hygrothermal coupling is introduced through the Soret effect, whereas the influence of the electric and magnetic field on these quantities is negligible. Finally, Fig. 15 presents the thickness plots of the elements of the moisture concentration gradient and flux vectors. It is shown that the same profiles of the moisture concentration gradient components are obtained in each multifield simulation, in line with the 3D-FEM ones derived for the H-D case. Once again, the introduction of the Dufour matrix results in an additional flux, caused by the moisture concentration gradient, with respect to that of the uncoupled formulations. The accuracy with respect to the 3D-FEM outcomes in H-D models is verified in Fig. 15, where the dispersion of each component of the moisture concentration flux is compared to the three-dimensional numerical predictions.

Finally, the same multifield investigations are conducted on a laminated shallow spherical shell, characterized by the same lamination scheme as the other panels. As can be seen from Fig. 16, the structure tends to bend downwards under external mechanical surface loads as shown by the typical profile assumed in both in-plane and out-of-plane directions. On the other hand, in coupled multifield simulations an upward bending can be observed because the profile of the out-of-plane component is in the positive region, whereas the slope of the in-plane components assumes an opposite direction if compared to the mechanical elasticity simulation. A significant variation is found with respect to the mechanical case even in the three-dimensional strain components of Fig. 17. Finally, in Fig. 18 it is shown that an increase of the magnitude of both in-plane and out-of-plane normal stress components occurs in the central lamina when multifield loads are applied to the structure. Nevertheless, the equilibrium condition under external loads is always satisfied. The distributions of the scalar configuration variables of the multifield problem are presented in Fig. 16. As can be seen, also in this case the presence an external moisture concentration yields a different curve for the electric potential. In addition, a change in slope of the curve is seen in the central core of the shell panel. The thickness plots of the electric potential obtained in the fully-coupled H-T-M-E-D and H-T-D simulations are not significantly influenced by hygrothermal coupling,

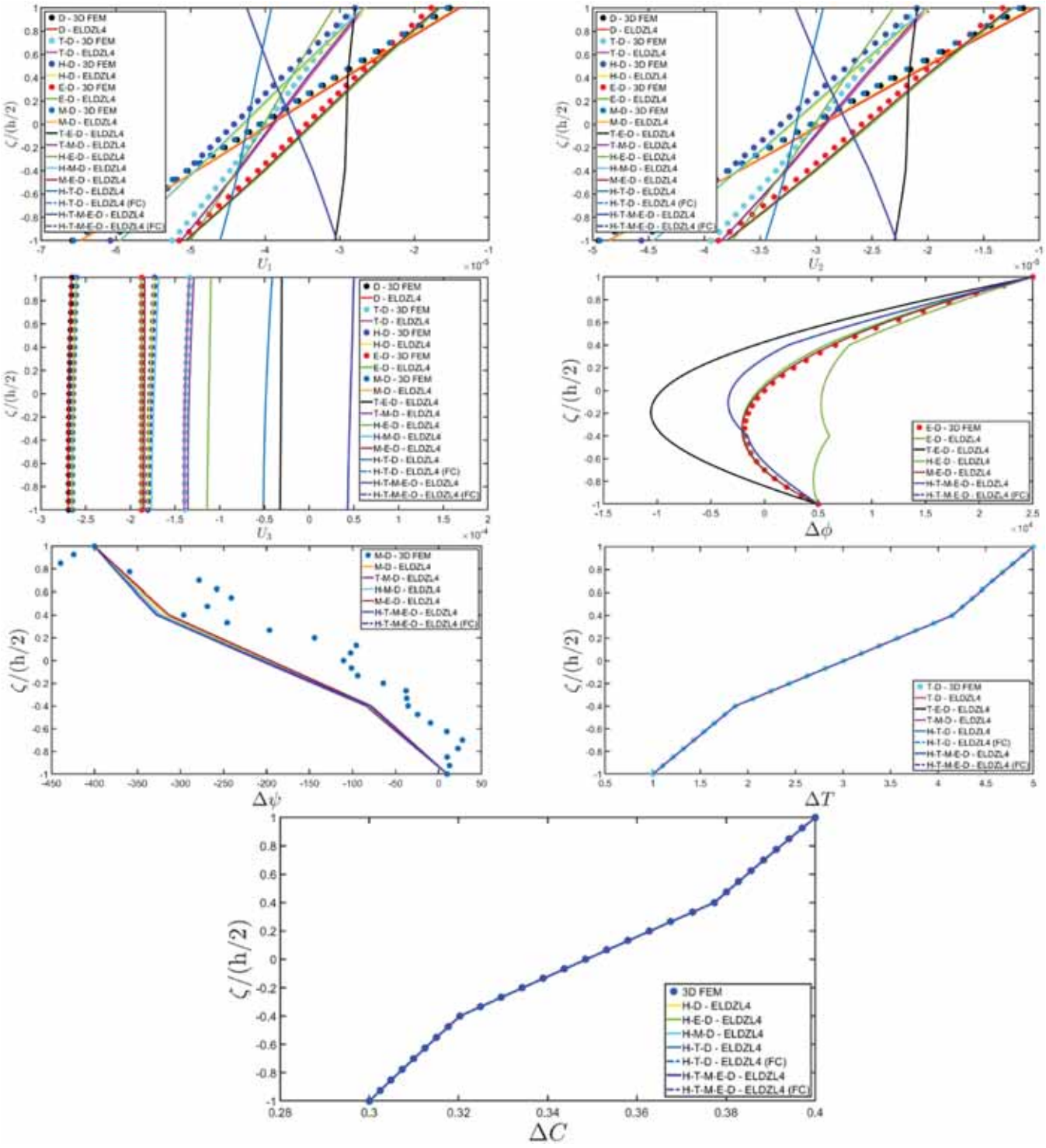

Figure 16. Distribution of the displacement field components, electric potential, magnetostatic potential, temperature variation and concentration variation along the thickness direction of a simply supported spherical panel subjected to a sinusoidal generalized action. Effect of the coupling in various multifield simulations. Thickness plots are provided at $(0.25{\cdot}L_1, 0.25{\cdot}L_2)$ within the physical domain.

as the same curve is obtained without considering these effects. On the other hand, the distribution of the magnetic scalar potential undergoes slight variations as external multifield loadings are introduced into the model. The same temperature and moisture concentration profile is derived in all simulations. The variation of the electric response of the spherical panel in different multifield investigations can also be seen in Fig. 19, where the components of the electric field and the electric displacement are reported. It can be seen that the out-of-plane electric field is amplified in the layer of soft adaptive wood for T-E-D and H-T-M-E-D models, whereas the in-plane electric field components exhibit slight variations if compared to the outcomes of E-D simulations, both in 3D-FEM and the semi-analytical model. The introduction of couplings in the formulation adds a linear quantity to the profiles of the in-plane components of the electrostatic field, leading to more significant variations in the third lamina than the first one. In contrast, the components of the magnetostatic field and the magnetic flux vector, reported in

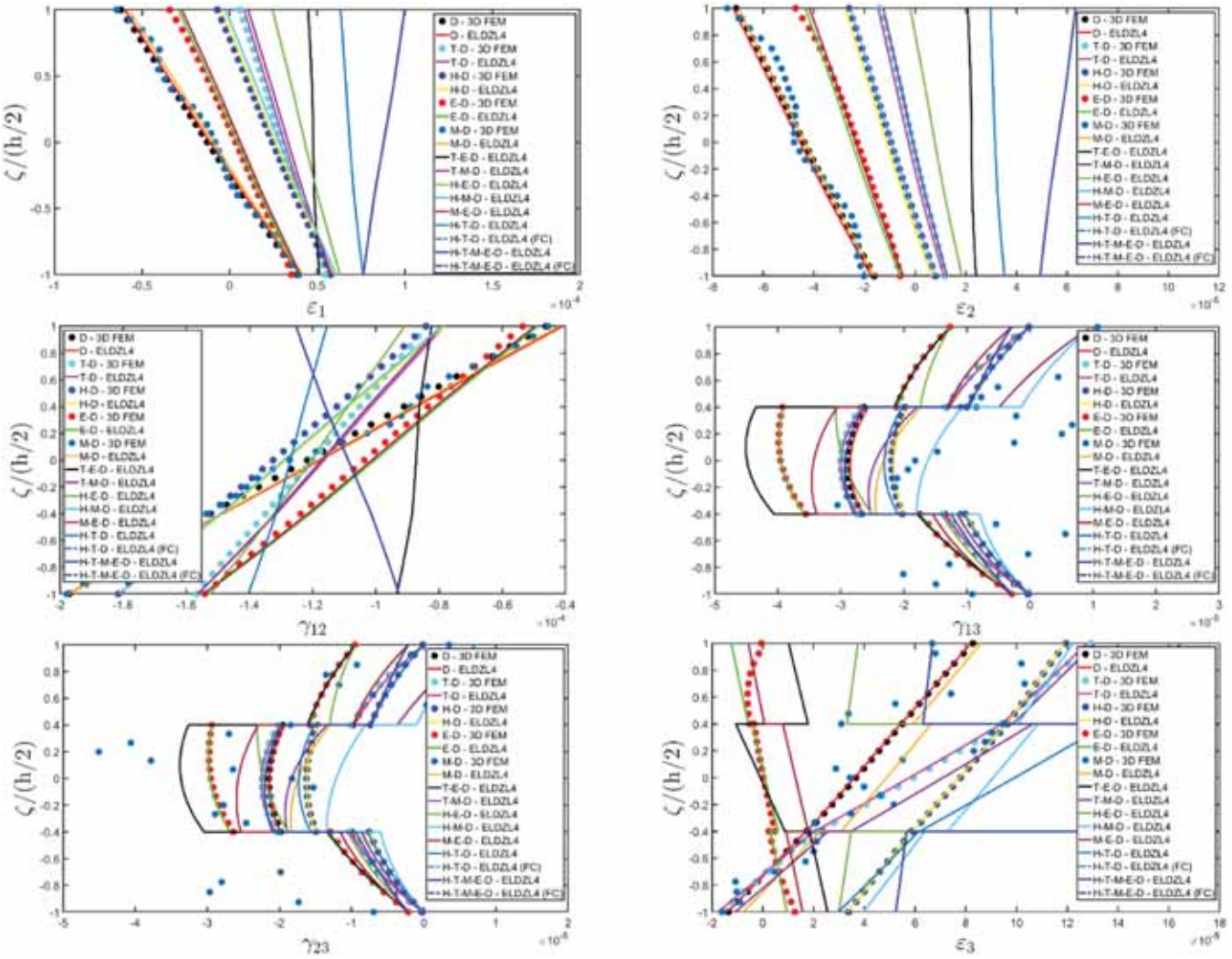

Figure 17. Distribution of the three-dimensional strain components along the thickness direction of a simply supported spherical panel subjected to a sinusoidal generalized action. Effect of the coupling in various multifield simulations. Thickness plots are provided at $(0.25{\cdot}L_1, 0.25{\cdot}L_2)$ within the physical domain.

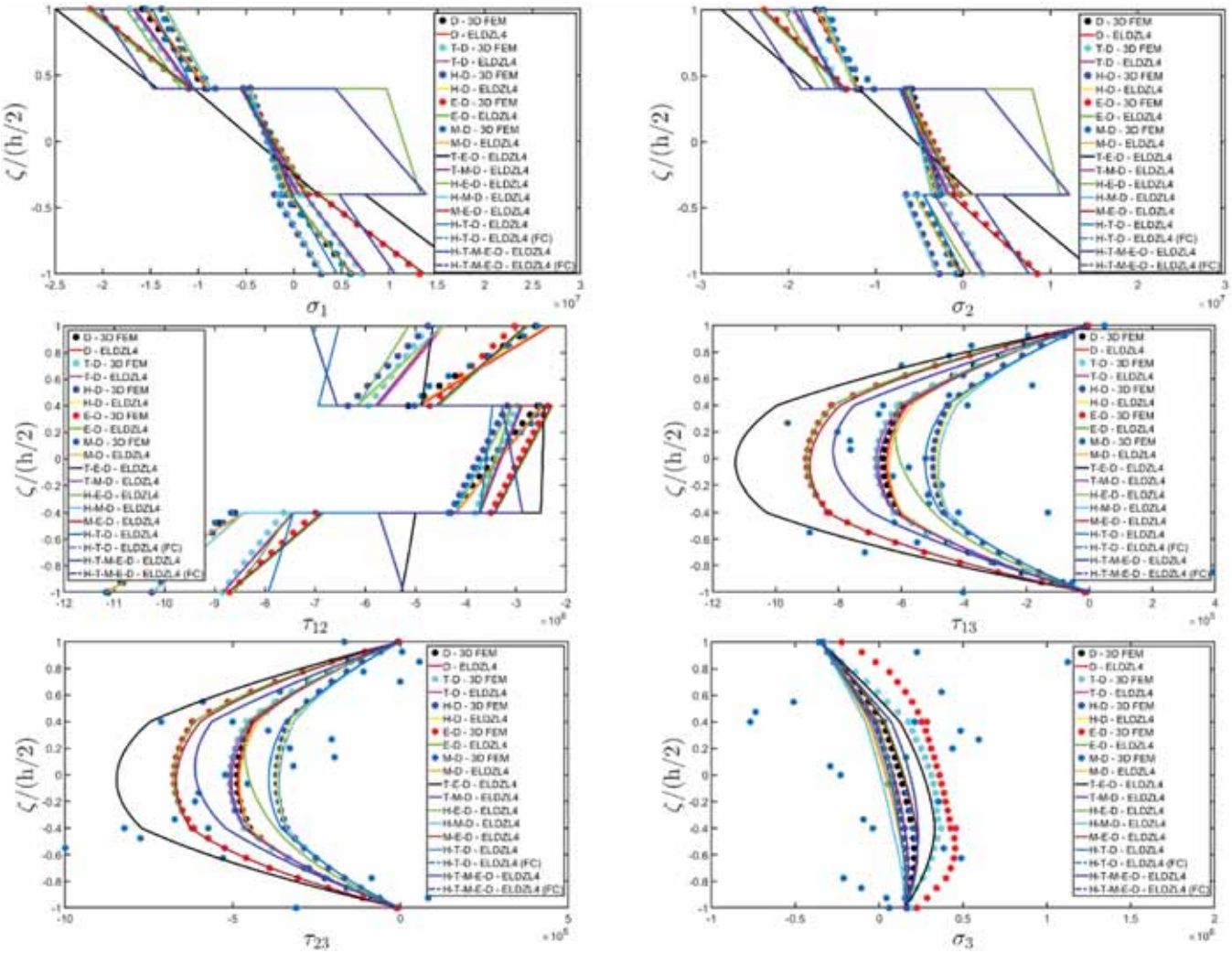

Figure 18. Distribution of the three-dimensional stress components [Pa] along the thickness direction of a simply supported spherical panel subjected to a sinusoidal generalized action. Effect of the coupling in various multifield simulations. Thickness plots are provided at $(0.25{\cdot}L_1, 0.25{\cdot}L_2)$ within the physical domain.

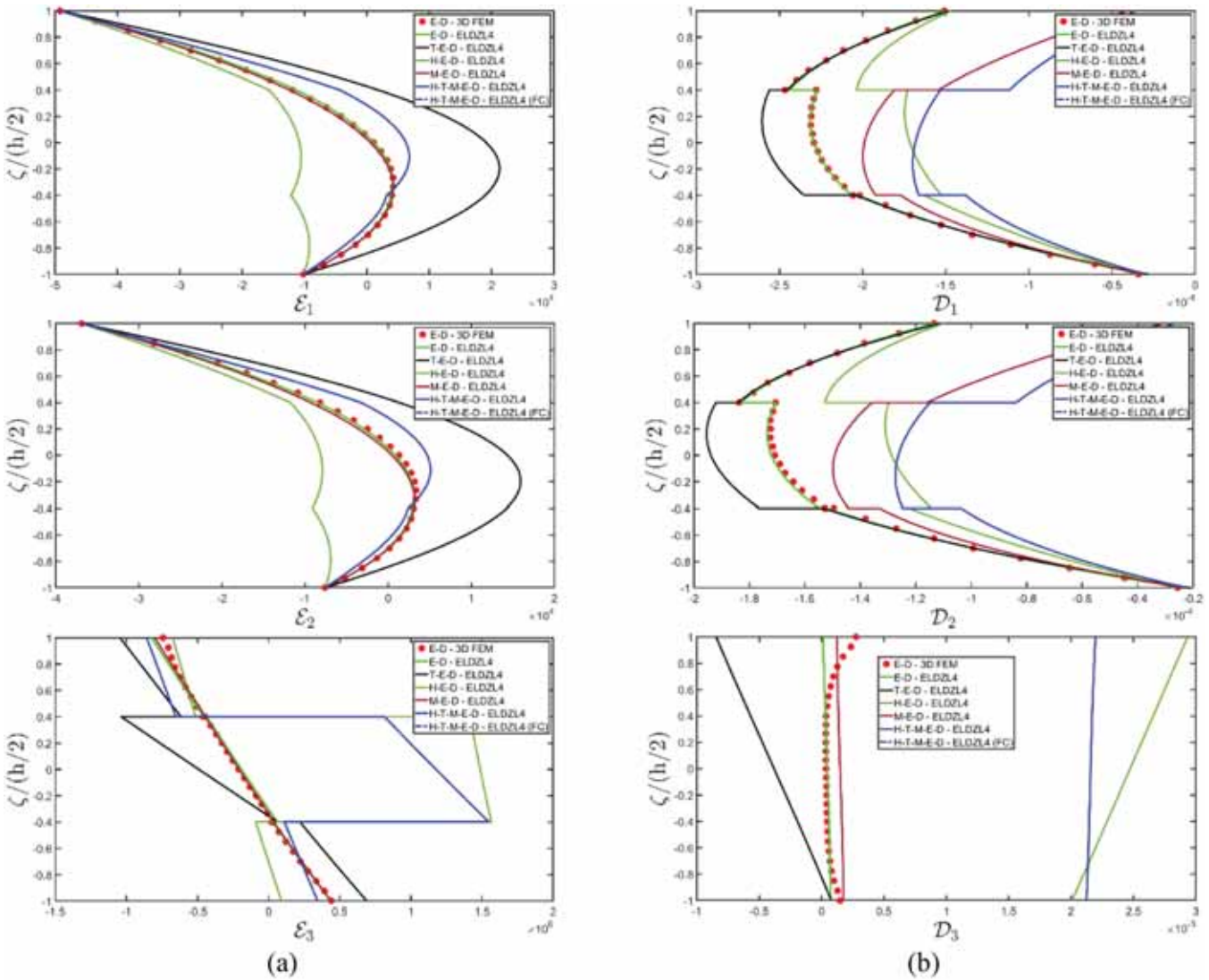

Figure 19. Distribution of the components of the electrostatic field (a) and the magnetostatic field (b) along the thickness direction of a simply supported spherical panel subjected to a sinusoidal generalized action. Effect of the coupling in various multifield simulations. Thickness plots are provided at $(0.25{\cdot}L_1, 0.25{\cdot}L_2)$ within the physical domain.

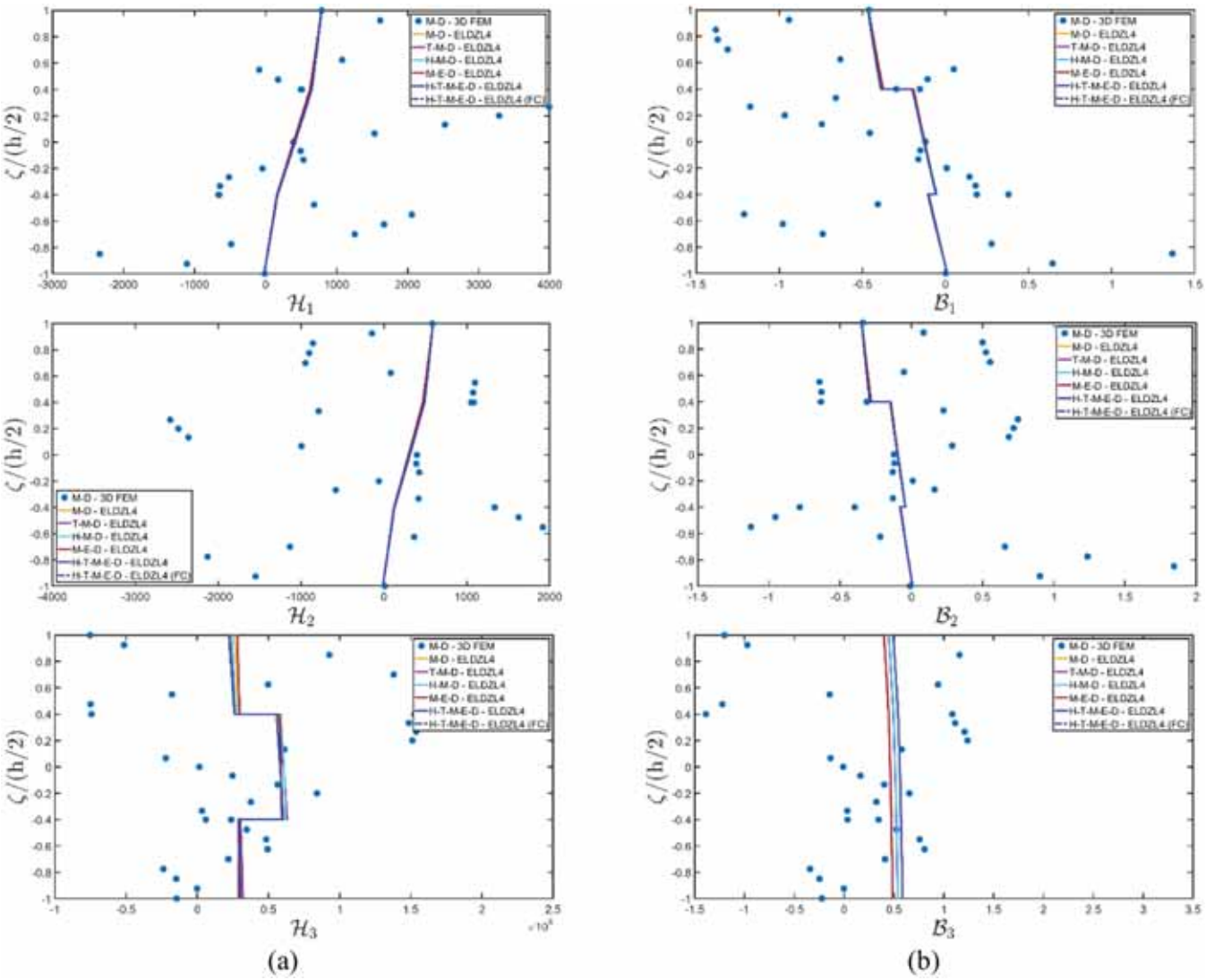

Figure 20. Distribution of the components of the electric displacement (a) and the magnetostatic flux (b) along the thickness direction of a simply supported spherical panel subjected to a sinusoidal generalized action. Effect of the coupling in various multifield simulations. Thickness plots are provided at $(0.25{\cdot}L_1, 0.25{\cdot}L_2)$ within the physical domain.

Fig. 20, are translated with respect to the M-D results. The Soret effect is only visible in the out-of-plane component of the thermal flux vector, as shown in Fig. 21. Accordingly, a new profile of this quantity is observed which comes from the presence of a moisture concentration gradient. All the other quantities remain unchanged in multifield semi-analytical investigations. Finally, the moisture concentration flux is significantly influenced by the temperature gradient, as can be seen in the thickness plots of Fig. 22 regarding H-T-D and H-T-M-E-D (FC) simulations. On the other hand, the mass concentration in H-T-M-E-D investigations is not affected by the other multifield couplings since the heat transfer and the mass diffusion equations are independent. In addition, the predictions of the 3D-FEM model for H-D analysis are perfectly matched.

10. Conclusions

In the present study, a two-dimensional formulation has been adopted for the coupled multifield modelling of curved and layered panels under the assumption of quasistatic processes and equilibrium thermodynamic conditions. Each configuration variable has been expanded along the thickness direction according to the ELW approach, taking into account higher order interpolating polynomials. The fundamental equations have been derived from the Master Balance principle, and a semi-analytical solution has been found using the Navier's method. Then, the three-dimensional distribution of each primary and secondary variable is obtained from the balance multifield equations written in the thickness direction. Some examples of investigation have been proposed, in which the prediction of the present formulation are compared to the results obtained from three-dimensional Finite Element models. These comparisons show a high level of accordance between these approaches. The proposed formulation enables the derivation of the multifield response of laminated curved panels using a semi-analytical method. Furthermore, the recovery procedure, applied to the two-dimensional solution and carried out with a numerical technique, provides a highly accurate prediction of the multifield response of the three-dimensional doubly-curved shell solids.

CRediT authorship contribution statement

Francesco Tornabene: Writing – review & editing, Visualization, Validation, Supervision, Software, Methodology, Investigation, Formal analysis, Data curation, Conceptualization. **Matteo Viscoti:** Writing – original draft, Validation, Investigation, Data curation. **Rossana Dimitri:** Writing – review & editing, Validation, Supervision, Investigation, Formal analysis, Conceptualization.

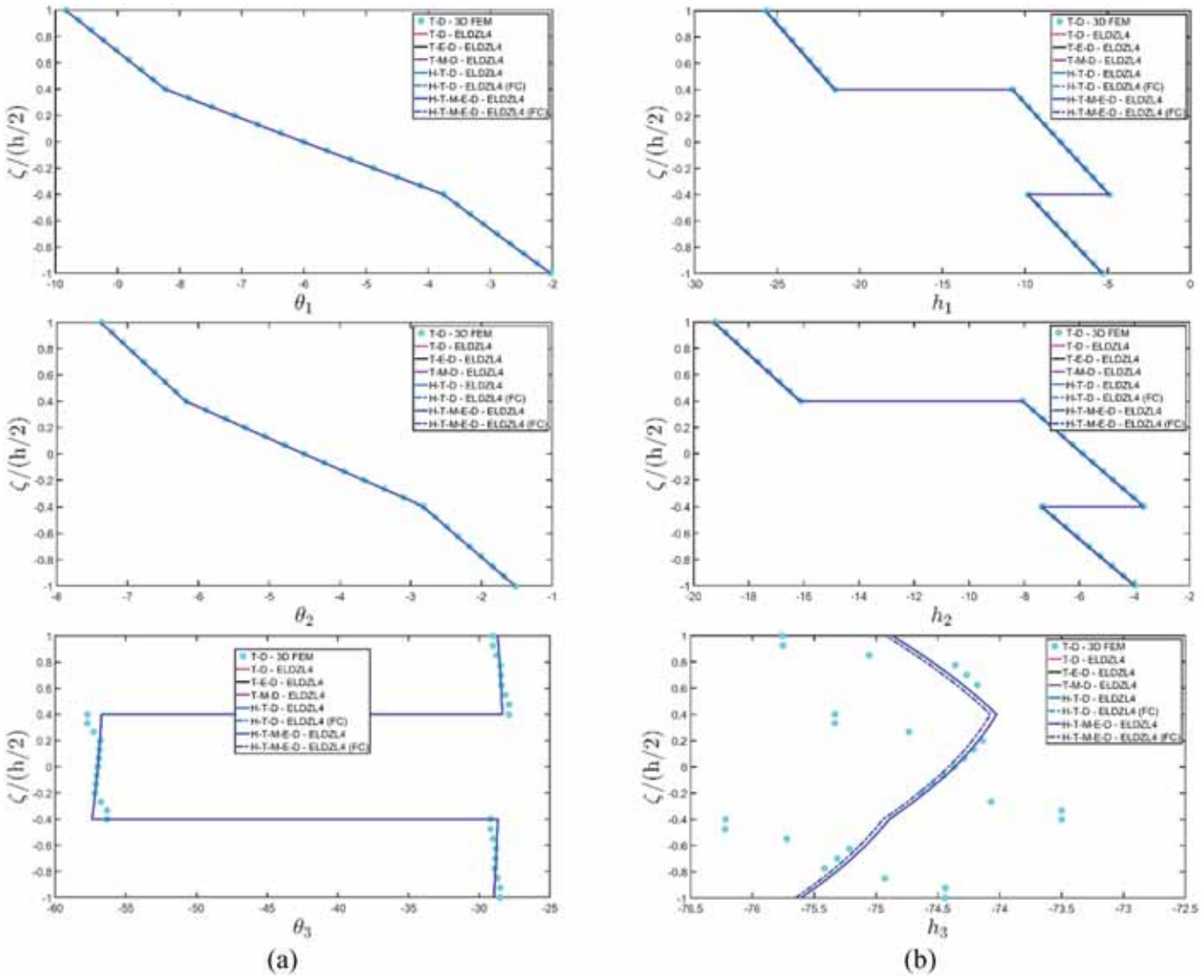

Figure 21. Distribution of the components of the thermal gradient (a) and the thermal flux (b) along the thickness direction of a simply supported spherical panel subjected to a sinusoidal generalized action. Effect of the coupling in various multifield simulations. Thickness plots are provided at $(0.25{\cdot}L_1, 0.25{\cdot}L_2)$ within the physical domain.

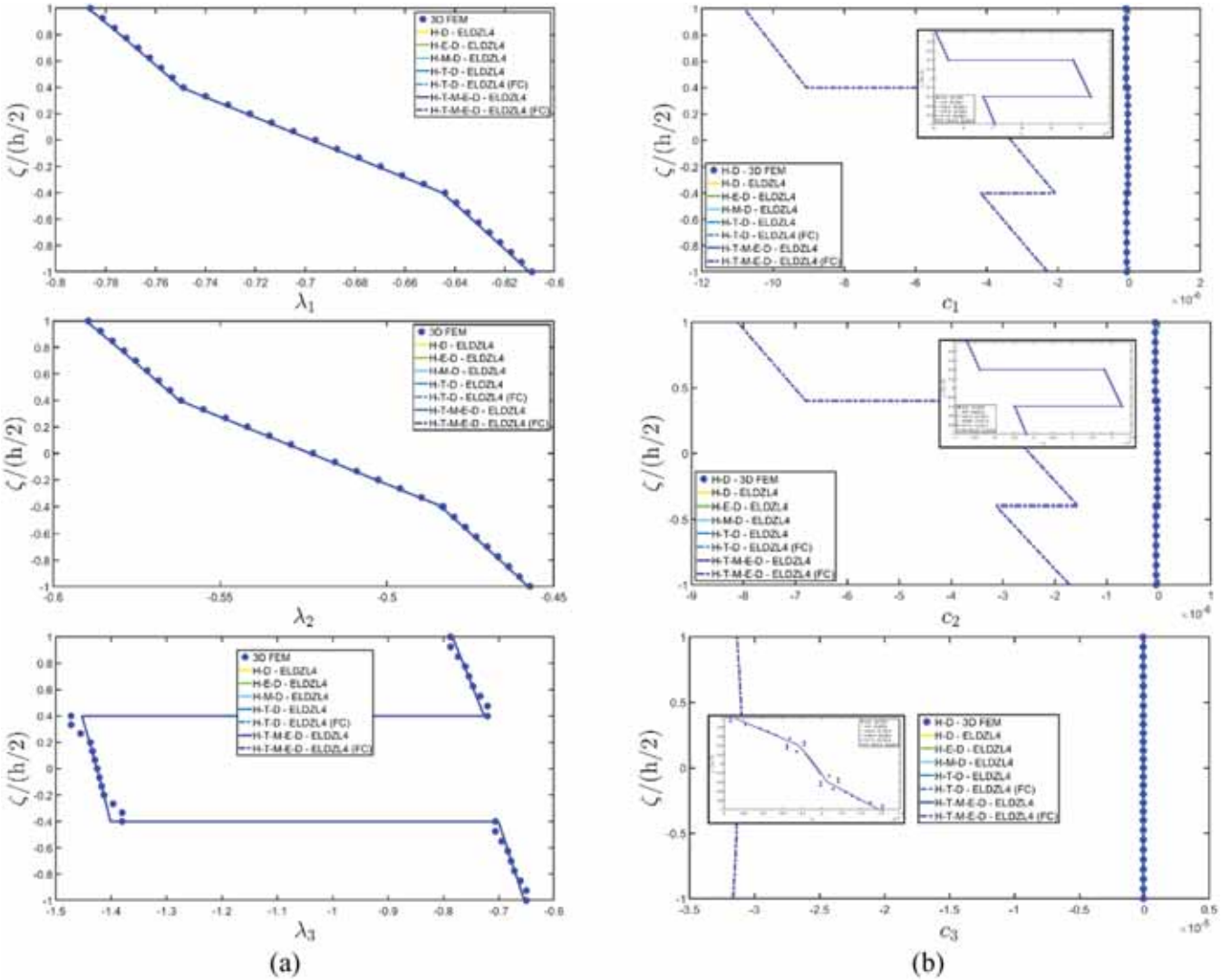

Figure 22. Distribution of the components of the concentration gradient (a) and the hygroscopic flux (b) along the thickness direction of a simply supported spherical panel subjected to a sinusoidal generalized action. Effect of the coupling in various multifield simulations. Thickness plots are provided at $(0.25{\cdot}L_1, 0.25{\cdot}L_2)$ within the physical domain.

Declaration of competing interest

The authors declare that they have no known competing financial interests or personal relationships that could have appeared to influence the work reported in this paper.

Data availability

No data was used for the research described in the article.

References

[1] H.S. Tzou, Piezoelectric shells: Distributed sensing and control of continua, Kluwer Academic Publishers, 1993.

[2] H.S. Tzou, C.I. Tseng, Distributed piezoelectric sensor/actuator design for dynamic measurement/control of distributed parameter systems: a piezoelectric finite element approach, Journal of Sound and Vibration 138 (1990) 17–34.

[3] S. Kapuria, P. Kumari, J.K. Nath, Efficient modeling of smart piezoelectric composite laminates: a review, Acta Mechanica 214 (2010) 31–48.

[4] S.J. Lee, J.N. Reddy, F. Rostam-Abadi, Transient analysis of laminated composite plates with embedded smart-material layers, Finite Elements in Analysis and Design 40 (2004) 463–483.

[5] H.S. Tzou, Y. Bao, Modeling of thick anisotropic composite triclinic piezoelectric shell transducer laminates, Smart Materials and Structures 3 (1994) 285.

[6] J.N. Reddy, J.I. Barbosa, On vibration suppression of magnetostrictive beams, Smart Materials and Structures 9 (2000) 49.

[7] S.C. Pradhan, T.Y. Ng, K.Y. Lam, J.N. Reddy, Control of laminated composite plates using magnetostrictive layers, Smart Materials and Structures 10 (2001) 657.

[8] P.K. Mahato, D.K. Maiti, Aeroelastic analysis of smart composite structures in hygro-thermal environment, Composite Structures 92 (2010) 1027–1038.

[9] Z. Chen, A. Akbarzadeh, Advanced thermal stress analysis of smart materials and structures, Springer, Berlin, 2020.

[10] S. Brischetto, Hygrothermal loading effects in bending analysis of multilayered composite plates, Computer Modeling in Engineering & Sciences 88 (2012) 367–417.

[11] M. Vinyas, S.C. Kattimani, Hygrothermal analysis of magneto-electro-elastic plate using 3D finite element analysis, Composite Structures 180 (2017) 617–637.

[12] F.Z. Jouneghani, R. Dimitri, F. Tornabene, Structural response of porous FG nanobeams under hygro-thermo-mechanical loadings, Composites Part B: Engineering 152 (2018) 71–78.

[13] T. Ikeda, Fundamentals of Piezoelectricity, Oxford University Press, 1996.

[14] H.F. Tiersten, Thickness vibrations of piezoelectric plate, The Journal of the Acoustical Society of America 35 (1963) 53–58.

[15] K.Y. Lam, X.Q. Peng, G.R. Liu, J.N. Reddy, A finite-element model for piezoelectric composite laminates, Smart Materials and Structures 6 (1997) 583.

[16] C.Y. Chee, L. Tong, G.P. Steven, A review on the modelling of piezoelectric sensors and actuators incorporated in intelligent structures, Journal of intelligent material systems and structures 9 (1998) 3–19.

[17] W.S. Hwang, H.C. Park, Finite element modeling of piezoelectric sensors and actuators, AIAA Journal 31 (1993) 930–937.

[18] G.C. Sih, M.T. Shih, Hygrothermal stress in a plate subjected to antisymmetric time-dependent moisture and temperature boundary conditions, Journal of Thermal Stresses 3 (1980) 321–340.
[19] M. Mohammadimehr, M. Salemi, B.R. Navi, Bending, buckling, and free vibration analysis of MSGT microcomposite Reddy plate reinforced by FG-SWCNTs with temperature-dependent material properties under hydro-thermo-mechanical loadings using DQM, Composite Structures 138 (2016) 361–380.
[20] M. Mohammadimehr, M. Emdadi, H. Afshari, B.R. Navi, Bending, buckling and vibration analyses of MSGT microcomposite circular-annular sandwich plate under hydro-thermo-magneto-mechanical loadings using DQM, International Journal of Smart and Nano Materials 9 (2018) 233–260.
[21] G.A. Holzapfel, Nonlinear solid mechanics: a continuum approach for engineering science, John Wiley & Sons, 2002.
[22] S. Brischetto, E. Carrera, Coupled thermo-electro-mechanical analysis of smart plates embedding composite and piezoelectric layers, Journal of Thermal Stresses 35 (2012) 766–804.
[23] B.P. Patel, M. Ganapathi, D.P. Makhecha, Hygrothermal effects on the structural behaviour of thick composite laminates using higher-order theory, Composite Structures 56 (2002) 25–34.
[24] S. Brischetto, Hygrothermoelastic analysis of multilayered composite and sandwich shells, Journal of Sandwich Structures & Materials 15 (2013) 168–202.
[25] S. Brischetto, R. Torre, Thermo-elastic analysis of multilayered plates and shells based on 1D and 3D heat conduction problems, Composite Structures 206 (2018) 326–353.
[26] F. Moleiro, C.M. Soares, E. Carrera, Three-dimensional exact hygro-thermo-elastic solutions for multilayered plates: Composite laminates, fibre metal laminates and sandwich plates, Composite Structures 216 (2019) 260–278.
[27] J. Tichý, J. Erhart, E. Kittinger, J. Privratska, Fundamentals of piezoelectric sensorics: mechanical, dielectric, and thermodynamical properties of piezoelectric materials, Springer Science & Business Media, 2010.
[28] J.C. Monge, J.L. Mantari, Three-dimensional numerical solution for the bending study of magneto-piezo-elastic spherical and cylindrical shells, Engineering Structures 238 (2021) 112158.
[29] S. Brischetto, R. Torre, D. Cesare, Three-dimensional coupling between elastic and thermal fields in the static analysis of multilayered composite shells, Computer Modeling in Engineering & Sciences 136 (2023) 1–44.
[30] Y. Wang, R. Xu, H. Ding, J. Chen, Three-dimensional exact solutions for free vibrations of simply supported magneto-electro-elastic cylindrical panels, International Journal of Engineering Science 48 (2010) 1778–1796.
[31] T.H. Wu, X.Y. Li, Elliptical crack problem in magneto-electro-thermo-elasticity of transversely isotropic materials: 3D analytical and numerical solutions, International Journal of Engineering Science 144 (103136) (2019) 1–27.
[32] C. Yu, G. Kang, A multiscale magneto-thermo-mechanically coupled model for ultra-low-field induced magneto-elastocaloric effect in magnetostrictive-shape memory alloy composite system, International Journal of Engineering Science 168 (103539) (2021) 1–38.
[33] J.N. Reddy, Mechanics of laminated composite plates and shells: theory and analysis, CRC Press, Boca Raton, 2003.
[34] C.P. Wu, Y.C. Liu, A review of semi-analytical numerical methods for laminated composite and multilayered functionally graded elastic/piezoelectric plates and shells, Composite Structures 147 (2016) 1–15.
[35] G. Qing, J. Qiu, Y. Liu, A semi-analytical solution for static and dynamic analysis of plates with piezoelectric patches, International Journal of Solids and Structures 43 (2006) 1388–1403.
[36] H. Li, F. Pang, X. Miao, Y. Du, H. Tian, A semi-analytical method for vibration analysis of stepped doubly-curved shells of revolution with arbitrary boundary conditions, Thin-Walled Structures 129 (2018) 125–144.
[37] F. Pang, H. Li, X. Wang, X. Miao, S. Li, A semi analytical method for the free vibration of doubly-curved shells of revolution, Computers & Mathematics with Applications 75 (2018) 3249–3268.
[38] J.C. Monge, J.L. Mantari, R.A. Arciniega, Computational semi-analytical method for the 3D elasticity bending solution of laminated composite and sandwich doubly-curved shells, Engineering Structures 221 (2020) 110938.
[39] H.T. Thai, S.E. Kim, Analytical solution of a two variable refined plate theory for bending analysis of orthotropic Levy-type plates, International Journal of Mechanical Sciences 54 (2012) 269–276.
[40] D.W. Cooke, M. Levinson, Thick rectangular plates—II: The generalized Lévy solution, International Journal of Mechanical Sciences 25 (1983) 207–215.
[41] S. Brischetto, Exact elasticity solution for natural frequencies of functionally graded simply-supported structures, Computer Modeling in Engineering Science 95 (2013) 391–430.
[42] J.C. Monge, J.L. Mantari, Exact solution of thermo-mechanical analysis of laminated composite and sandwich doubly-curved shell, Composite Structures 245 (2020) 112323.
[43] R.A. Chaudhuri, H.R. Kabir, Vibration of clamped moderately thick general cross-ply plates using a generalized Navier approach, Composite Structures 24 (1993) 311–321.
[44] K.M. Liew, Z.Z. Pan, L.W. Zhang, An overview of layerwise theories for composite laminates and structures: Development, numerical implementation and application, Composite Structures 216 (2019) 240–259.
[45] F. Tornabene, M. Viscoti, R. Dimitri, Equivalent single layer higher order theory based on a weak formulation for the dynamic analysis of anisotropic doubly-curved shells with arbitrary geometry and variable thickness, Thin-Walled Structures 174 (2022) 109119.
[46] J.N. Reddy, An evaluation of equivalent-single-layer and layerwise theories of composite laminates, Composite Structures 25 (1993) 21–35.
[47] J.N. Reddy, D.H. Robbins Jr, Theories and computational models for composite laminates, Applied Mechanics Reviews 47 (1994) 147–169.
[48] F. Tornabene, N. Fantuzzi, M. Bacciocchi, J.N. Reddy, An equivalent layer-wise approach for the free vibration analysis of thick and thin laminated and sandwich shells, Applied Sciences 7 (2016) 17.
[49] M.A. Al-Osta, An exponential-trigonometric quasi-3D HSDT for wave propagation in an exponentially graded plate with microstructural defects, Composite Structures 297 (2022) 115984.
[50] A.J.M. Ferreira, C.M.C. Roque, R.M.N. Jorge, Analysis of composite plates by trigonometric shear deformation theory and multiquadrics, Computers & Structures 83 (2005) 2225–2237.
[51] M. Arefi, E.M.R. Bidgoli, R. Dimitri, M. Bacciocchi, F. Tornabene, Application of sinusoidal shear deformation theory and physical neutral surface to analysis of functionally graded piezoelectric plate, Composites Part B: Engineering 151 (2018) 35–50.
[52] U. Icardi, F. Sola, Assessment of recent zig-zag theories for laminated and sandwich structures, Composites Part B: Engineering 97 (2016) 26–52.
[53] H. Murakami, Laminated Composite Plate Theory with Improved In-Plane Responses, ASME Journal of Applied Mechanics 53 (1986) 661–666.
[54] F. Tornabene, M. Viscoti, R. Dimitri, J.N. Reddy, Higher order theories for the vibration study of doubly-curved anisotropic shells with a variable thickness and isogeometric mapped geometry, Composite Structures 267 (2021) 113829.
[55] H. Aminipour, M. Janghorban, O. Civalek, Analysis of functionally graded doubly-curved shells with different materials via higher order shear deformation theory, Composite Structures 251 (2020) 112645.
[56] F. Tornabene, M. Viscoti, R. Dimitri, Generalized higher order layerwise theory for the dynamic study of anisotropic doubly-curved shells with a mapped geometry, Engineering Analysis with Boundary Elements 134 (2022) 147–183.
[57] D. Ballhause, M. D'Ottavio, B. Kröplin, E. Carrera, A unified formulation to assess multilayered theories for piezoelectric plates, Computers & Structures 83 (2005) 1217–1235.
[58] F. Tornabene, E. Viola, N. Fantuzzi, General higher-order equivalent single layer theory for free vibrations of doubly-curved laminated composite shells and panels, Composite Structures 104 (2013) 94–117.
[59] K. Washizu, Variational Methods in Elasticity & Plasticity, Pergamon Press, Oxford, 1975.
[60] J.N. Reddy, A generalization of two-dimensional theories of laminated composite plates, Communications in Applied Numerical Methods 3 (1987) 173–180.
[61] F. Tornabene, M. Viscoti, R. Dimitri, Static analysis of anisotropic doubly-curved shell subjected to concentrated loads employing higher order layer-wise theories, Computer Methods in Engineering Science (2022) 22237.
[62] F. Tornabene, M. Viscoti, R. Dimitri, Static analysis of doubly-curved shell structures of smart materials and arbitrary shape subjected to general loads employing higher order theories and generalized differential quadrature method, Computer Methods in Engineering Science (2022) 22210.
[63] Z.B. Kuang, Theory of electroelasticity, Springer Berlin, Heidelberg, 2014.
[64] S. Brischetto, R. Torre, 3D shell model for the thermo-mechanical analysis of FGM structures via imposed and calculated temperature profiles, Aerospace Science and Technology 85 (2019) 125–149.
[65] S. Brischetto, An exact 3D solution for free vibrations of multilayered cross-ply composite and sandwich plates and shells, International Journal of Applied Mechanics 6 (2014) 1450076.
[66] Y:H. Tsai, C.P. Wu, Y.S. Syu, Three-dimensional analysis of doubly curved functionally graded magneto-electro-elastic shells, European Journal of Mechanics-A/Solids 27 (2008) 79–105.
[67] J. Verhoogen, The chemical potential of a stressed solid, Eos, Transactions American Geophysical Union 32 (1951) 251–258.
[68] M. Vinyas, On frequency response of porous functionally graded magneto-electro-elastic circular and annular plates with different electro-magnetic conditions using HSDT, Composite Structures 240 (2020) 112044.
[69] W. Nowacki, Thermoelasticity, Polish Scientific Publishers, Warszawa, 1986.
[70] G.C. Sih, J.G. Michopoulos, S.C. Chou, Hygrothermoelasticity, Martinus Nijhoff Publishers, 1986.
[71] L.D. Landau, E.M. Lifshitz, The classical theory of fields, Pergamon Press, Oxford, 1951.
[72] F. Tornabene, Hygro-Thermo-Magneto-Electro-Elastic Theory of Anisotropic Doubly-Curved Shells, Esculapio, Bologna (2023).
[73] H. Mehrer, Diffusion in solids: fundamentals, methods, materials, diffusion-controlled processes, Springer Science & Business Media, Berlin, 2007.
[74] H.S. Carslaw, J.C. Jaeger, Conduction of heat in solids, Oxford University Press, 1947.
[75] F.P. Incropera, D.P. DeWitt, T.L. Bergman, A.S. Lavine, Fundamentals of heat and mass transfer, John Wiley & Sons, 1996.
[76] S. Brischetto, E. Carrera, Thermomechanical effect in vibration analysis of one-layered and two-layered plates, International Journal of Applied Mechanics 3 (2011) 161–185.
[77] J.K. Platten, The Soret effect: a review of recent experimental results, Journal of Applied Mechanics 73 (2006) 5–15.
[78] L. Onsager, Reciprocal relations in irreversible processes. I, Physical review 37 (1931) 405.
[79] L. Onsager, Reciprocal relations in irreversible processes. II, Physical review 38 (1931) 2265.
[80] R.J. Hartranft, G. Sih, The influence of the Soret and Dufour effects on the diffusion of heat and moisture in solids, International Journal of Engineering Science 18 (1980) 1375–1383.

[81] C.H. Shen, G.S. Springer, Moisture absorption and desorption of composite materials, Journal of Composite Materials 10 (1976) 2–20.
[82] H.A. Zambrano, et al., Thermophoretic motion of water nanodroplets confined inside carbon nanotubes, Nano letters 9 (2009) 66–71.
[83] S.L. Goren, Thermophoresis of aerosol particles in the laminar boundary layer on a flat plate, Journal of Colloid and Interface Science 61 (1977) 77–85.
[84] N.J. Pagano, Exact solutions for composite laminates in cylindrical bending, Journal of Composite Materials 3 (1969) 398–411.
[85] N.J. Pagano, Exact solutions for rectangular bidirectional composites and sandwich plates, Journal of Composite Materials 4 (1970) 20–34.
[86] J.C. Monge, J.L. Mantari, 3D elasticity numerical solution for the static behavior of FGM shells, Engineering Structures 208 (2020) 110159.
[87] W. Ye, et al., Higher order semi-analytical solution for bending of angle-ply composite laminated cylindrical shells based on three-dimensional theory of elasticity, Thin-Walled Structures 145 (2019) 106392.
[88] J.N. Reddy, Exact solutions of moderately thick laminated shells, Journal of Engineering Mechanics 110 (1984) 794–809.
[89] S. Kapuria, P. Kumari, J.K. Nath, Analytical piezoelasticity solution for vibration of piezoelectric laminated angle-ply circular cylindrical panels, Journal of Sound and Vibration 324 (2009) 832–849.
[90] M. Sobhy, Levy solution for bending response of FG carbon nanotube reinforced plates under uniform, linear, sinusoidal and exponential distributed loadings, Engineering Structures 182 (2019) 198–212.
[91] J.N. Reddy, Theory and analysis of elastic plates and shells, Taylor and Francis, Philadelphia, 1999.
[92] F. Tornabene, M. Viscoti, R. Dimitri, On the Importance of the Recovery Procedure in the Semi-Analytical Solution for the Static Analysis of Curved Laminated Panels: Comparison with 3D Finite Elements, Materials 17 (2024) 588.
[93] F. Tornabene, J.N. Reddy, FGM and laminated doubly-curved and degenerate shells resting on nonlinear elastic foundations: a GDQ solution for static analysis with a posteriori stress and strain recovery, Journal of the Indian Institute of Science 93 (2013) 635–688.
[94] S. Brischetto, F. Tornabene, Advanced GDQ models and 3D stress recovery in multilayered plates, spherical and double-curved panels subjected to transverse shear loads, Composites Part B: Engineering 146 (2018) 244–269.
[95] J.N. Reddy, Introduction to the finite element method, McGraw-Hill Education, New York, 2019.
[96] O.C. Zienkiewicz, R.L. Taylor, The finite element method: solid mechanics, 2, McGraw-Hill, New York, 1967.
[97] F. Tornabene, N. Fantuzzi, F. Ubertini, E. Viola, Strong formulation finite element method based on differential quadrature: a survey, Applied Mechanics Reviews 67 (2015) 0208101.
[98] C. Shu, Differential quadrature and its application in engineering, Springer Science & Business Media, Berlin Heidelberg, 2012.
[99] C. Shu, B.E. Richards, Application of generalized differential quadrature to solve two-dimensional incompressible Navier-Stokes equations, International Journal for Numerical Methods in Fluids 15 (1992) 791–798.
[100] F. Tornabene, Generalized Differential and Integral Quadrature, Esculapio, Bologna, 2023.
[101] F. Tornabene, M. Viscoti, R. Dimitri, Free vibration analysis of laminated doubly-curved shells with arbitrary material orientation distribution employing higher order theories and differential quadrature method, Engineering Analysis with Boundary Elements 152 (2023) 397–445.
[102] A.G. Striz, X. Wang, C.W. Bert, Harmonic differential quadrature method and applications to analysis of structural components, Acta Mechanica 111 (1995) 85–94.
[103] W. Chen, X. Wang, T. Zhong, The structure of weighting coefficient matrices of harmonic differential quadrature and its applications, Communications in Numerical Methods in Engineering 12 (1996) 455–459.
[104] C. Shu, W. Chen, H. Xue, H. Du, Numerical study of grid distribution effect on accuracy of DQ analysis of beams and plates by error estimation of derivative approximation, International Journal for Numerical Methods in Engineering 51 (2001) 159–179.
[105] C. Shu, W. Chen, On optimal selection of interior points for applying discretized boundary conditions in DQ vibration analysis of beams and plates, Journal of Sound and Vibration 222 (1999) 239–257.
[106] F. Tornabene, M. Viscoti, R. Dimitri, Thermo-Mechanical analysis of laminated Doubly-Curved Shells: Higher order Equivalent Layer-Wise formulation, Composite Structures (2024), https://doi.org/10.1016/j.compstruct.2024.117995.
[107] F. Tornabene, M. Viscoti, R. Dimitri, Higher order theories for the modal analysis of anisotropic doubly-curved shells with a three-dimensional variation of the material properties, Engineering Analysis with Boundary Elements 158 (2024) 486–519.
[108] F. Tornabene, M. Viscoti, R. Dimitri, M.A. Aiello, Higher order formulations for doubly-curved shell structures with a honeycomb core, Thin-Walled Structures 164 (2021) 107789.
[109] R.A. Alashti, M. Khorsand, Three-dimensional thermo-elastic analysis of a functionally graded cylindrical shell with piezoelectric layers by differential quadrature method, International Journal of Pressure Vessels and Piping 88 (2011) 167–180.
[110] M.H. Mansouri, M. Shariyat, Differential quadrature thermal buckling analysis of general quadrilateral orthotropic auxetic FGM plates on elastic foundations, Thin-Walled Structures 112 (2017) 194–207.
[111] P. Malekzadeh, H.M.R. Golbahar, M.M. Atashi, Free vibration analysis of elastically supported functionally graded annular plates subjected to thermal environment, Meccanica 46 (2011) 893–913.
[112] C.C. Hong, Thermal vibration and transient response of magnetostrictive functionally graded material plates, European Journal of Mechanics-A/Solids 43 (2014) 78–88.